

## **YEAR END TECHNICAL REPORT**

September 29, 2018 to September 28, 2019

# **Chemical Process Alternatives for Radioactive Waste**

**Date submitted:**

January 17, 2020

**Principal Investigator:**

Leonel E. Lagos, Ph.D., PMP®

**Florida International University Collaborators:**

Dwayne McDaniel, Ph.D., P.E. (Project Manager)

Anthony Abrahao, M.S.

Aparna Aravelli, Ph.D.

Amer Awwad, M.S., P.E.

Ahmadreza Abbasi Baharanchi, Ph.D.

Mayren Echeverria Boan, Ph.D.

Shervin Tashakori, Ph.D.

Mackenson Telusma, M.S.

DOE Fellows

**Submitted to:**

U.S. Department of Energy

Office of Environmental Management

Under Cooperative Agreement DE-EM00000598



**Applied Research Center**

FLORIDA INTERNATIONAL UNIVERSITY

Addendum:

This document represents one (1) of four (4) reports that comprise the Year End Reports for the period of September 29, 2018 to September 28, 2019 prepared by the Applied Research Center at Florida International University for the U.S. Department of Energy Office of Environmental Management (DOE-EM) under Cooperative Agreement No. DE-EM0000598. Incremental funding under this cooperative agreement resulted in FIU having to execute carryover scope, which was completed in November 2019. The technical information for the carryover scope from FIU Performance Year 9 has therefore also been included in these reports.

The complete set of FIU's Year End Reports for this reporting period includes the following documents:

Project 1: Chemical Process Alternatives for Radioactive Waste  
Document number: FIU-ARC-2018-800006470-04b-264

Project 2: Environmental Remediation Science and Technology  
Document number: FIU-ARC-2018-800006471-04b-263

Project 3: Waste and D&D Engineering and Technology Development  
Document number: FIU-ARC-2018-800006472-04b-253

Project 4: DOE-FIU Science & Technology Workforce Development Initiative  
Document number: FIU-ARC-2018-800006473-04b-297

Each document will be submitted to OSTI separately under the respective project title and document number as shown above. In addition, the documents are available at the DOE Research website for the Cooperative Agreement between the U.S. Department of Energy Office of Environmental Management and the Applied Research Center at Florida International University: <http://doeresearch.fiu.edu>

### **DISCLAIMER**

This report was prepared as an account of work sponsored by an agency of the United States government. Neither the United States government nor any agency thereof, nor any of their employees, nor any of its contractors, subcontractors, nor their employees makes any warranty, express or implied, or assumes any legal liability or responsibility for the accuracy, completeness, or usefulness of any information, apparatus, product, or process disclosed, or represents that its use would not infringe upon privately owned rights. Reference herein to any specific commercial product, process, or service by trade name, trademark, manufacturer, or otherwise does not necessarily constitute or imply its endorsement, recommendation, or favoring by the United States government or any other agency thereof. The views and opinions of authors expressed herein do not necessarily state or reflect those of the United States government or any agency thereof.

## TABLE OF CONTENTS

---

TABLE OF CONTENTS.....	i
LIST OF FIGURES .....	iii
LIST OF TABLES .....	vii
PROJECT 1 OVERVIEW .....	1
MAJOR TECHNICAL ACCOMPLISHMENTS .....	3
TASK 17: ADVANCED TOPICS FOR HLW MIXING AND PROCESSES .....	4
Task 17: Executive Summary .....	4
Subtask 17.2: Evaluation of Pipeline Flushing Requirements for HLW at Hanford and Savannah River .....	4
Subtask 17.2: Introduction .....	4
Subtask 17.2: Objectives.....	6
Subtask 17.2: Methodology .....	6
Subtask 17.2: Results and Discussion.....	7
Subtask 17.2: Conclusions .....	11
Subtask 17.2: References .....	12
TASK 18: TECHNOLOGY DEVELOPMENT AND INSTRUMENTATION EVALUATION.....	13
Task 18: Executive Summary .....	13
Subtask 18.2: Development of Inspection Tools for DST Primary Tanks .....	14
Subtask 18.2: Introduction .....	14
Subtask 18.2: Objectives.....	15
Subtask 18.2.1: Preparation for the Deployment of Mini-Inspection Tool at Hanford .....	16
Subtask 18.2.1: Magnetic Arm Rover.....	16
Subtask 18.2.1: Caterpillar Rover .....	20
Subtask 18.2.1: Capsule Controller .....	22
Subtask 18.2.1: UT Sensor Module .....	26
Subtask 18.2.1: Conclusions and Future Work.....	27
Subtask 18.2.4: 6-Inch Crawler Testing and Design Modifications .....	28
Subtask 18.2.4: Proposed Inspection .....	28
Subtask 18.2.4: Testing.....	34
Subtask 18.2.4: Conclusions and Future Work.....	35
Subtask 18.2.4: References .....	35

Subtask 18.3: Evaluation of Coatings for the H-Canyon Exhaust Tunnel  
 (NEW).....36  
 Subtask 18.3: Introduction ..... 36  
 Subtask 18.3: Objectives..... 37  
 Subtask 18.3.2: Bench-scale testing for the SRS H-Canyon (NEW) ..... 37  
 Subtask 18.3.2: Literature Review ..... 37  
 Subtask 18.3.2: Materials and Methods ..... 45  
 Subtask 18.3.2: Results and Discussion..... 47  
 Subtask 18.3.2: Conclusions and Future Work..... 49  
 Subtask 18.3.2: References ..... 50  
**TASK 19: PIPELINE INTEGRITY AND ANALYSIS .....52**  
 Task 19: Executive Summary ..... 52  
 Subtask 19.1: Pipeline Corrosion and Erosion Evaluation .....53  
 Subtask 19.1: Introduction ..... 53  
 Subtask 19.1: Objectives..... 54  
 Subtask 19.1: Methodology ..... 54  
 Subtask 19.1: Results and Discussion..... 58  
 Subtask 19.1: Conclusions and Future Work..... 69  
 Subtask 19.1: References ..... 70  
 Subtask 19.2: Evaluation of Nonmetallic Components in the Waste Transfer  
 System.....72  
 Subtask 19.2: Introduction ..... 72  
 Subtask 19.2: Objectives..... 72  
 Subtask 19.2: Methodology ..... 72  
 Subtask 19.2: Results and Discussion..... 74  
 Subtask 19.2: Conclusions and Future Work..... 83  
 Subtask 19.2: References ..... 84  
**ACKNOWLEDGEMENTS .....85**  
**CONFERENCE PARTICIPATION, PUBLICATIONS & AWARDS .....86**  
**APPENDIX.....88**

## LIST OF FIGURES

---

Figure 1. Two initial condition modes for the flushing studies. ....	5
Figure 2. Schematic of a pipeline for flushing experiments. ....	6
Figure 3. Pipeline constructed for flushing experiments. ....	7
Figure 4. Fully-flooded (top) and gravity-drained (bottom) initial conditions created in the pipeline.....	8
Figure 5. Pipeline condition after flushing with 1 (up) and 1.5 (bottom) line volume of water from fully-flooded (F.F) initial conditions; sections #1, 2, and 3 are start, middle, and end of loop, respectively. ....	9
Figure 6. Post-flush conditions of loop at start and end point clear sections one-day after flushing. ....	9
Figure 7. Flow quantities during flushing of fully flooded pipeline with target FTLV of 1.5. ....	10
Figure 8. During-flush (up) and post-flush (bottom) assessments gravity-drained pipeline with target FTLV of 1. ....	11
Figure 9. Inspection entry points of the AY-102 double-shell tank. ....	15
Figure 10. (Left) CAD drawing of the back view of the modified rover with magnetic arms. (Right) Initial 3D printed prototype to evaluate the feasibility of the modified design. ....	16
Figure 11. Miniature inspection tool equipped with magnetic, free-rotating arm traversing over weld seams. ....	17
Figure 12. Alternate rover design with the motor controls. ....	17
Figure 13. Assembly of adjusted arms. ....	18
Figure 14. Modified design of the magnetic arm mini rover. ....	18
Figure 15. New design for camera and light of the magnetic arm mini rover. ....	19
Figure 16. Testing mini rover in the main mock-up. ....	19
Figure 17. Testing mini rover in our lab mock-up. ....	19
Figure 18. Alternate rover design with the motor controls. ....	20
Figure 19. Images showing rover traveling over 1.5” diameter weld seam. ....	20
Figure 20. Modifiable segments allow sensors mounted to PCBs to be placed according to inspection needs. ....	21
Figure 21. Modified caterpillar design. ....	21
Figure 22. PCBs to be placed according to inspection needs. ....	22
Figure 23. Schematic of the control for mini rover. ....	23
Figure 24. Schematic of the control for the capsule. ....	24
Figure 25. The initial bench testbed for the controller. ....	25

Figure 26. New board design for controller..... 25

Figure 27. New design for the capsule..... 25

Figure 28. New design for the capsule..... 26

Figure 29. Secondary unit designs that include a UT sensor..... 26

Figure 30. Secondary unit designs in order to include a UT sensor. .... 27

Figure 31. UT sensor deployment process..... 27

Figure 32. Leak detection systems at Hanford’ DSTs. .... 29

Figure 33. Typical DST’s drain slots foundation..... 29

Figure 34. FIU’s inspection system. .... 30

Figure 35. Existing condition of DST’s drain lines (WRPS)..... 30

Figure 36. Mother pipe crawler prototype. .... 31

Figure 37. Pneumatic crawlers control box. .... 31

Figure 38. Original (left) and redesigned (right) gripper..... 32

Figure 39. Redesigned gripper model (left) and prototype (right)..... 32

Figure 40. Pipe cross-section mockup conceptual design. .... 33

Figure 41. Alternative guide designs. .... 33

Figure 42. Miniature child-rover conceptual design..... 33

Figure 43. Child inspection tool prototype. .... 34

Figure 44. Preliminary maneuverability tests. .... 34

Figure 45. The full-scale mockup foundation..... 35

Figure 46. Images of HCAEX tunnel degradation [2], [11]. .... 38

Figure 47. Schematic of the acid aging chamber..... 46

Figure 48. Images of concrete specimens (sample 2) immersed in 0.025M (top) and 0.5 M (bottom) nitric acid solutions. (The numbers 1 and 2 identify the same coarse aggregate for the two tested specimens at different times. Samples were wet when the pictures were taken, except for the control sample)..... 47

Figure 49. Average weight loss of concrete immersed in 0.025M and 0.5M nitric acid solutions. .... 48

Figure 50. pH Changes of the 0.025M and 0.5M Nitric acid solutions with time..... 49

Figure 51. Experimental set up with heater and sensors in the chamber..... 55

Figure 52. Data acquisition system (left) and experimental set up (right)..... 55

Figure 53. a) Erosion Coupon b) UT sensor and coupon [4] c) UT pencil sensor on FIU’s loop.56

Figure 54. SRNL Coupons on the pipe loop, endoscopic images of the pipe internal surface with the coupons. .... 56

Figure 55. Fiberstrike a) sensor system b) sensor [6] c) monitoring system layout [6]. ..... 57

Figure 56. a) Fiber optic sensors on the loop; b) single transducer (LCM-500); c) LCM-2500 Interrogator and user control station. .... 58

Figure 57. Results obtained during the environmental chamber testing, a) manual and b) automated. .... 59

Figure 58. Dynamic environmental conditions in the UT sensor’s testing chamber. .... 61

Figure 59. Microscopic images of the coupon surfaces (5X magnification). .... 63

Figure 60. SRNL coupon (new) a) before the test and b) after the test. .... 64

Figure 61. a) New coupon surface; b) Coupon 1 (after testing); c) Coupon 2 (after testing). .... 64

Figure 62. a) Coupon 3 (after testing); b) Coupon 4 (after testing); c) Coupon 5 (after testing). 64

Figure 63. Microscopic images (5X magnification) of coupon surfaces for coupons 1, 2, 3 respectively. .... 65

Figure 64. Microscopic images (5X magnification) of coupon surfaces for coupons 4 and 5 respectively. .... 65

Figure 65. Sensor baseline profile of pipe loop (no activity - top and pump operating - below). 67

Figure 66. Sensor profile (0.25” hole opened and closed). .... 67

Figure 67. Sensor profile (0.5” hole opened and closed). .... 68

Figure 68. Sensor profile (pipeline strike 13 sec - top and 2 sec magnified - below). .... 68

Figure 69. Water only aging loop. .... 73

Figure 70. Flow meter, pressure transducer and thermocouple. .... 74

Figure 71. Coupon aging vessel (left) and EPDM dog bone (right). .... 74

Figure 72. Tensile strength testing of an EPDM dog bone. .... 75

Figure 73. EPDM dog bone tensile strength. .... 75

Figure 74. Hose burst test apparatus. .... 76

Figure 75. Ruptured HIHTL specimen WO-01. .... 76

Figure 76. Ruptured HIHTL specimens WO-02. .... 76

Figure 77. WO-01 burst pressure graph. .... 77

Figure 78. WO-02 burst pressure graph. .... 77

Figure 79. Average hose burst pressure comparison. .... 78

Figure 80. Visual characteristics of the surface of the EPDM (dog-bone) specimens before and after aging. .... 78

Figure 81. SEM-EDS scan of baseline hose specimen. .... 79

Figure 82. SEM-EDS scan of hose specimen aged for 6-months at 130°F. .... 80

Figure 83. SEM-EDS scan of hose specimen aged for 12-months at 130°F. .... 81



Figure 84. SEM-EDS scan of hose specimen aged for 6-months at 170°F. .... 82  
Figure 85. SEM-EDS scan of hose specimen aged for 12-months at 170°F. .... 83

## LIST OF TABLES

---

Table 1. Overlay Material Characteristics [13]..... 40

Table 2. Characteristics of Potential Concrete Repair Materials for Aggressive Environments [15]..... 43

Table 3. Review of Details for Acid Immersion Testing from Literature ..... 44

Table 4. Mix Proportions of Conventional Concrete [24] ..... 46

Table 5. UT Sensor Measurements during the Experiment..... 60

Table 6. UT Sensor Measurements during the Experiment..... 61

Table 7. Mass Loss in the SRNL Coupons during the Experiment ..... 62

Table 8. SRNL Coupon Mass and Height Loss ..... 66

## PROJECT 1 OVERVIEW

---

The Department of Energy's (DOE's) Office of Environmental Management (EM) has a mission to clean up the contaminated soils, groundwater, buildings and wastes generated over the past 60 years by the R&D and production of nuclear weapons. The nation's nuclear weapons complex generated complex radioactive and chemical wastes. This project is focused on tasks to support the safe and effective storage, retrieval and treatment of high-level waste (HLW) from tanks at Hanford and Savannah River sites. The objective of this project is to provide the sites with modeling, pilot-scale studies on simulated wastes, technology assessment and testing, and technology development to support critical issues related to HLW retrieval and processing. Florida International University (FIU) engineers work directly with site engineers to plan, execute and analyze results of applied research and development.

Although a number of tasks have been initiated and completed over the course of the cooperative agreement, at the end of this past year, there were 4 active tasks. These tasks are listed below and this report contains a detailed summary of the work accomplished for FIU's Performance Year 9.

### **Task 17: Advanced Topics for HLW Mixing and Processes**

The objective of this task is to develop a test loop that can bridge technical gaps associated with the flushing of HLW within the transfer and processing lines at Hanford and Savannah River. This loop will aid in implementing optimal flush operations with minimized water usage and the possibility of water hammer and plug formations. These practices will aim to develop a correlation for flush parameters based on characteristics of the system at the start of flushing. The data and correlations will be useful for improving existing guidelines. Characterization of post-flush pipeline cleanliness is an additional objective of the task which will be implemented using various elements of the loop. With discussions between FIU and engineers from Hanford and SRNL, these evaluations will help to establish criterion for flushing operations.

### **Task 18: Technology Development and Instrumentation Evaluation**

The objective of this task is to develop inspection tools that will assist engineers in evaluating the structural integrity of the primary and secondary tank floors in the double shell tanks (DSTs) at the Hanford Site. This effort has led to the development of multiple inspection tools that are able to provide live visual feedback. These include a magnetic wheeled miniature motorized rover that can travel through the refractory cooling channels under the primary tank and a pneumatic pipe crawler that can inspect tank ventilation pipes and its central plenum. In addition, FIU is developing a marsupial robotic system that can navigate through the drain lines and inspect the secondary liner via the drain slots.

An additional objective is to investigate coatings or fixatives that can be used to mitigate and prevent further degradation of concrete walls exposed to adverse environments in the HCAEX tunnel. Efforts will focus on defining important aspects regarding the concrete specimens such as configuration (cylindrical, square, etc.), dimensions (length, thickness), exposure mode to the aggressive environment (e.g. full immersion), etc. The effort will also cover the design and development of new test setups, the experimental design (potential variables definition, number of samples), concrete samples preparation, as well as the selection of measurements to evaluate

the performance of the concrete. Initial bench-scale testing will be performed including the aforementioned considerations.

### **Task 19: Pipeline Corrosion and Erosion Evaluation**

The objective of this task is to provide the sites with a means to evaluate the structural integrity of waste transfer pipeline components. This has involved the evaluation of potential sensors and the viability of utilizing them to provide real time data for long durations of time. The sensors can be installed and provide thickness measurements of pipeline components and fittings found in jumper pits, evaporators, and valve boxes.

The objective of this task is also to provide the Hanford Site with data obtained from experimental testing of the hose-in-hose transfer lines, Teflon® gaskets, EPDM O-rings, and other nonmetallic components used in their tank farm waste transfer system under simultaneous stressor exposures. The experiments will be limited to various combinations of simultaneous stressor exposure to caustic solutions, high temperatures and high pressure. Evaluation of baseline materials will be conducted for comparison to materials that have been conditioned with the various simultaneous stressors.

## MAJOR TECHNICAL ACCOMPLISHMENTS

---

### Task 17: Advanced Topics for HLW Mixing and Processes

- The flushing test loop was completed and initial testing was conducted for both fully flooded and drained systems using a kaolin/water mixture as the simulant. A Coriolis meter was also added to the loop to provide real time flow and density data. Results have demonstrated for the simulant and pipeline configuration tested, that 1.5 flow volume is needed for the flushing operation.

### Task 18: Technology Development and Instrumentation Evaluation

- A marsupial crawler was designed and manufactured and tested in a 6-inch bench scale experimental set up. A rover was also designed and is being developed to navigate through the drain slots of the Hanford DSTs. The rover will be deployed from the 6-inch crawler when the system traverses through the drain line and reaches the foundation drain slots.
- Design modifications to the miniature rover system have been included that provide the means to meet criteria established by WRPS engineers for deployment at Hanford. These modifications include traversing over weld seams and operation without significant loss of video signal or power.
- A test plan was developed to create a platform for the evaluation of coatings that could be used to protect the degrading walls of the exhaust tunnel at the H-Canyon facility. The plan involves aging concrete specimens with nitric acid to create concrete surfaces with similar chemistry and surface morphology. Initial bench scale tests were conducted to validate the approach.

### Task 19: Pipeline Corrosion and Erosion Evaluation

- Testing with the Permasence UT sensors continued with elevated temperature and environmental exposure. Results indicated that the sensors were able to operate properly at temperatures up to 120°F and 95% RH.
- Testing with SRNL mass loss coupons demonstrated the potential for use in the DOE's waste transfer system. The coupons are capable of detecting very small changes in pipes due to erosion or corrosion.
- Additional aging and testing was conducted on HIHTL coupons and EPDM dog bone coupons. The aging processes used were 170°F water and was intended to differentiate aging from caustic exposure and elevated temperature.
- SEM-EDX scans were completed on the previously aged HIHTL coupons and indicate that there was penetration of the caustic solution through the EPDM. It is not clear from the scans whether there was significant enough penetration to affect the polyester support weave in the hose.

## **TASK 17: ADVANCED TOPICS FOR HLW MIXING AND PROCESSES**

---

### **Task 17: Executive Summary**

Pipelines which carry high-level waste within the DOE complex should be properly flushed in the cases where stationary or moving beds of solid sediment occur, or lines are prone to hydrogen gas buildup. Present guidelines establish a minimum for the amount of water (flush volume) and flush velocity values used for post-transfer flushing operations to achieve satisfactory cleaning of pipelines. However, further studies are needed to find optimal operating velocity modes/values in order to minimize the flush volume and consequent downstream waste. These efforts are significantly helpful to DOE waste remediation sites by preserving tank storage, preventing additional waste processing, and minimizing dilution and changes in waste chemistry. An experimental test loop was recently developed for study of non-Newtonian slurry flushing at Florida International University (FIU). This loop was designed to create sediment beds of various materials and bed heights and to investigate parameters that affect the efficiency of flushing operations. The objective is to find flush velocity values/modes which lead to satisfactory cleaning of transport lines with a minimum amount of water usage.

A 165 ft experimental test loop made of 3-inch carbon steel pipes was constructed and used in initial testing campaigns. This pipe loop was equipped with real-time monitoring instruments to record variation of pressure, density, mass flow rate, and temperature during testing. Post-flush in-situ no-flow evaluations were performed using ultrasonic, endoscopy, and visual inspection. Additional post-flush evaluations were conducted using filtration and density monitoring of residuals within a designated circulations loop. These provisions enable comparison of pipeline cleanness before the start and after termination of flushing operations for efficiency evaluation.

This report presents efforts associated with flushing of kaolin-water mixtures at different concentrations and with various flush volume and flush velocity values/modes. In initial testing, efforts focused on creating repeatable sediment beds inside the pipeline in both fully-flooded (no pre-flush drainage) and gravity-drained (pre-flush drained) systems. Bed characterization (i.e., measurement of sediment height and solids concentration) was conducted to ensure consistency of initial conditions between tests. Preliminary results for a flushing study of 10% vol. kaolin-water mixtures starting from a fully-flooded initial condition showed that flushing with 1-line volume (65 gallons) could remove up to 72 percent of solids from the pipeline.

### **Subtask 17.2: Evaluation of Pipeline Flushing Requirements for HLW at Hanford and Savannah River**

---

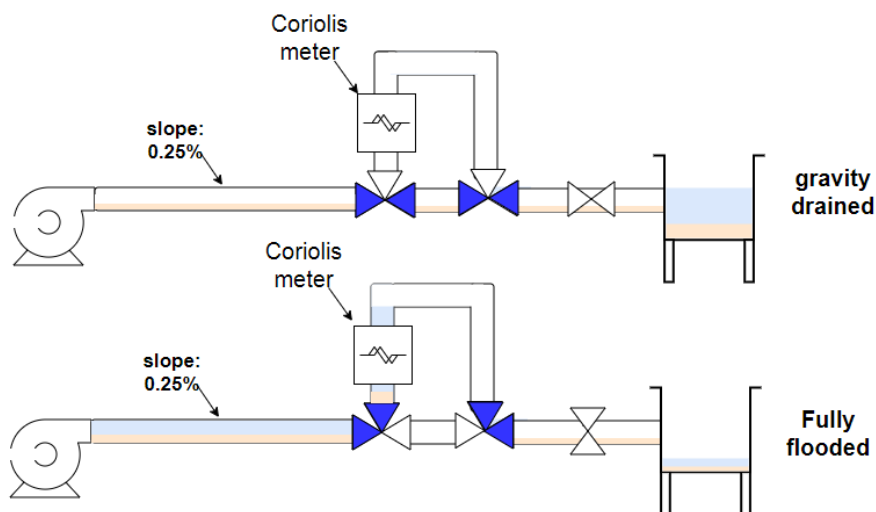
#### **Subtask 17.2: Introduction**

Pipelines which transport radioactive waste at Department of Energy sites should be operated above the critical velocity to avoid formation of stationary or moving beds of solid sediments inside pipes. These formations can result in partial line plugging (which may lead to excessive pumping load and erosion) or full line plugging (which may lead to pump burst or pipeline

failure). The pretreatment facility design strategy requires that each slurry transfer in process lines be followed by a flush with water in order to minimize the likelihood of plugging. Recently, the Defense Nuclear Facilities Safety Board (DNFSB/TECH-40, Kazban 2016) has indicated needs for vigorous investigations on the technical basis for prescribing flush velocity in pipelines.

Previous reports related to pipeline flushing of several simulants were noted in WTP-RPT-175 Rev. 0 (Poloski et al., 2009) and WTP-RPT-178 Rev. 0 (Yokuda et al., 2009). Our study revealed that, in a number of tests, the minimum required flush volumes were more than minimum required values provided by the design guidelines in 24590-WTP-GPG-M-0058, Rev. 0 (Hall 2006). In addition, flush velocities in the pipeline exceeded the maximum velocity stated in the flushing guidelines, RPP-RPT-59600, Rev. 0 (Nguyen et al., 2016). In addition, no assessments of flushing effectiveness (post-flush pipeline cleanliness) were reported.

This effort is intended to determine effective flushing operations using a minimal amount of water usage and provide additional guidelines in support of recently developed flushing standards (TFC-ENG-STD-26). Successful execution requires creation and characterization of sediment beds, flushing in different modes, and evaluation of operation effectiveness through measurement of post-flush pipeline residues. To extend previous flushing studies, our strategy will be creating different case studies targeting different materials and pipe lengths. In addition, existing ultrasonic and visualization methods inspired by the work conducted at PNNL, PNNL-20350 FINAL (Denslow et al., 2011) and PNNL-19441 Rev. 0 (Bontha et al., 2010), will be used in the collection and assessment of data. In each round of testing, focus will be on influential parameters set for one simulant in a fixed pipe length. These parameters are flush velocity mode (continuous one-step, continuous two-step, and pulsing) and initial conditions (gravity drained versus fully flooded systems, as shown in Figure 1). These initial conditions can be simply created before start of flushing operations by directing the flow in different directions using two ball valves.



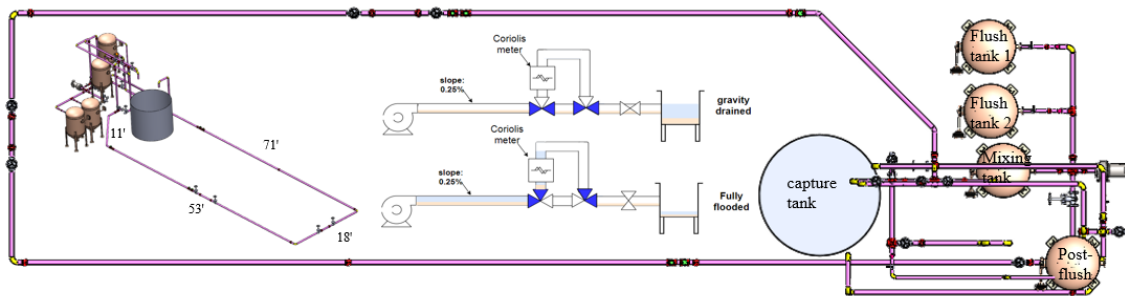
**Figure 1. Two initial condition modes for the flushing studies.**

**Subtask 17.2: Objectives**

- Implementing optimal flush operations with minimized waste production and pipeline erosion.
- Developing a correlation for flush parameters based on characteristics of the system at the start of flushing (initial conditions). Data and correlations will be useful for determination of pumping requirements improving existing guidelines.
- Establishing a criterion for flushing satisfaction through discussions between FIU and experts from Hanford Site and the national labs.

**Subtask 17.2: Methodology**

To achieve the objectives of this study, a 50.3 m (165 ft) test loop made of 3 inch schedule 40 carbon steel pipes and fittings was constructed (Figure 2 and Figure 3). The pipeline was sloped at the rate of 0.15% (3 inch drop in 100 ft) to emulate conditions at Hanford site and facilitate gravity draining. This experimental loop can perform various functions such as slurry circulation (to load the system), draining (to create gravity-drained initial condition and to empty the system), pump cleaning, flushing, sediment and water retrieval, filtration, and post-flush circulation.



**Figure 2. Schematic of a pipeline for flushing experiments.**





**Figure 3. Pipeline constructed for flushing experiments.**

A 15 hp slurry pump (AMT 427B-95) capable of delivering  $0.87 \text{ m}^3/\text{s}$  (230 gpm) of water at 2.74 atm (40.3 psi or 93 feet of head), was used for slurry circulation, flushing, and post-flush evaluations. This pump was controlled via a HopeWind variable frequency drive (VFD) which has made it possible to reduce ramp-up and ramp-down times to 0.5 seconds (time to reach 1,750 rpm from rest and vice versa). To protect the loop from over-pressurization (in situations where plugs form or pumping against a closed valve occurs), safety elements such as relief valves and a burst disk were added. The loop was also equipped with three clear sections in the beginning, middle, and end locations for visualization purposes. These sections assist with characterization of initial conditions and monitoring of bed variations during flushing operations.

Simulant preparation was performed using a 0.5 hp 32V136 Dayton mixer with a 6 inch propeller inside the mixing tanks. To achieve target concentrations, kaolin or water content was adjusted in the mixing tank using data obtained from a Krohne Optimass 1000 Coriolis meter in the loop. The Coriolis meter was also a key instrument to monitor variation of density and mass flow rate during flushing operations and post-flush evaluations. Post-flush in-situ no-flow evaluations were possible through ultrasonic, endoscopy, and visual inspection (clear sections). Additional post-flush evaluations were conducted using filtration of residuals within designated bypass lines. These provisions enable comparison of pipeline cleanness before the start and after termination of flushing operations for efficiency evaluations.

### **Subtask 17.2: Results and Discussion**

Initial tests were performed using kaolin-water with 10 vol.% (19 wt.%) concentration. EPK kaolin with a density of 2.65 gr/cc was used in tests with both gravity drained and fully flooded

conditions. The fully-flooded condition was created by allowing kaolin to settle for one day in the loop after stopping the slurry pump and without changing any valve configurations. The gravity drained condition was created by opening a drain valve after full settlement. Sediment bed height was observed in the clear sections at the beginning and end of the loop for quantification of initial conditions (Figure 4) in both modes. This figure shows the presence of a consistent bed at both clear sections in the case of the fully-flooded initial condition. However, different bed heights were observed across the loop for the drained initial conditions. Presence of a thicker bed at the end of the pipe loop can be associated with accumulative settling of particles toward the end of the pipeline during drainage process.



**Figure 4. Fully-flooded (top) and gravity-drained (bottom) initial conditions created in the pipeline.**

#### *Testing with Fully-flooded Initial Conditions*

Flushing tests were started with the system loaded with 10 vol. % (19 wt. %) kaolin-water and in the fully-flooded condition. In the flush operations, the slurry pump was stopped at target flush-to-line-volume (FTLV) values of 1 and 1.5 (corresponding to 65 and 97.5 gallons, respectively). Condition of the pipeline in three points immediately after flushing is shown in Figure 5. This figure shows a cloudy condition inside the third clear section (post-flush residues), indicative of insufficient cleaning with use of 1 line of flush water. Clean conditions were obtained by use of 1.5 line volume of water in all three clear sections.





**Figure 5. Pipeline condition after flushing with 1 (up) and 1.5 (bottom) line volume of water from fully-flooded (F.F) initial conditions; sections #1, 2, and 3 are start, middle, and end of loop, respectively.**

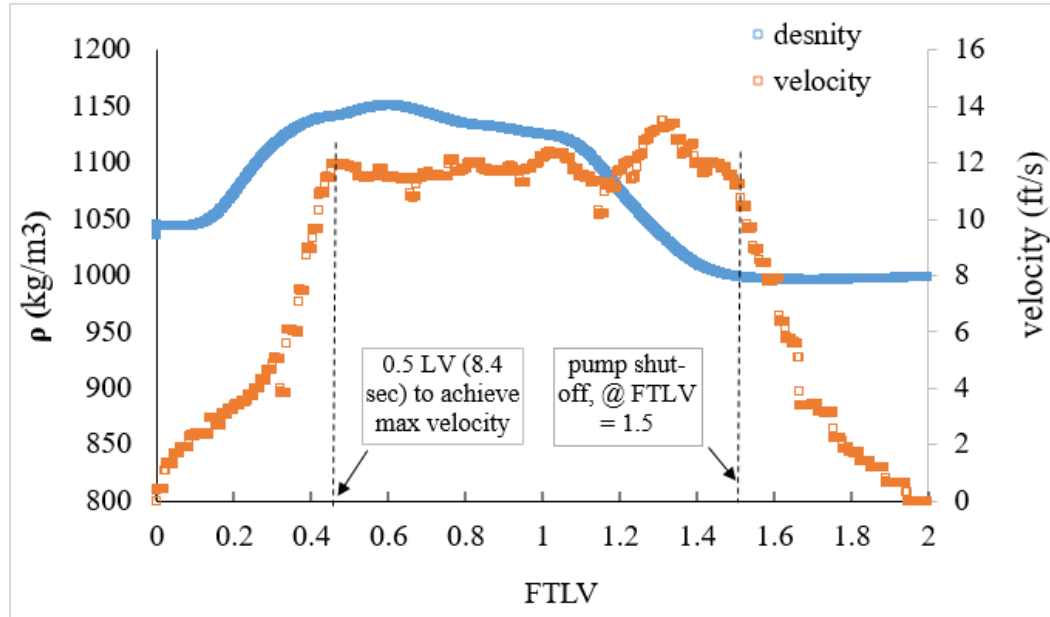
Further, loop content was circulated in the post-flush circulation initially filled with 50 gallons of fresh water and allowed to settle for two days. After this period, a strip of kaolin was observed in the pipe invert. Solids concentration of this bed was found to be 1.6 vol. % through sampling from the loop (density measurements) and matched with a value obtained from geometric reconstruction. No post-flush residues (strips of kaolin) were found in the case of the target 1.5 FTLV. Similarly, no difference was found between density values of fresh water and recirculated post-flush streams displayed by the Coriolis meter.



**Figure 6. Post-flush conditions of loop at start and end point clear sections one-day after flushing.**

Flow quantities such as mass flow rate and density were also recorded using a Field Point 2010 data acquisition module and a PRO-FLO200 totalizer. Data is displayed for the target 1.5 FTLV case in Figure 7. Mass flow rate data show a large inertia of the system to reach maximum startup velocity and reach stagnation at pump shut-down, resulting in final FTLV of 2. Increase of mass flow rate toward the end of this operation could be associated with progressive drop of

system loss (solids leaving the pipeline). Density data reached a plateau at FTLV=1.5 which suggested a sufficient cleaning of the system at this FTLV. Further, content of the loop was circulated in the post-flush loop where constant density of  $996 \text{ kg/m}^3$  was observed at the Coriolis meter.



**Figure 7. Flow quantities during flushing of fully flooded pipeline with target FTLV of 1.5.**

In the next step, flushing of the system with gravity-drained initial conditions was performed. The loop was initially loaded with a 10 vol.% kaolin-water mixture and allowed to rest for one day. At this point, a valve at pump discharge was closed and a drain valve at the pipeline exit was opened. The drain valve was closed when no more material exited the pipeline due to gravity. At this point, the system was allowed to rest for 4 hours which led to conditions shown in Figure 5. To start flushing, the valve at the pump discharge was opened simultaneously with pump startup and the pump was shut off at the target FTLV of 1.

Figure 8 shows data from the Coriolis meter during flushing of the gravity drained pipe. Density data shows small perturbations due to air being pushed through the Coriolis meter. Field observations (video recording) discovered a 10 second travel time for flush water to reach the end of pipeline at the location of the meter. This observation matched with the delay in the rise of mass flow curve. However, delay in the rise of density can only be explained by presence of air in the meter meaning that meter was not fully flooded. Full removal of air from vertical pipes inside the meter took about 4 seconds. Interestingly, the start of the density rise occurred after the pump was shut off and successive processes occurred due to system inertia as explained in the figure. Figure 8 also shows the condition of the clear sections immediately after the flush operation. All clear sections were found completely empty of kaolin and  $997 \text{ kg/m}^3$  was reported by the Coriolis meter.

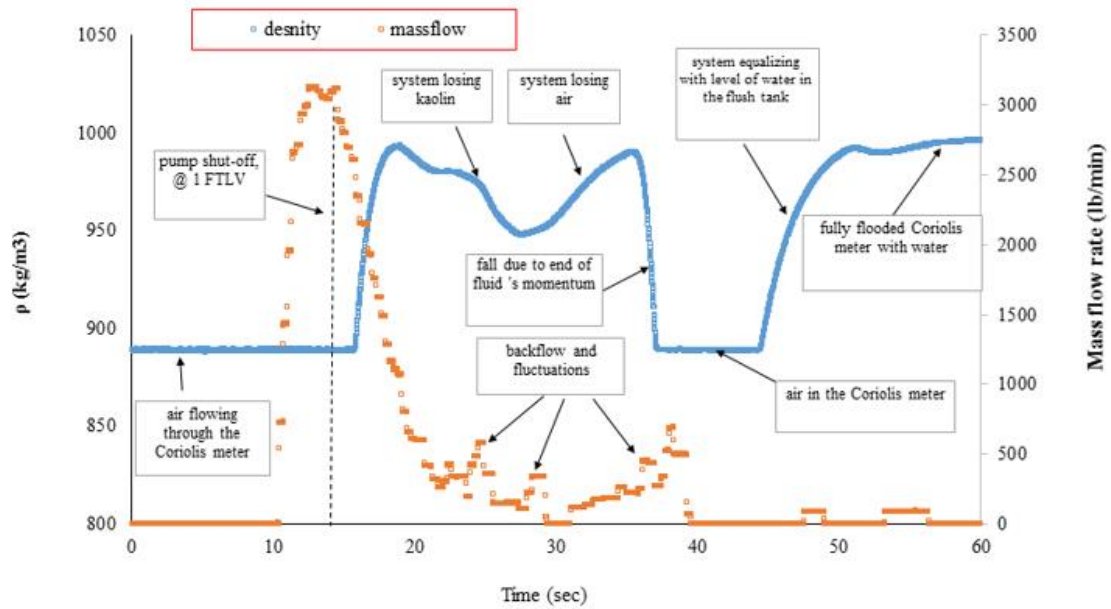


Figure 8. During-flush (up) and post-flush (bottom) assessments gravity-drained pipeline with target FTLV of 1.

**Subtask 17.2: Conclusions**

Results of the initial flushing test using 10 vol.% kaolin-water mixture inside a 165 ft experimental loop were presented. Flushing of lines starting with gravity-drained and fully-flooded initial conditions was performed and it was found possible to clean the pipeline with less than 2 line volumes of water.

For the fully-flooded initial condition, flushing with 1 line volume resulted in residues with 1.6 vol.% concentration in the pipeline. Mass balance calculations were performed to obtain cleaning effectiveness of the flush operation. Therefore, by considering the initial mass of kaolin in the pipeline (117 lb) and final mass of kaolin in the pipeline and post-flush tank (33.24), 72% of solids were removed from the system. Flushing results showed that at least 1.5 line volume was required to sufficiently clean the system with the simulant used.

In the case of the gravity drained system, sufficient cleaning was achieved through flushing with 1 line volume. Results showed that with the conditions used in this testing (early termination at 1 FTLV), presence of air was a challenging factor in accurate tracking of solids migration from the system. Perhaps longer flushing tests (more challenging simulants) where complete air removal occurs early in the process can create better scenarios for more accurate tracking of solids during future flushing tests.

**Subtask 17.2: References**

- R. Bontha, H. E. Adkins, K. M. Denslow, J. J. Jenks, C. A. Burns, P. P. Schonewill, G. P. Morgen, M. S. Greenwood, J. Blanchard, T. J. Peters, P. J. MacFarlan, E. B. Baer, W. A. Wilcox, "Test Loop Demonstration and Evaluation of Slurry Transfer Line Critical Velocity Measurement Instruments", PNNL-19441 Rev. 0 (2010)
- M. Denslow, J. J. Jenks, J. R. Bontha, H. E. Adkins, C. A. Burns, P. P. Schonewill, N. N. Bauman, D. F. Hopkins, "Hanford Tank Farms Waste Certification Flow Loop Phase IV: PulseEcho Sensor Evaluation", PNNL-20350 FINAL (2011)
- N. Hall, "Minimum Flow Velocity for Slurry Lines", 24590-WTP-GPG-M-0058, Rev 0 (2006)
- K. Hansen, "WTP Pretreatment Facility Potential Design Deficiencies - Sliding Bed and Sliding Bed Erosion Assessment", SRNL-STI-2015-00014, Revision 0 (2015)
- Kazban, A., "Plugging and Wear of Process Piping at The Waste Treatment and Immobilization Plant", DNFSB/TECH-40 (2016)
- Lee, "Ultrasonic Technique for Measuring the Thickness of Scale on the Inner Surfaces of Pipes", Journal of the Korean Physical Society, Vol. 56, No. 2, p. 558-561 (2010)
- C. Nguyen, M. S. Fountain, C. W. Enderlin, A. J. L. Fuher, L. F. Pease, "One System River Protection Project Integrated Flowsheet-Slurry Waste Transfer Line Flushing Study", RPP-RPT-59600, Rev.0 (2016)
- P. Poloski, M. L. Bonebrake, A. M. Casella, M. D. Johnson, P. J. MacFarlan, J. J. Toth, H. E. Adkins, J. Chun, K. M. Denslow, M. L. Luna, J. M. Tingey, "Deposition Velocities of Newtonian and Non-Newtonian Slurries in Pipelines", PNNL-17639, WTP-RPT-175 Rev. 0, (2009)
- T. Yokuda, A. P. Poloski, H. E. Adkins, A. M. Casella, R. E. Hohimer, N. K. Karri, M. Luna, M. J. Minette, J. M. Tingey, "A Qualitative Investigation of Deposition Velocities of a Non-Newtonian Slurry in Complex Pipeline Geometries", PNNL-17973, WTP-RPT-178 Rev. 0, (2009)

## TASK 18: TECHNOLOGY DEVELOPMENT AND INSTRUMENTATION EVALUATION

---

### Task 18: Executive Summary

Recent integrity issues in the double-shell tanks (DST) at Hanford have motivated the need for developing innovative tools that can provide information regarding the health of the tanks. These issues include the primary linear failure of AY-102 and recent concerns of thinning in the DST secondary liners. Other concerns include erosion or corrosion on transfer lines and processing pipes. In recent years, FIU has supported DOE-EM by developing tools that can assist in understanding the health of tanks and the waste transport system at Hanford.

More specifically, FIU has developed a miniature rover that can be deployed through small risers and gain access to refractory slots in the Hanford DSTs. It traverses through the slots on the primary liner upside down via magnets to avoid debris in the slots. Recent modifications include a spring loaded magnetic arm that allows the unit to traverse over large weld seams but does not reduce the overall functionality of the system. The system has also incorporated a control capsule that will sit within the annulus of the tank and improves on issues related to signal and voltage loss over long tether lines. Lastly, the unit is also being augmented with a second module that will include a means to prep the tank surface and obtain a thickness measurement using a dual element ultrasonic sensor.

FIU has also developed a 6-inch peristaltic pipe crawler that operates similar to the previous pipe crawlers developed at FIU. This crawler is a marsupial type crawler that will navigate through the 6-inch drain lines, and deploy a small rover at the entrance of the drain slots. This rover will also traverse upside down on the secondary liner and provide information regarding the health of the liner. An initial prototype for the crawler unit has been developed, assembled and tested. The system is pneumatic and consists of three modules – two grippers and one extender. The validation tests are conducted in a mockup of the drain lines and demonstrate the system's ability to navigate through long pipe lengths and elbows.

In addition to the Hanford site, FIU is supporting the Savannah River site (SRS) facility to investigate technologies to evaluate the H-Canyon for degradation and potentially help avoid further degradation. Robotic inspections of the tunnel revealed significant degradation of the reinforced concrete structure that was associated with acid attack, and could compromise the structural stability of the tunnel. Thus, the identification and evaluation of potential repair materials that could be applied on the degraded walls to mitigate and prevent further degradation is important. FIU has been supporting this task by 1) development and evaluation of aged concrete under accelerated aging conditions and, 2) evaluation of potential repair materials applied on aged and non-aged concrete under simulated aggressive conditions. In order to develop and evaluate concrete samples exposed to accelerated aging conditions in simulated aggressive environments, a literature review of the HCAEX tunnel was conducted that included 1) characterization and extent of the concrete damage, 2) environmental conditions inside the tunnel and 3) primary deterioration mechanisms. In addition, potential coatings and/or repair materials for degraded concrete surfaces exposed to aggressive environments (primarily acidic) were selected from the literature review and the most common testing and measurements for evaluating acid attack phenomena, erosion, etc. were reviewed.



From the literature review findings, a preliminary bench-scale test plan for the concrete accelerated aging under aggressive conditions (acid fumes, humidity, etc.) was developed. Donated concrete samples (composition different to the tunnel) were exposed to the aging conditions (e.g. immersion in acid solutions) and visual inspection, mass loss and pH change (acid solution) were recorded over time. Correlations between the visual inspection, mass loss and pH changes results and the aging time or the aging conditions were developed. Specimens submitted to the highest acid concentration showed the fastest and most intense degradation. The type of coarse aggregate (limestone) used for the concrete seemed to be the cause of the fastest aging observed, compared to the cement paste. The research findings created the foundation for the ongoing investigation, in which new concrete samples with a mix design similar to the HCAEX tunnel will be tested and will serve as the substrate for testing the selected coatings and /or repair materials. In summary, the literature review and the preliminary results from the aging tests of concrete are provided in this year-end report.

## **Subtask 18.2: Development of Inspection Tools for DST Primary Tanks**

---

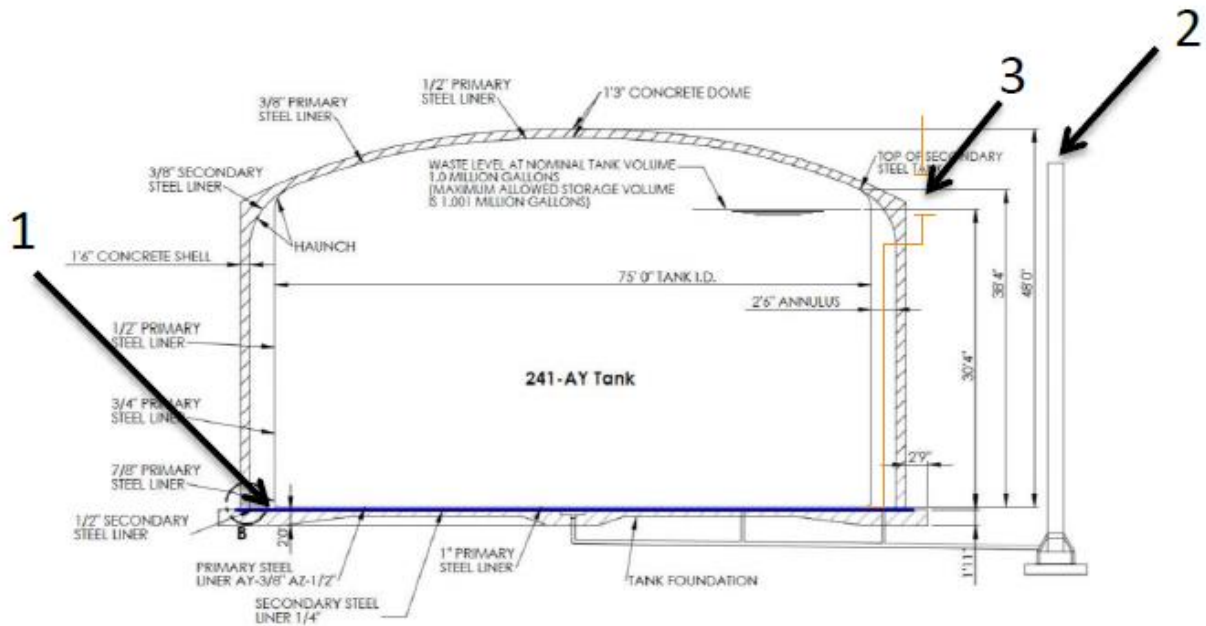
### **Subtask 18.2: Introduction**

In August of 2012, traces of waste were found in the annulus of the AY-102 double-shell tank storing radioactive waste at the Hanford Site, prompting the need for developing inspection tools that can help assess the structural integrity of the DST primary liner. In addition, evaluations of the DST secondary liners within the tank annulus have also shown thinning of the secondary liner. This has prompted the development an inspection tool for the secondary liner as well.

Figure 9 shows three possible entry points for inspection in a typical DST (AY-102):

1. refractory air slots through the annulus,
2. leak detection piping, and
3. Ventilation header piping.





**Figure 9. Inspection entry points of the AY-102 double-shell tank.**

Among the inspection tools that are currently being developed and tested at FIU are:

- A *magnetic miniature rover* that will travel through the refractory air slots,
- A *pneumatic pipe crawler* that will inspect the ventilation header piping, and
- A new *marsupial crawler* that will inspect the secondary liner.

The new marsupial crawler has a design that includes a pneumatic pipe crawler that travels through the 6” leak detection piping and houses a rover that has similar features as the magnetic miniature rover.

**Subtask 18.2: Objectives**

The objective of this task is to develop inspection tools that can provide information regarding the DST bottoms from within the insulation refractory pads and concrete foundation leading to the tank liners. FIU engineers will continue to work directly with site engineers to develop and test systems that can assist in the health assessment of the tanks. After the technologies have successfully demonstrated specified capabilities, FIU will work with site engineers to meet requirements for deployment at the sites. Specific subtasks include:

- Improvement of the design concepts that will allow for the navigation of a remotely controlled device through the refractory pad channels and/or the drain slots of DST tanks and provide visual feedback. A prototype of the inspection tool has been validated in a full-scale sectional mock-up test bed; however, minor modifications are needed for deployment of the system at Hanford. FIU will also continue to incorporate a secondary unit that will house and deploy a UT sensor for point thickness measurement of the tank floor.
- Development and improvement of the design concepts that will allow for the navigation of the miniature rover through the straight sections and 90 degree turns in tank AY-101. The

current design is a modular system (caterpillar system) that utilizes magnets to control the rotation and potential navigation around the turns.

- Testing and improvement of the design for a 6-inch crawler that can navigate through the drain lines to the concrete foundation of the DSTs. A new miniature rover housed in the 6-inch crawler will then be deployed to inspect the secondary liners.

## Subtask 18.2.1: Preparation for the Deployment of Mini-Inspection Tool at Hanford

---

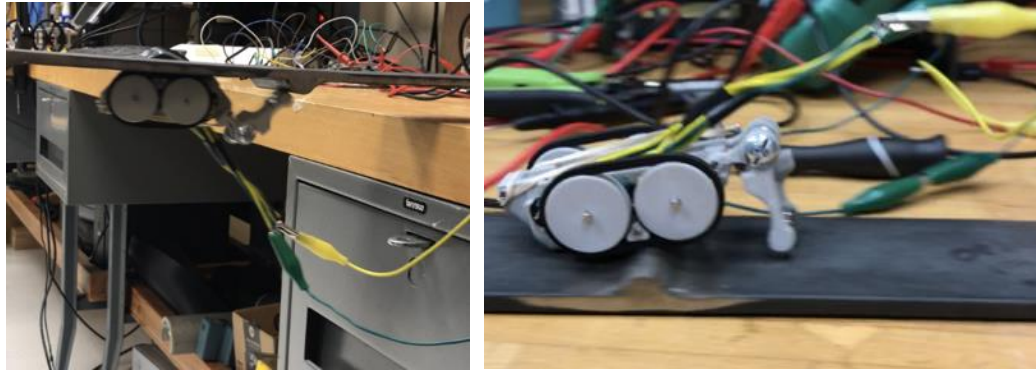
### Subtask 18.2.1: Magnetic Arm Rover

For this subtask, efforts for the miniature rover continued to focus on addressing design issues related to deployment of the unit in the DSTs at Hanford. One of the issues identified was improving the rover's weld seam traversing capability. A design modification to the rover included the addition of two free-rotating arms attached to the front and back of the rover, as showed in the figure below. The end of the arm is connected to a magnetic roller, similar in design to a steamroller, to maintain contact with the tank surface, while the rover is traversing weld seams on the primary liner. Torsion springs at the arm-joints have also been added to generate a vertical stabilizing torque. After the arm rolls over a weld seam, the higher tension of the pivoted end of the arm will cause the rover to tilt forward, allowing the front wheels of the rover to regain contact with the tank surface. An initial 3D printed prototype was fabricated to test the feasibility of modified design.



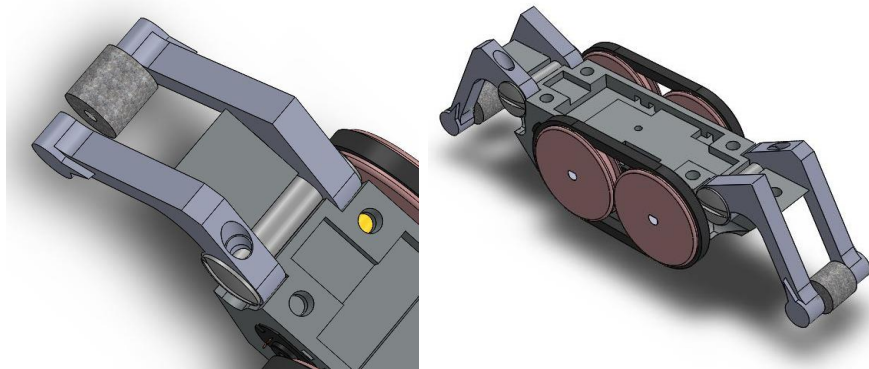
**Figure 10. (Left) CAD drawing of the back view of the modified rover with magnetic arms. (Right) Initial 3D printed prototype to evaluate the feasibility of the modified design.**

Initial bench tests using the simulated weld seams with different heights showed that the modified version managed to traverse weld seams of 0.375 inches. This satisfies the minimum requirement specified by WRPS engineers. The figure below shows snapshots of the bench tests performed in the lab.



**Figure 11. Miniature inspection tool equipped with magnetic, free-rotating arm traversing over weld seams.**

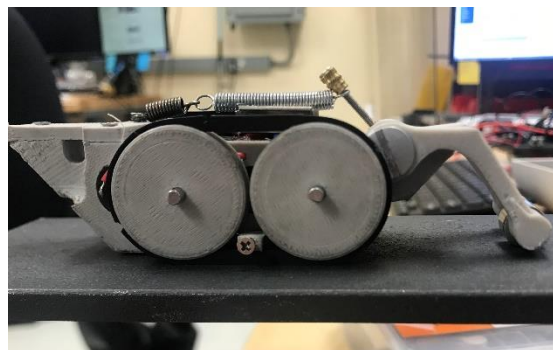
As noted previously, the front of the arms contains a cylindrical magnet that rolls very similar to a bulldozer. It is secured into place using a rod and two bearings, in order to maintain its passive nature. This magnet’s purpose is strictly to remain in contact with the surface, and does not need to provide any torque/active motion.

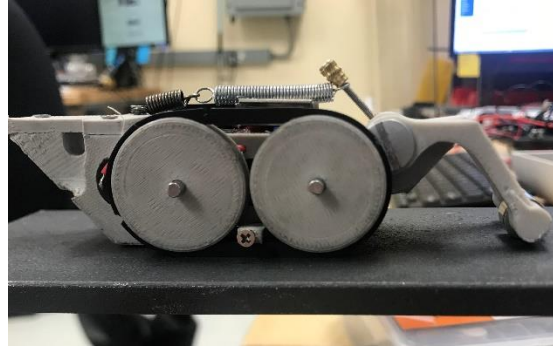


**Figure 12. Alternate rover design with the motor controls.**

The arms are secured in place to a barrel screw, which is temporarily fastened to the body using a cover. The spring (not pictured) extends from the arm to the opposite end of the body, in order to allow the unit to snap back to the nominal orientation when passing over the weld seam.

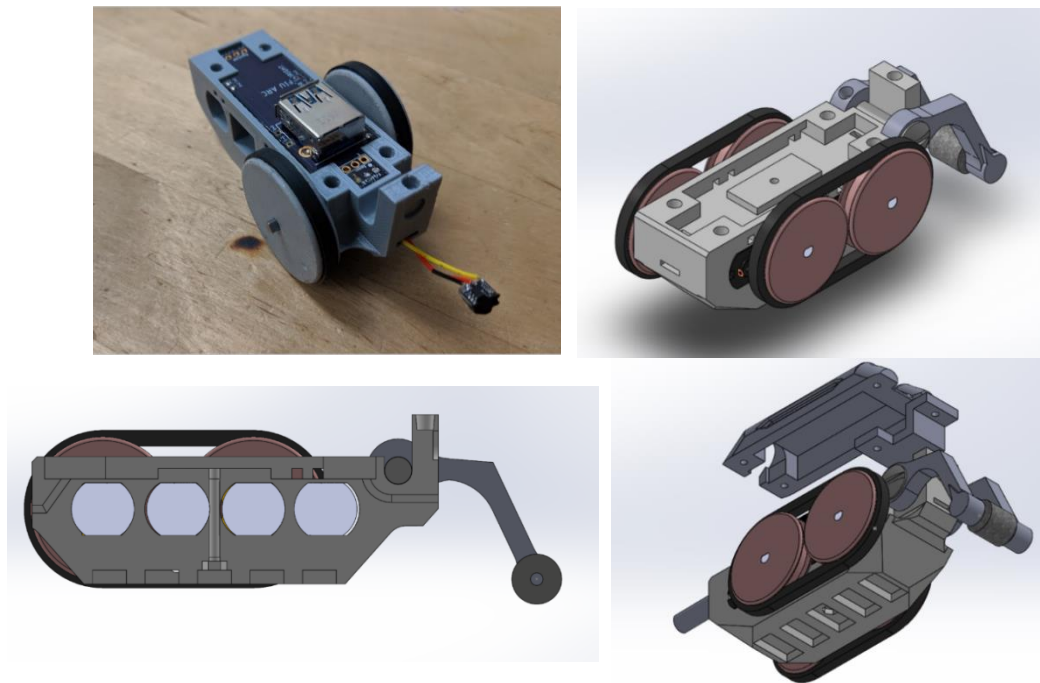
Although this design successfully navigated over the seams, it struggled over more discrete seams. An alteration was made to the design that utilizes a 120 degree angle instead of the previous 90 degree angle of the arm. In addition, the geometry of the bottom of the rover was also adjusted to eliminate contact points that could interfere with the unit’s traction force.





**Figure 13. Assembly of adjusted arms.**

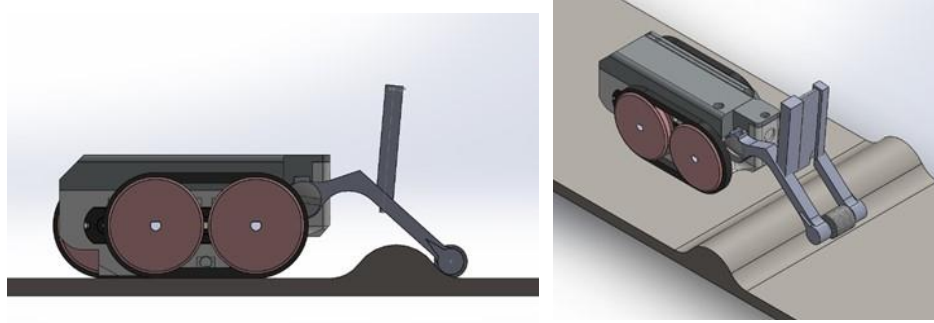
In preparation for testing of the miniature rover for the full-scale mock-up test, a few minor modifications were made. This included a dedicated holder and cable channels for the LEDs and camera. While testing the unit’s ability to traverse weld seams, it was observed that the unit would slightly yaw as it traversed over the seam since one track would reach the seam before the other. To account for this, a free rotating wheel was added to provide the stability needed. Some of these modifications are shown in the figures below.



**Figure 14. Modified design of the magnetic arm mini rover.**

In addition, to improve the quality of the video for monocular visual odometry and autonomous control, a new light and camera module was designed to raise the height of the camera and light. This module fits on top of the magnetic arm and is shown in the figure below.



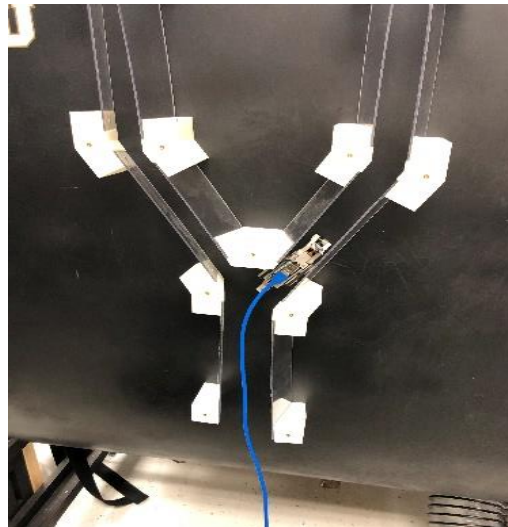


**Figure 15. New design for camera and light of the magnetic arm mini rover.**

Tests were conducted to validate the new magnetic arm design which included lighting tests and full scale mock-up testing. The new lighting approach provides significantly higher quality images as shown in the figures below.



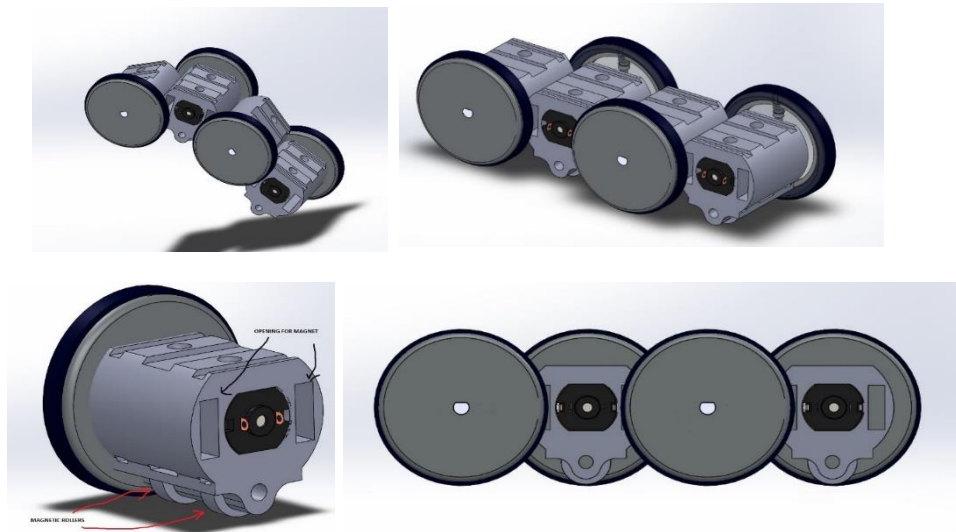
**Figure 16. Testing mini rover in the main mock-up.**



**Figure 17. Testing mini rover in our lab mock-up.**

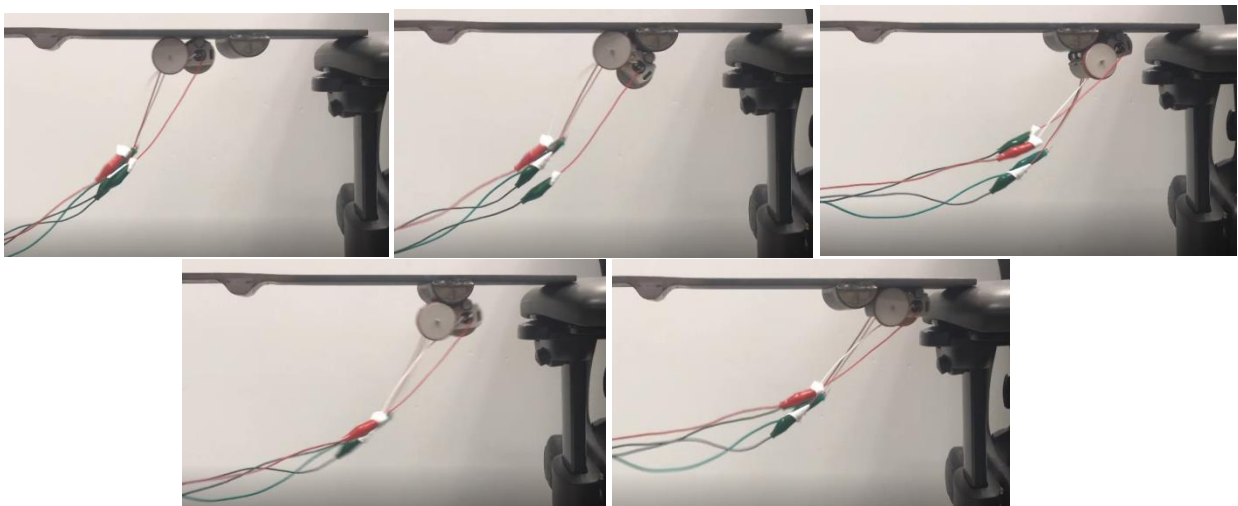
**Subtask 18.2.1: Caterpillar Rover**

To address challenges of inspecting the AY-101 primary liner, an alternate design is being developed for the rover to navigate around the 90 degree turns in the AY-101 refractory pad. The rover was split into separate sections, with each section housing a motor and a series of magnets. The segments are held together through a combination of stringers and magnets. Magnets are placed in the rectangular openings (referenced in the diagram below) in order to help maintain the natural, horizontal position between each motor segment. Magnetic rollers are used to maintain contact with the ferrous surface. The two holes on the top of each segment serve the purpose of securing a PCB and holding the motor in place. Each segment has a separate PCB, linked together using ribbon wire or flex PCB.



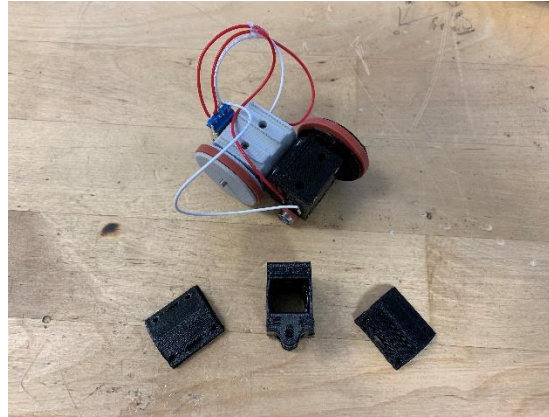
**Figure 18. Alternate rover design with the motor controls.**

This new design of the rover was subjected to initial testing shown below. This multi-segmented version can not only address the weld seam challenge, but it can also navigate through 90° turns.



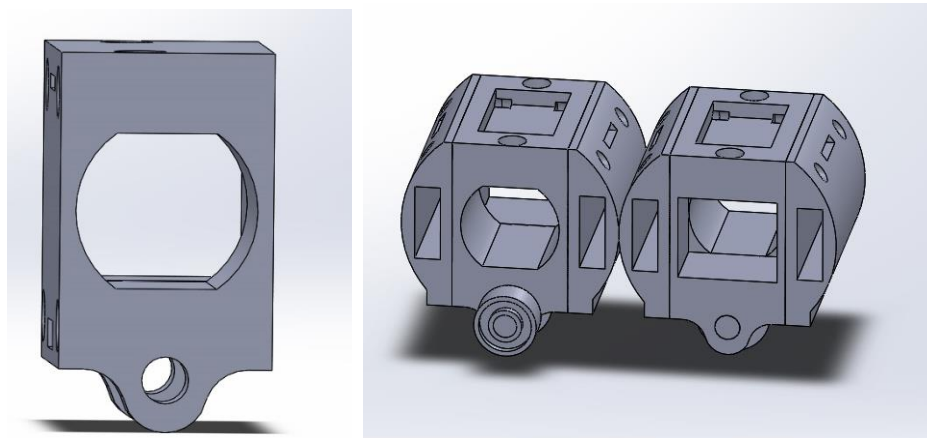
**Figure 19. Images showing rover traveling over 1.5” diameter weld seam.**

During this performance period, a number of design changes were made to the rover which included adjusting the separation between the motor in each segment and the surrounding magnets and modifying the wheel diameter. Bearings were also added opposite of the active wheels on each segment, which improves stability to each individual segment. Finally, the motor housing was reduced into 3 separate segments, allowing for further customization of the sensor placement. After these modifications, the unit was able to successfully traverse over weld seams up to a diameter of 1.5 inches (height of 0.75 inch).



**Figure 20. Modifiable segments allow sensors mounted to PCBs to be placed according to inspection needs.**

A ribbon cable connector was used when connecting the caterpillar segments together to improve the flexibility of the design. The rear segment has a detachable port to connect the rear facing camera and allow for easy maintenance. The overall design was slightly altered in order to ensure there is minimal interference from the magnets.



**Figure 21. Modified caterpillar design.**

In addition to the design changes, a new PCB board was developed for the caterpillar rover. Each segment will have its own PCB board which will be connected to the DC motor and also adjacent segments. The last segment will carry the USB connection in addition to former connections.

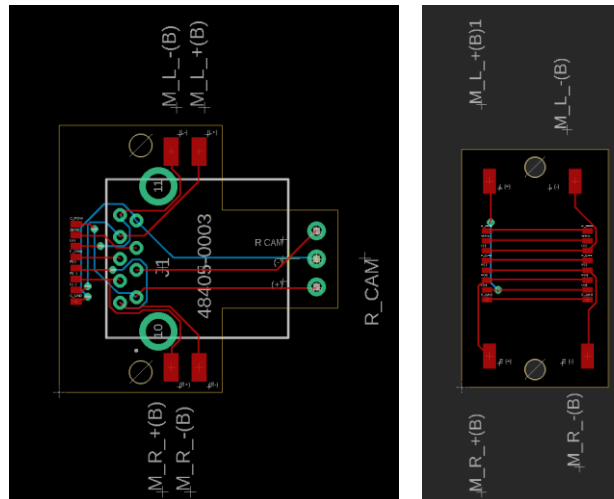


Figure 22. PCBs to be placed according to inspection needs.

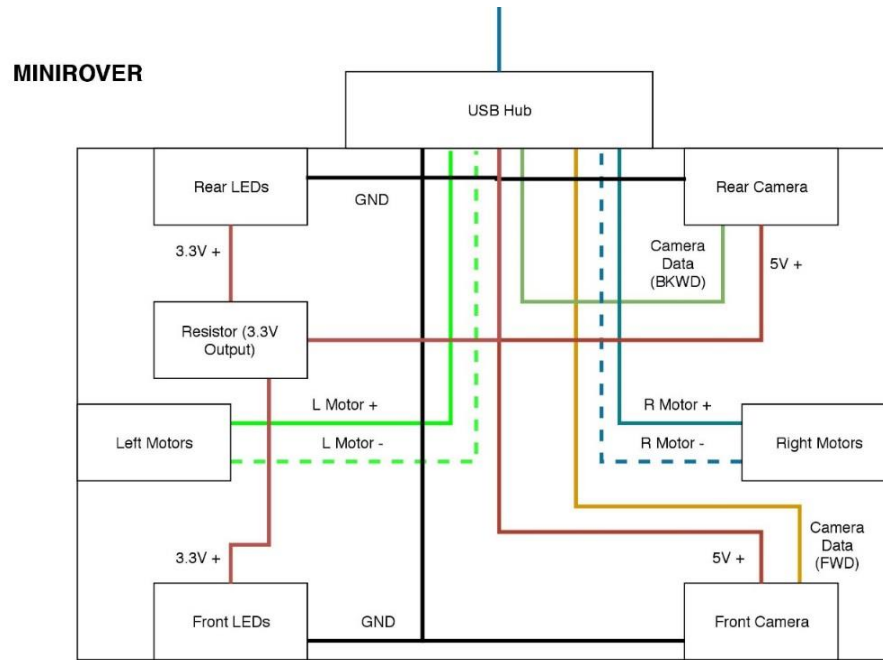
### Subtask 18.2.1: Capsule Controller

The capsule controller is a component that houses electronics for the rover and would sit within the annulus of the tank during operation. The capsule is being developed to address multiple needs for deployment:

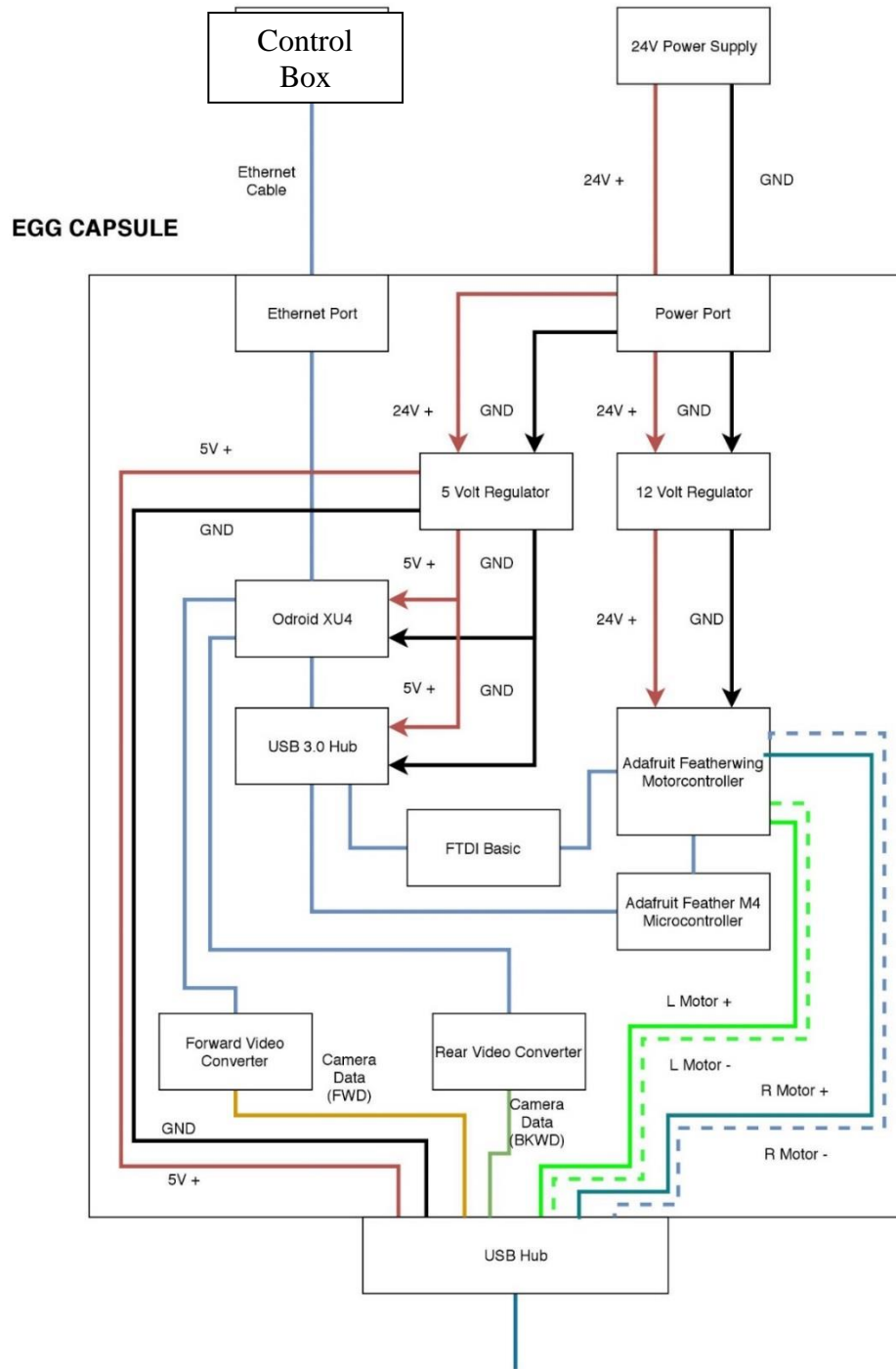
- 1.) The motors of the unit require 12 V for operation, while the cameras, LEDs, Odroid XU4, and USB hubs operate from 3.3-5V. A 150 ft cable carries a significant voltage drop due to the length of the cable. To remedy this, the cable will be split into two sections. A 100 ft cable will run from the control box to the capsule, and a 50 ft cable will run from the capsule to the rover. Higher voltage will be applied from the control box and will run down the 100 ft cable, which will then step down through voltage regulators located inside of the capsule (step down to 12 V and 5 V). The 50 ft cable will carry these voltages to the components onboard the rover.
- 2.) The cameras (at both the front and rear of the unit) transmit analog data. This poses a similar challenge to the voltage drop, as the signal is not able to carry from the unit to the exterior control box across a 150 ft cable. To solve this, the capsule will contain analog to digital converters. The 100 ft cable connected from the capsule to the control box will be Ethernet, which will allow the digital data to travel successfully to the control box.

Schematics of the controls are shown for both the mini rover and the control capsule in the figures below.



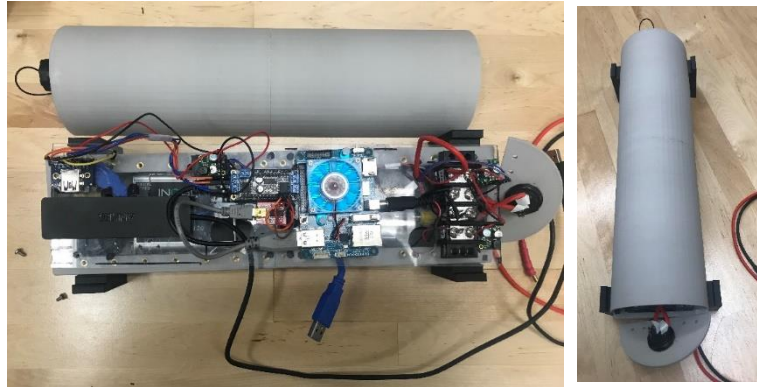


**Figure 23. Schematic of the control for mini rover.**



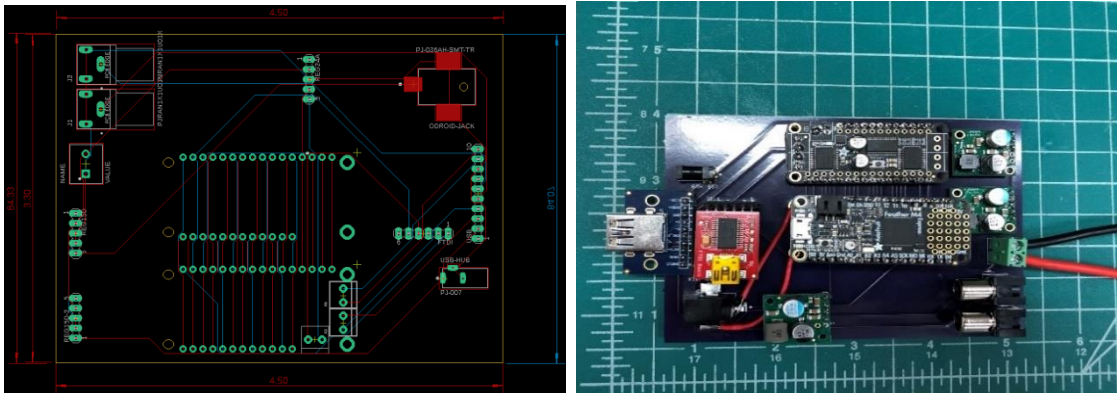
**Figure 24. Schematic of the control for the capsule.**

In addition to the design of the controls architecture, an initial control bench testbed was manufactured. This was developed to shorten the time it takes to evaluate new units. This testbed does not require the assembly of a full PCB, allowing the motors to be directly wired into a motor controller. The dynamics/maneuverability of new units can then be evaluated rapidly.

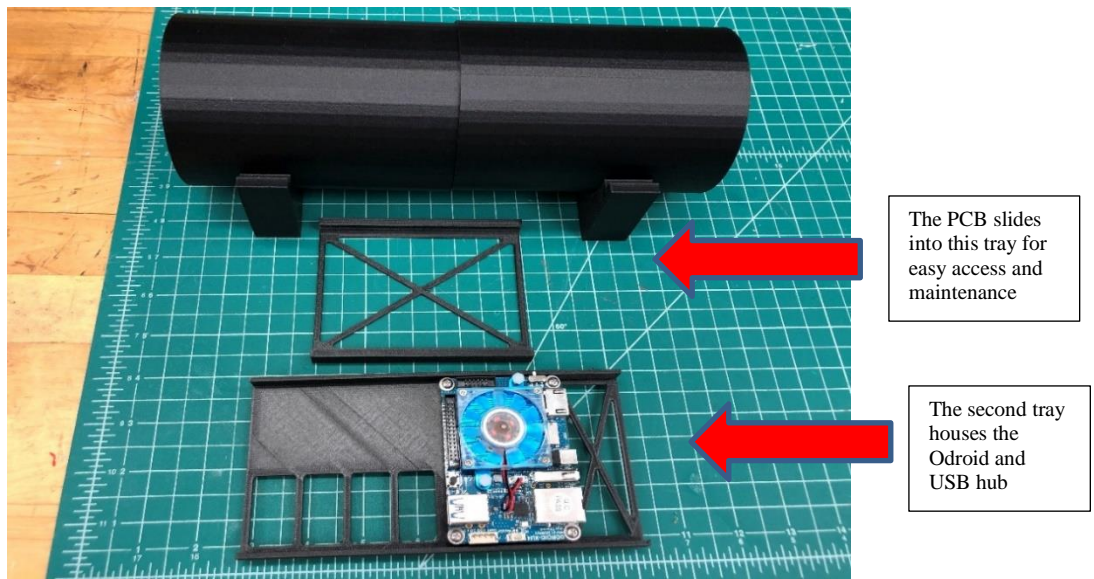


**Figure 25. The initial bench testbed for the controller.**

After the initial evaluation of the control system, a final version of the capsule controller was designed and developed. The new design incorporated a PCB that eliminates all wires and a two-tray design provides easy access for troubleshooting and maintenance. This design is shown in figures below.



**Figure 26. New board design for controller.**



**Figure 27. New design for the capsule.**

The new controller was successfully tested for real time video and control. The final assembly of the capsule is shown in the figure below.

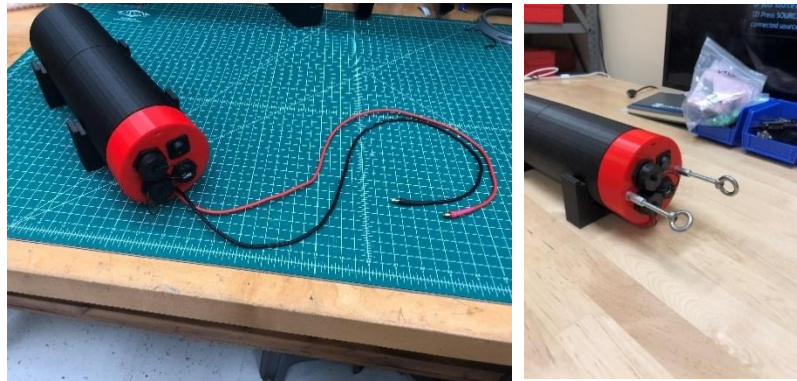


Figure 28. New design for the capsule.

**Subtask 18.2.1: UT Sensor Module**

To improve the functionality of the rover, an additional module is being developed to house a UT sensor that can obtain thickness measurements of the liner. Renderings of the initial design concepts are shown in the figure below. Significant considerations include UT contact force required to obtain quality measurements and surface preparation required.

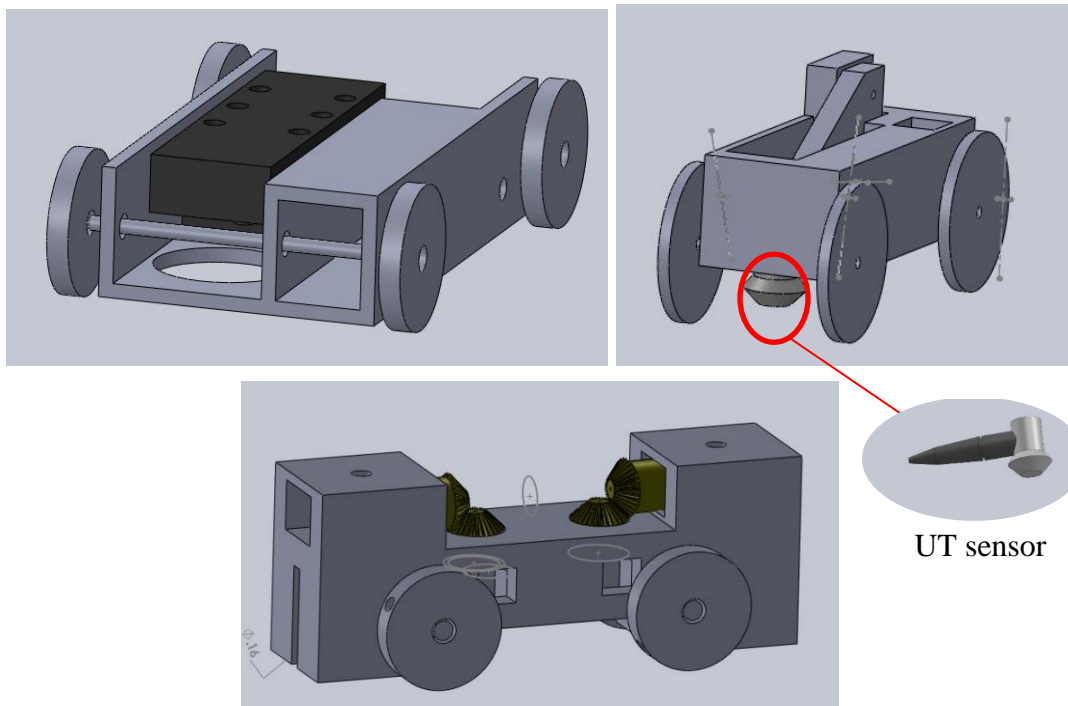
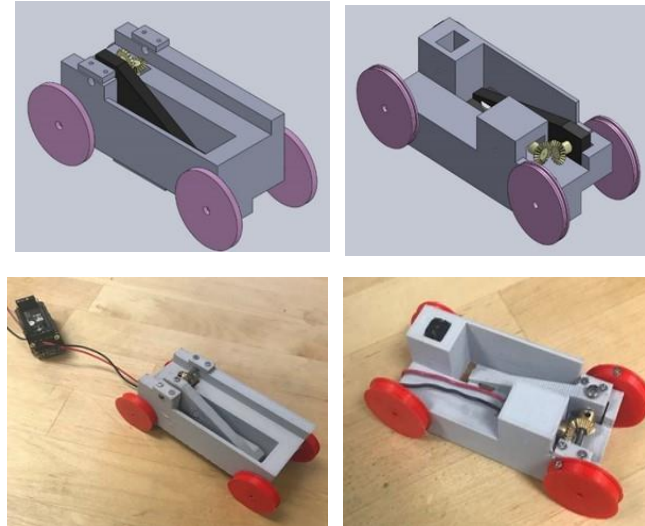


Figure 29. Secondary unit designs that include a UT sensor.

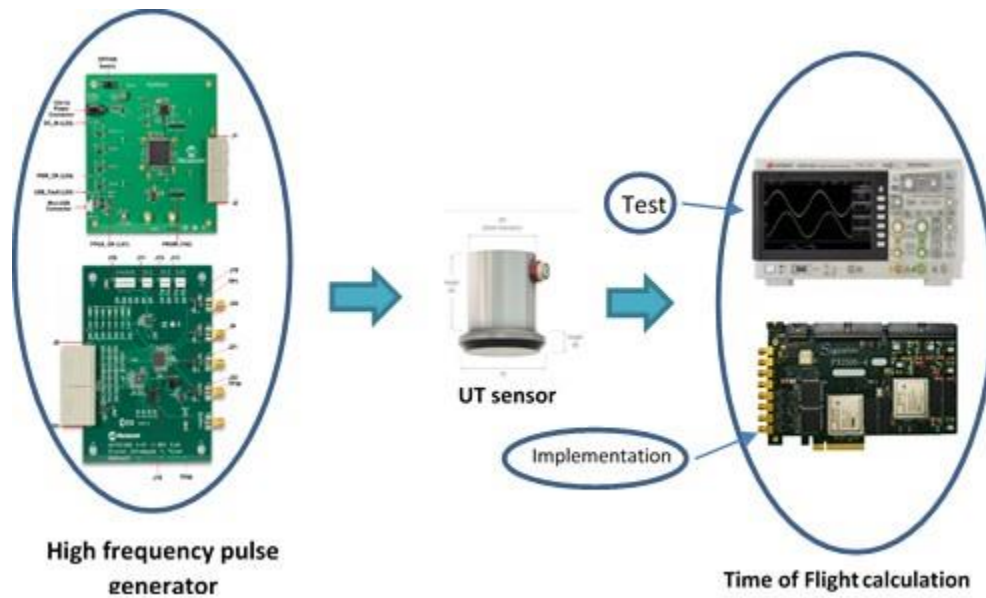
Simple prototypes of the designs were 3D printed and assembled in order to evaluate the UT sensor deployment operation. Each design consists of a rotating arm that will position the UT sensor on the intended surface.





**Figure 30. Secondary unit designs in order to include a UT sensor.**

In addition, the designs of the signal processing board of the UT sensor were evaluated. The evaluation utilized a high frequency pulse generator, an Ultrasound TX Pulsar Evaluation Board and a Microchip Ultrasound Platform Board (MUPB001). These components will be utilized to generate a high frequency pulse to actuate the UT sensor. An oscilloscope with a minimum 500MHz BW and two high-impedance probes will be used for the calculation of the time of flight. In the future, we plan to use an FPGA board for this function.



**Figure 31. UT sensor deployment process.**

**Subtask 18.2.1: Conclusions and Future Work**

A modified version of the magnetic arm rover was developed and created. This version improved the ability of the rover to traverse weld seams of varying heights located on the primary liner. A new hood for the mini-rover was also designed that allows for the attachment of a spring

mechanism to the top of the rover and provides a secure means for the retrieval of the inspection tool in case of failure.

An additional design for a rover was developed to navigate in the refractory slots of AY-101. The rover is split into separate sections, each housing a motor and a series of magnets. The segments are held together through a combination of stringers and magnets. This multi-segmented version can navigate over weld seams as well as around 90° turns. This design resembles the body of a caterpillar and thus has been named the caterpillar rover.

In addition, an initial version of a controller module was developed. The module was designed to address the problem of significant voltage drop and poor video signal transmission due to the length of the cable. The module houses an Odroid XU4, an Adafruit Featherwing motor controller, an Adafruit Feather M4 microcontroller, a 5V voltage regulator, a 12V voltage regulator, and 2 analog to digital video converters. The controller was successfully tested for real time video and mini rover control.

Preliminary concepts for a secondary unit of the miniature rover were also investigated. The secondary unit will be attached to the primary unit and carry/deploy the UT sensor mechanism. Simple prototypes of the designs were 3D printed and assembled in order to evaluate the UT sensor deployment operation. Each design consists of a rotating arm that will position the UT sensor on the intended surface.

Future work includes preparing for the deployment of the mini inspection tool into the DST refractory slots at the Hanford. This will require additional testing in terms of functionality and durability in our full-scale sectional mock-up of the DSTs. Research efforts will also be focused on development of the UT sensor module and caterpillar rover.

## **Subtask 18.2.4: 6-Inch Crawler Testing and Design Modifications**

---

### **Subtask 18.2.4: Proposed Inspection**

Recent concerns about the structural integrity of the containment liner of DSTs has prompted FIU to continue developing a specialized tool, in coordination with WRPS engineers, to inspect for potential thinning of the secondary liners under the refractory pads. The development of the inspection tool is a three-year effort with the first year focusing on surveying and conceptualization of the design. In the second year (current year), FIU has been designing, building and testing a functional prototype. The last year will focus on full-scale testing, hardening and necessary deployment arrangements and customizations.

The only access to the secondary liner under the tank refractory is through the leak detection systems in the foundation of the DSTs. Figure 32 shows 4 different configurations for the leak detection systems with all having a DN 150 (NPS 6) drain pipeline providing access to the drains slots under the tank. Figure 33 illustrates a typical configuration of the drain slots in the foundation of the Hanford's DSTs. The system consists of a maze of channels about 115 mm (4.5 inches) with 65 mm (2.5 inches) high. Most of the configurations use an entry manifold that slopes up from the drain pipeline to the plenum at the middle of the tank.

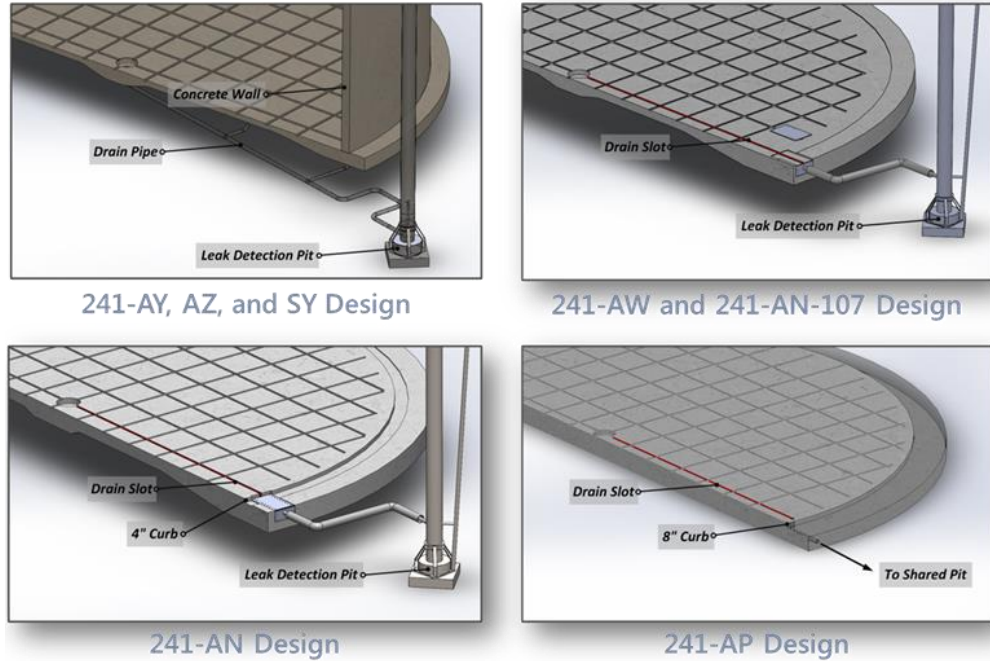


Figure 32. Leak detection systems at Hanford’ DSTs.

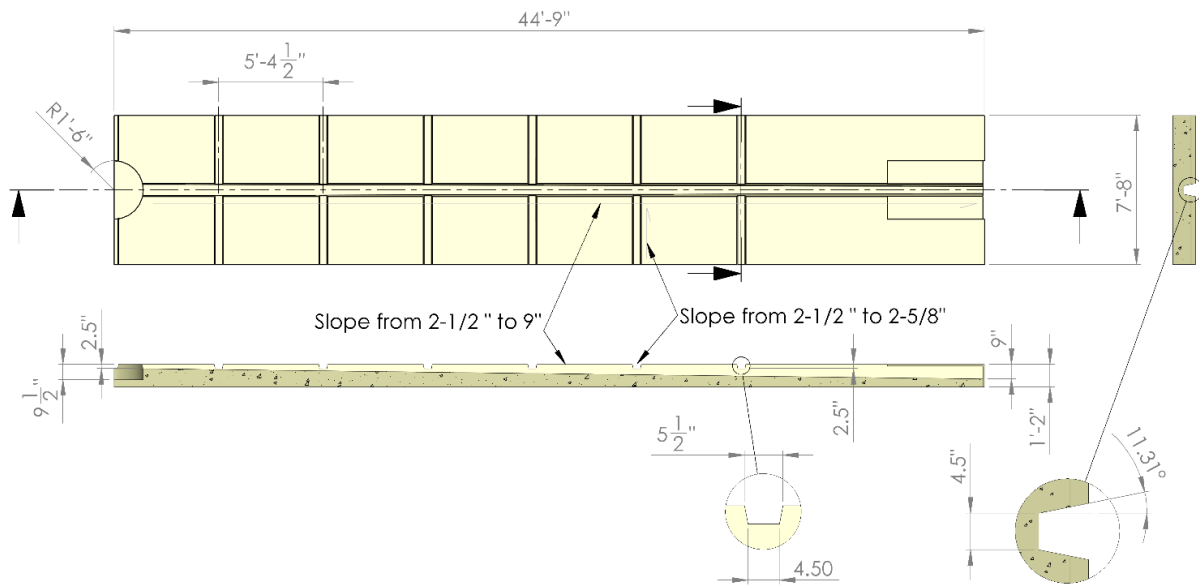
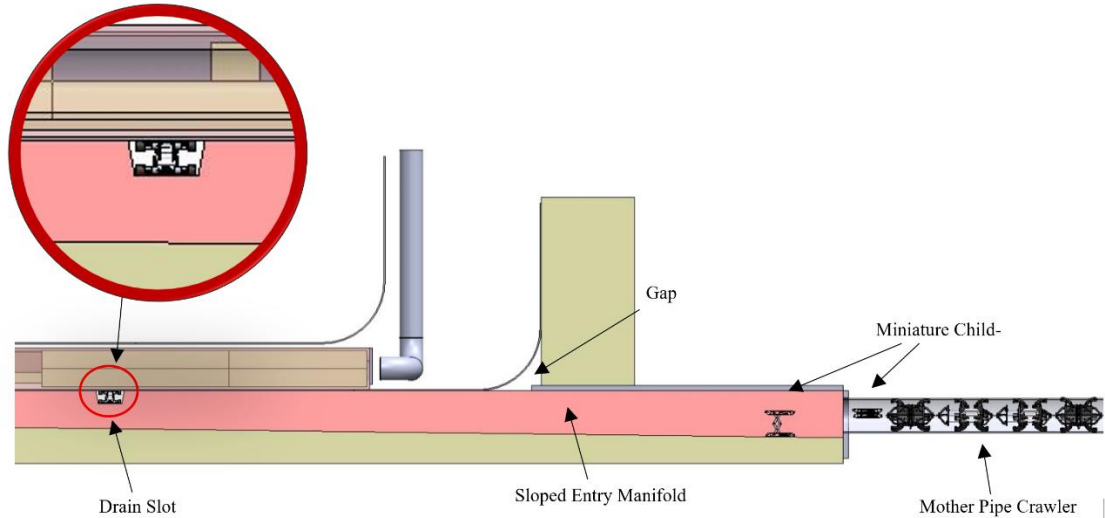


Figure 33. Typical DST’s drain slots foundation.

*Marsupial crawler for secondary liner inspection*

The tool FIU has been developing is a robotic marsupial system that uses a mother pipe crawler to navigate through the ND 150 (6”) drain pipeline and deploys a miniature child-rover into the drain slots. Figure 34 shows a rendering of the conceptual design and approach.



**Figure 34. FIU’s inspection system.**

The mother pipe crawler has multiple functions including:

- 1) traversing the entry drain pipeline,
- 2) deploying the miniature child-rover,
- 3) managing the tethers of both units, and
- 4) rescuing the miniature tool in case of failure.

The crawler operates using pneumatic actuators on the same peristaltic principles of other inspection tools previously developed at FIU [1-3]. This configuration provides a high payload to weight ratio, and should be suitable for tough environments found in the existing DST’s drain pipeline, as shown in Figure 35, and experienced in previous inspections attempted by WRPS. Previous efforts at the site have fallen short of reaching the central plenum due to debris and mud within the pipeline.



**Figure 35. Existing condition of DST’s drain lines (WRPS).**

The current system includes two gripper modules and extender modules. Figure 36 shows a functional prototype that only includes one extender module. The primary difference between this crawler and previous systems is that it can traverse through 6-inch pipes and the grippers use actuation elements that are aligned perpendicular to the axis. The final design will include a new front module housing that will carry, deploy and provide support to the miniature child-rover



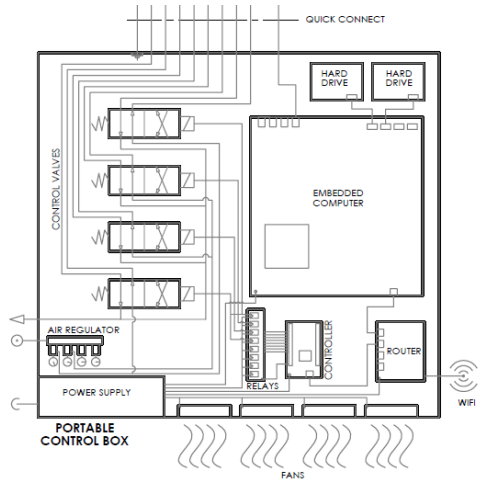
when the crawler reaches the foundation.



**Figure 36. Mother pipe crawler prototype.**

The current system uses a retrofitted portable control box from a previous pipe crawler. As illustrated on Figure 37, the design is self-contained and the front panels provide:

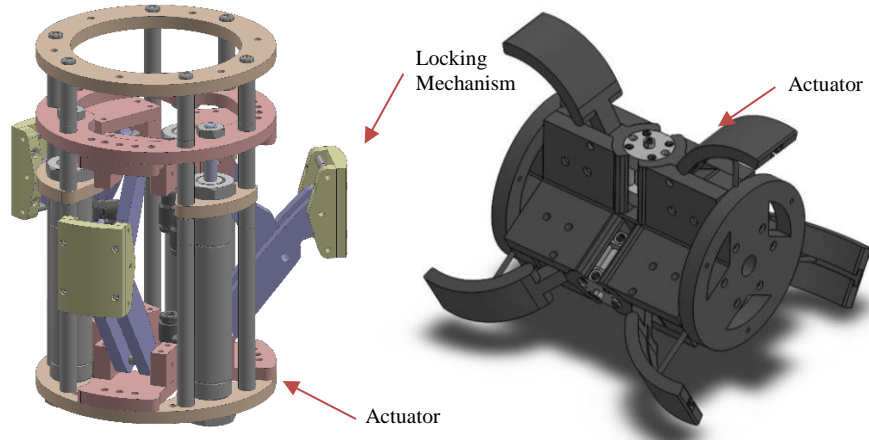
- a) quick disconnect for all pneumatic and electric lines,
- b) pressure control,
- c) pressure gauge (for troubleshooting),
- d) internet and USB access, and
- e) a touch screen interface.



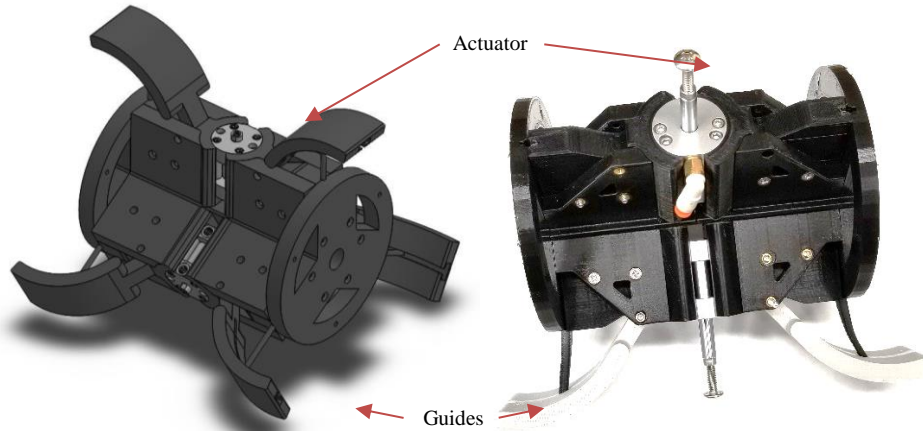
**Figure 37. Pneumatic crawlers control box.**

The major control box retrofit includes implementing the Robot Operating System (ROS) to the system. The improvement provides a common communication infrastructure allowing better integration with other systems, and also taking advantage of robust algorithms already developed by the vibrant community behind ROS’ collaborative research environment.

The grippers have been redesigned to incorporate less moving parts as illustrated in Figure 38. The new streamlined design takes advantage of the module large diameter (about 5”) and replaces the original locking mechanism with radially distributed pneumatic actuators acting directly to the pipe surface. A functional prototype of the redesigned grippers is as shown in Figure 39.



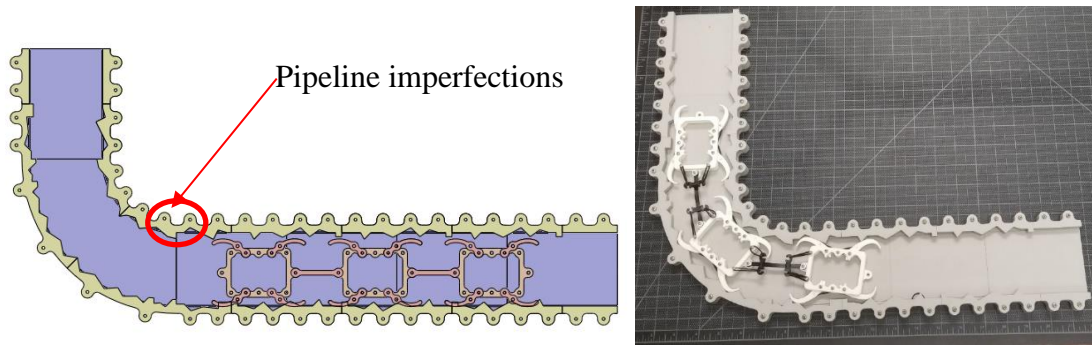
**Figure 38. Original (left) and redesigned (right) gripper.**



**Figure 39. Redesigned gripper model (left) and prototype (right).**

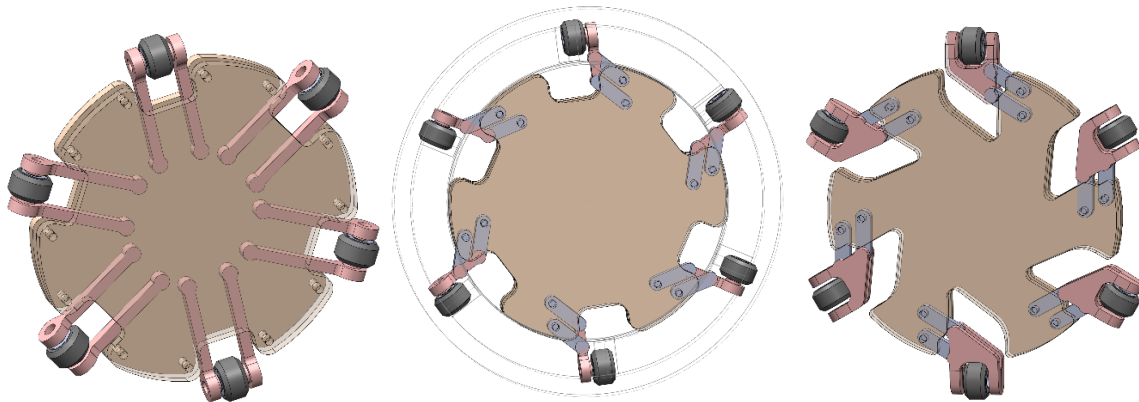
Each module in the crawler uses spring loaded guides that assist in passing through pipes with significant scaling and potential obstacles, such as defects, buildups and pipe sediments. The guides also minimize the unit drag and the bulldozer effect, where debris is collected in front of the camera during the crawling.

Figure 40 shows simplified two-dimensional cross-section tests that were used to optimize the curvature of the guides in each module and improve efficiency while minimizing potential sediment accumulation.



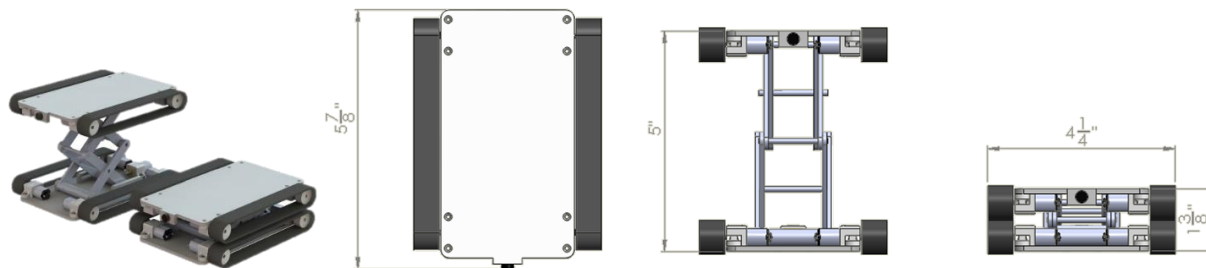
**Figure 40. Pipe cross-section mockup conceptual design.**

Other alternative guide mechanisms similar to the traditional suspension system are being investigated. Sample designs are illustrated in Figure 41. The use of radial springs and wheels has the potential to minimize friction to better handle the potential obstacles. However, they add extra complexity to the system.



**Figure 41. Alternative guide designs.**

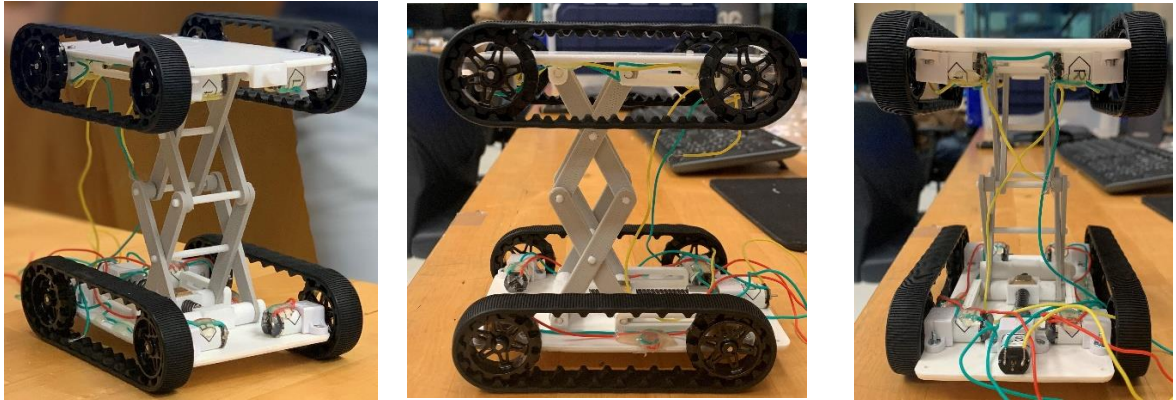
The miniature child rover, shown in **Error! Reference source not found.**, is a modified version of the magnetic mini-rover developed to inspect the primary liner tank floor. The primary modification includes a scissor lift mechanism that allows the tool to travel at the bottom of the central slot and extend to magnetically attach to the bottom of the secondary liner. This approach is taken to provide a means to pass the gap in the cover of the drain line shown in **Error! Reference source not found.**



**Figure 42. Miniature child-rover conceptual design.**

Figure 43 show images of our first working prototype. The unit's larger size allows the design to be enhanced with surrounding cameras, wheel encoders, an inertial measurement unit and other

advanced sensors such as radiation, ultra-sound, LiDAR and surface camera. The integration will take advantage of the sensors and software framework being developed for other tasks at FIU.



**Figure 43. Child inspection tool prototype.**

Current efforts include designing of front module housing and engineering cable management strategies for tether handling and retrieval of the miniature inspection tool during secondary liner inspections. Evaluating strategies for automatic collapsing the scour-lift mechanism in case of retrieval and power loss will be considered.

**Subtask 18.2.4: Testing**

Several bench-scale tests have been conducted to evaluate the system performance and durability, including successful runs of the mother pipe crawler through pipelines with multiple fittings, as illustrated in Figure 45. The crawler is capable of pulling up to 445 N (100 lbs) before it stalls. The team plans to run additional testing considering mud deposit in the pipeline.



**Figure 44. Preliminary maneuverability tests.**

After the integration of the child rover with the parent crawler, the system will be tested in the mockup of the DSTs at FIU. Figure 45 shows the 8 ft. wide sectional mock-up with the drain slots in the foundation.





Figure 45. The full-scale mockup foundation.

#### Subtask 18.2.4: Conclusions and Future Work

The design of the marsupial system to assist in the inspection of the secondary liners in DSTs at Hanford will continue to focus on enhancing the design, new prototype development and conducting bench and full scale testing. Efforts will mainly be concentrated on several aspects as described next.

The mother pipe crawler will be streamlined per need. The child rover design will be finalized and the control and sensor systems will be integrated with the final design. A front module housing will be designed, prototyped to attach to the crawler. Finally, the child rover will be integrated to the mother pipe crawler system. Additional work will include engineering a cable management strategy for tether handling and retrieval of the miniature inspection tool. Finally, exhaustive full-scale tests will be conducted at the FIU mock up to verify and validate the complete crawler system.

#### Subtask 18.2.4: References

1. M. DiBono, et. al., "Engineering Scale Testing of Robotic Inspection Tools for Double Shell Tanks at Hanford," in *Proceedings of the Waste Management Symposia*, Phoenix, AZ, 2018.
2. A. Abrahao, et al., "Development of Inspection Tools for the AY-102 Double-Shell Tank at the Hanford DOE Site," in *Proceedings of the Waste Management Symposia*, Phoenix, AZ, 2016.
3. A. Abrahao, et al., "Development of Robotic Crawlers for Inspection of Radioactive Waste Tanks and Transfer Lines," in *Proceedings of the Waste Management Symposia*, Phoenix, Arizona, 2019.
4. A. Abrahao, et al., "Development and Testing of Robotic Inspection Tools for the High-Level Waste Double Shell Tanks at Hanford," in *Proceedings of the Waste Management Symposia*, Phoenix, 2017.
5. L. Lagos, "Chemical Process Alternatives for Radioactive Waste," Florida International Univeristy, Miami, 2016.
6. T. Pribanic, et. al., "Design Optimization of Innovative High-Level Waste Pipeline Unplugging Technologies," in *Proceedings of the Waste Management Symposia*,

Phoenix, 2013.

## **Subtask 18.3: Evaluation of Coatings for the H-Canyon Exhaust Tunnel (NEW)**

---

### **Subtask 18.3: Introduction**

H-canyon is the only remaining chemical processing facility in America capable of reprocessing plutonium, highly-enriched uranium and other radioactive materials [1]. The exhaust air flow from the H-canyon chemical processing areas and HB-line are transported through the H-Canyon Exhaust (HCAEX) tunnel, where radioactive contamination is removed. Structural integrity and visual inspections of the HCAEX tunnel have revealed severe and ongoing degradation of the reinforced concrete structure [1-2], which could compromise the mechanical strength of the structure. The ability of the HCAEX tunnel to withstand a design basis earthquake is uncertain so the search for solutions to mitigate and prevent further degradation is necessary.

The application of coatings and/or repair materials on the degraded concrete surfaces could be an option to mitigate and prevent further degradation, increasing the service life and improving the safety of the tunnel. The selection of repair materials is a key step in any repair action. Several aspects need to be carefully analyzed including: 1) knowledge of the root problem, 2) the degradation state of the concrete surface that will be repaired, 3) the aggressiveness of the environment, 4) the remaining service life of the concrete structure, and 5) associated costs [3]. There are a number of coatings and repair materials available on the market [4-9], but not all of them are adequate for the aggressive and challenging environment of the HCAEX tunnel.

For this effort, we divided the investigation in two phases: 1) Development and evaluation of aged concrete under accelerated aging conditions (preliminary results included in this report) and, 2) Evaluation of potential repair materials applied on aged and non-aged concrete under simulated aggressive conditions. During the last year, work was conducted on tasks related to phase 1, including a literature review and the beginning of bench-scale testing for concrete aging. The literature review included aspects such as 1) the current conditions of the HCAEX tunnel, 2) concrete degradation mechanisms in aggressive environments, and 3) concrete repair options to prevent further degradation. This will support further selection of potential coatings and/or repair materials to be evaluated (phase 2). Also, test methods and measurements to evaluate the performance of protected vs non-protected concrete under aggressive conditions were reviewed. This literature review constituted the first objective of the investigation. From the literature review findings, a preliminary bench-scale test plan for concrete aging was proposed by the FIU-ARC team consisting of accelerated tests in simulated aggressive conditions (acid solutions). The idea was to develop aged concrete surfaces, similar to the degraded HCAEX tunnel walls after 60 years of operation, which would serve as the substrate for the evaluation of selected coatings and repair materials. Hence, conducting preliminary bench-scale tests for the concrete aging under aggressive and accelerated conditions was the second objective of this investigation.

Research findings of the bench-scale testing, as well as the lessons learned during this period have supported the ongoing investigation. Recently, FIU prepared the first batch of concrete

samples using a mix design believed to have been used in the construction of the tunnel. The same proportions and raw materials (as similar as possible) were used for preparing the concrete in order to increase the reliability of the results. Also, a new test setup for the concrete aging, where only one face of the samples is exposed (similar to the tunnel), is being developed. This is in addition to the old setup (full immersion) that simulates a worst scenario inside the tunnel.

### **Subtask 18.3: Objectives**

The identification and evaluation of potential repair materials to mitigate and prevent further degradation of the concrete walls of the HCAEX tunnel is the main objective of this subtask. On that note, the FIU-ARC team has been working and continue to work very closely with the Savannah River Site's engineering team in order to meet the objective. The first stage of the investigation is to develop and evaluate aged concrete specimens under accelerated aging conditions (preliminary results included in this report) that will be later used (second stage) as the substrate for evaluating potential repair materials.

In this year-end report two objectives were proposed related to this subtask, 1) to do a literature review of relevant aspects related to the H-Canyon study (characterization and extent of the damage, identify concrete degradation mechanisms, preselect potential repair materials for degraded concrete, aging tests in aggressive environments, etc.), and 2) to perform initial aging tests of concrete specimens (primarily in acidic conditions). These two objectives will support the ongoing investigation (concrete aging phase).

### **Subtask 18.3.2: Bench-scale testing for the SRS H-Canyon (NEW)**

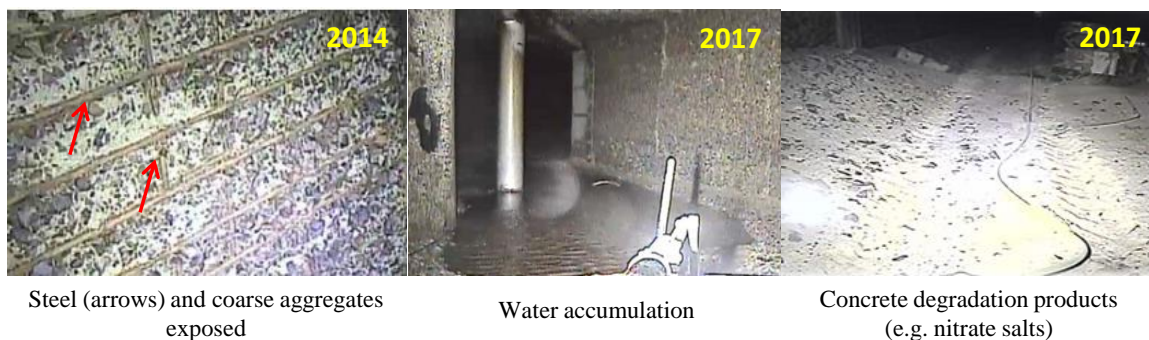
---

#### **Subtask 18.3.2: Literature Review**

In this section, a summary of the literature review of the H-Canyon study is presented below. For the development of this task, important information from the Savannah River Site personnel and documentation has been obtained. Additional information has been obtained from technical journal papers, reports, patents and standards.

#### *H-Canyon exhaust (HCAEX) tunnel background*

The HCAEX tunnel ventilation system mitigates the release of radioactive materials by pulling exhaust air from the H-Canyon chemical processing areas and the HB-line through the sand filter, where radioactive materials are removed [10]. Reinforced concrete was the material used for the construction of the tunnel, which was originally covered with a protective liner. The HCAEX tunnel has been visually inspected over the years by means of pole cameras and robotic crawlers, demonstrating the ongoing degradation of the concrete tunnel walls. Figure 46 shows images of the degradation observed of the tunnel interior walls at different times. The extent of the concrete tunnel degradation was characterized by: 1) exposure of steel rebar (large areas), 2) eroded surfaces exposing coarse aggregates (generalized), 3) formation of concrete degradation compounds (e.g. nitrates and carbonates) accumulated on the tunnel floor, and 4) water accumulation at some locations. Also, at multiple locations of the tunnel, the degradation is so severe that the two layers of steel rebar (vertical and horizontal) were completely exposed, indicating that more than 2 in. of concrete were lost [10].



**Figure 46. Images of HCAEX tunnel degradation [2], [11].**

A recent study reported the characterization results of concrete cores exposed to the aggressive environment of the HCAEX tunnel [11]. The concrete cores depicted a distinct transition between the affected areas (~ 2-3 in from the portion closest to the tunnel environment) and unaffected areas (inner zone), that could have a negative effect on the facility structural strength. Chemical and petrographic analysis of the concrete cores at different depths demonstrated the presence of high concentration of nitrate ions (up to 3000 ppm) up to 1.5 in from the exposed surface, as well as portlandite being replaced by calcium carbonate, and leaching of calcium from the concrete to the exposed surface. All of these findings are a consequence of acid attack and carbonation [2].

The degradation observed is due to the combined action of physical, chemical and mechanical factors like nitric acid fumes, radioactive materials (up to 10 mSv), strong winds (~30mph) with debris, moderate temperatures (up to 105°F) and high relative humidity (RH) (80-90%), which characterizes the HCAEX tunnel aggressive environment.

#### *Degradation mechanisms of reinforced concrete*

The initial high alkalinity (pH >12.5) of the concrete protects the steel rebar embedded in it due to the formation of a protective passive layer (iron corrosion products). The entry of water, oxygen, and other chemicals through the concrete pores, with time will lead to alkalinity reduction (pH < 9) and at some point will promote the steel depassivation. Consequently, steel corrosion will take place. The iron corrosion products formed increase the volume of the steel around 3 to 10 times, promoting the formation of cracks, etc. and reducing the material durability [12].

The alkaline nature (high pH) of the concrete makes it vulnerable to the action of acids leading to chemical degradation processes (e.g., acid attack and carbonation) through acid-base reactions. In an acid attack, the acidic solution reacts with the concrete alkaline compounds (calcium hydroxide and some hydration products (C-S-H)), causing their decomposition with the consequent formation of salts and water. This chemical reaction will lead to a deterioration of the mechanical strength and durability of the concrete [12]. The resistance of the cement matrix to acid corrosion depends primarily on its pore structure characteristics (related to the permeability), the ability of the matrix components to neutralize acids (alkalinity) and also on the solubility of the salts formed during the degradation process (chemical reaction). The main reaction (1) for the nitric acid attack on concrete is represented below. This is an acid-base reaction where calcium nitrate ( $\text{Ca}(\text{NO}_3)_2$ ) and water is formed. Nitrate salts are very soluble due to the strong chemical character of the nitrate ( $\text{NO}_3$ )<sup>2-</sup> cation coming from the acid, leading to a

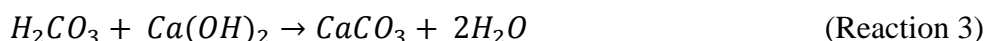


fast disintegration of the concrete (decalcification) and significantly reducing its alkalinity (pH). The type of acid (strong or weak), its concentration, and the contact time with the concrete are key factors that affect the intensity of the attack [12].



Pavlík compared the corrosion depth of hardened cement paste exposed to different acidic solutions (nitric, hydrochloric, sulfuric, acetic and formic) over time. A nitric acid solution promoted the highest corrosion depth (~ 10 mm) after 100 days of immersion, due to the greater solubility of nitrate salts [12].

However, carbon dioxide promotes concrete carbonation, with the further disruption of the steel passive layer and corrosion initiation. First, carbon dioxide in the presence of water lead to the formation of carbonic acid (reaction 2), followed by an acid-base reaction (reaction 3), degrading the concrete matrix by the formation of calcium carbonate salts (CaCO<sub>3</sub>) and water [12].



The temperature of the environment affects the kinetics of chemical reactions and it can promote concrete stresses and the emergence of failures. Also, the moisture or water content of the concrete surface is critical to the rate of deterioration. For example, the carbonation reaction is faster when concrete is partially saturated, with RH values ranging from around 50-70% [12]. In addition, the water acts as a solvent and a means of transport for aggressive agents (e.g. acids) and corrosion products formed (e.g. nitrates and carbonates) through the concrete pores.

The HCAEX tunnel environment, with a high relative humidity and high temperature, supports faster degradation [12]. Also, the action of strong winds of ~ 30 mph inside the tunnel, with debris and particles in suspension in the air flow, creates the ideal conditions to erode the concrete surface, leading to mass loss and dimension reduction of the tunnel walls [12]. The images taken during robotic inspections of the concrete tunnel provide evidence of these effects.

#### *Repair materials options for the HCAEX tunnel*

A preliminary selection of potential concrete protection methods was performed based on the literature review findings. A number of key factors in the selection process like cause and extent of the concrete degradation, the adverse environment of the tunnel, the availability in the market, the application method, etc. were considered [3]. Three primary methods for mitigating chemical attack on concrete have been reported, including: 1) optimizing the concrete mixture, 2) isolating the concrete from the aggressive agents, and 3) modifying the factors (e.g., temperature, composition). Of these, implementation of isolation materials (such as coatings and overlays) is the only viable alternative for the HCAEX tunnel case study.

Overlay materials have been proposed for concrete repair [13]; however, not all of them are suitable for the tunnel demands. Mineral admixtures-modified mortars, polymer-modified mortars and polymer mortars are overlay materials that could be used for the concrete tunnel repair (Table 1). Overlays are composed of ordinary Portland cement (OPC), fine aggregates, water and a modifying agent (polymers or mineral admixtures).

**Table 1. Overlay Material Characteristics [13]**

<b>Overlay Types</b>	<b>Composition</b>	<b>Properties</b>
<i>Mineral admixtures-modified mortar</i>	Cement mortar with mineral admixture (e.g. silica fume, fly ash, etc.)	Mineral admixtures increase bond strength and cohesiveness of the mortar, provide resistance to chemical attack, increase strength and reduce permeability.
<i>Polymer-modified mortar</i>	Cement mortar with a polymer modifier	Compared with cement mortar, has excellent bond strength and cohesiveness, reduced permeability, and improved resistance to chemical attack.
<i>Polymer mortars</i>	Polymer binder and fine aggregates	Compared with cement mortar, has high bond strength, low permeability and good chemical resistance.

The beneficial effects of replacing OPC with mineral admixtures such as silica-fume, fly ash, blast furnace slag, etc., to mitigate concrete acid attack have been investigated. The improved performance of modified mortars with silica-fume and fly ash admixtures to reduce acid attack have been related to a decrease in mortar alkalinity as well as pore refinement. The mineral admixtures also lead to the formation of a denser and improved microstructure, increasing concrete mechanical resistance and durability. Typical polymers used for overlays include styrene butadiene, epoxy, styrene acrylic, vinyl acetate-ethylene, etc. The type of polymer selected will determine the resulting properties and the expected service life of the repair material [13]. More information about polymers that are resistant to adverse environments is presented in literature.

Based on the thickness of the overlay material, they are classified as deep, shallow and thin and the method of application will consequently vary [13]. Given the fact that large areas of the tunnel have lost ~ 2 in of the concrete cover (steel exposed), only shallow (16 mm to 25.4 mm thick) and thin (< 16 mm to 25.4 mm thick) mortar overlays without coarse aggregates could be used. Shallow and thin overlays can be applied by shotcrete (spray), which is a viable application method for the tunnel conditions, where only robotic units have access. Manual applications (e.g. brush) are not desirable because it may take longer time (compared with spray methods) and it would require the presence of specialized personnel for the application, not feasible for the tunnel environment.

Coatings are a well-known protection method. Most coatings protect the surface by creating a physical barrier to restrain or slow down the entrance of water, oxygen, ions, chemicals (e.g., acids) and consequently, delaying the concrete deterioration processes [13]. Coatings, also known as surface sealers, can be classified as organic, inorganic or hybrid, depending on the composition (i.e., type of polymer or resin). Coatings can be grouped in terms of function as: 1) surface coating (traditional), 2) hydrophobic impregnation (inorganic), 3) pore blocking surface treatment (inorganic), and 4) multifunctional surface treatment [7]. The inorganic surface treatments are more stable and have better resistance to aging, but limited studies about their application have been published [7].

*Traditional organic coatings* include polymeric resins such as epoxy, acrylic, polyurethane, vinyl, etc. and have been widely used in the construction industry. They are usually applied as a coating system (primer, intermediate and top coats) to enhance the barrier effect and, consequently, the surface protection. Coating thickness can range from 0.1–0.6 mm (100–600 µm), depending on the type of coating and the demands of the environment. Typical coating failures are blistering, cracking, holes, and loss of adhesion [8].

*Polymer nanocomposite coatings* (multifunctional surface treatment) have advantages over traditional polymeric coatings. The addition of nanoparticles or nanocomposites has led to higher abrasion resistance, heat resistance, thermal stability and mechanical strength. Also, the addition of nanocomposites can improve the barrier protection [9]. However, few investigations have been dedicated to the study of their properties and their potential application in the concrete industry is still under investigation [7].

*Hydrophobic impregnation coatings* (inorganic) include silane, siloxane and a mixture of these two components. Its main function is to create a hydrophobic (water-repellent) surface, penetrating the concrete pores.

*Phosphate ceramic coatings* (inorganic) or phosphate cements are typically developed with an acid-base reaction between phosphoric acid or an acidic phosphate and basic oxide/hydroxide component, obtaining a product that replicates the properties of cement, a ceramic or both [14]. These products can be pumped and sprayed onto concrete surfaces, creating a rapid-setting protective layer with excellent chemical stability, compressive strength, impermeability, heat resistance and good aesthetical appearance. The thickness of the ceramic layer can range from 0.51 mm (~20 mils) to as thick as 50.8 mm (2 in.) [14]. Organic coatings (epoxy, acrylic, urethanes, polyester, etc.) can be applied on top of the ceramic material, providing additional protection such as water resistance, stain resistance, crack resistance, and durability [14].

#### *Performance of coatings and overlays*

Acrylic coatings offer good resistance to alkali, oxidation and weathering, but its bonding strength and ductility are relatively poor compared to epoxy resin. A recent study evaluated the resistance to acid attack (nitric, hydrochloric, etc.) of several materials including epoxy resin, acrylic painting, fly ash-based geopolymeric mortar, OPC concrete, etc. The epoxy coatings demonstrated the best performance against acid attack (no matter the type and concentration of the acid) over the rest of the tested materials. Novolacs are multifunctional epoxy resins with enhanced chemical and heat resistance [15].

The behavior of coated and uncoated mortar specimens immersed in 2.5% sulfuric acid was also evaluated. The epoxy and polyurethane coatings showed the best performance to acid attack over acrylic polymer and chlorinated rubber coatings. A significant variation in the performance of the same generic type coating provided from different manufacturers was observed. Hence, it is recommended that testing be performed with the same type of coating from different manufacturers prior to a final selection [15].

The effectiveness of different surface treatments applied on concrete to prevent microbial degradation was assessed by simulated chemical tests (0.5% sulfuric acid solution, followed by air blowing and surface brushing) and microbiological tests (with sulfur oxidizing bacteria). The polyurea lining (topcoat) combined with the epoxy primer, as well as the single epoxy primer, offered the best protection with no loss of coating integrity after testing. The cementitious

coating and the hydrous silicate solution treatment depicted significant degradation. Another investigation evaluated the resistance to biogenic acids for geothermal cooling tower basins (pH=2.59, T=40°C) of different epoxy-based coatings and polymer-modified mortars (with epoxy and styrene butadiene as polymers). The epoxy coatings exhibited the best performance as evaluated by visual inspection and bond strength and they were recommended for protecting concrete substrate against acid producing bacteria [15].

A summary of the findings on the performance of possible repair materials in aggressive environments are presented in Table 2. Also included in the table are some repair materials recommended by the American Concrete Institute to prevent nitric acid attack on concrete [16]. The characteristics of the repair materials presented in the table do not represent a single material, but a family. For example, “epoxy” refers to a family of coatings using different chemical combinations of that resin, leading to different performance. The materials performance was evaluated as excellent (E), good (G), moderate (M) and poor (P).

**Table 2. Characteristics of Potential Concrete Repair Materials for Aggressive Environments [15]**

Repair Materials	Resistance to				Application (Spray)	Availability
	Acids <sup>a</sup>	Water Permeability	High Temp.	Abrasion		
<i>Coatings</i>						
Epoxy	E , G	E, G	E <sup>c</sup> , G (40°C),	E	X	X
Polyurethane	G (e.g. polyol-cured)	G, E	-	E (aliphatic urethane)	X	X <sup>b</sup>
Vinyls and latex-based materials	SB > WB coatings	-	-	-	X	X
Polyester and Vinyl ester materials	E	-	E <sup>c</sup>	-	Only manual	X
Silane, siloxane and siliconates	-	E	-	-	X	X
Epoxy-siloxane (Hybrid Coating)	G	E	-	G	X	X
Polyurea lining	E	-	-	E	X	X
Phosphate Ceramic Coatings	E (chemical resistant)	E	E <sup>c</sup>	E	X	X
Crystalline pore blockers	P	M	-	-	X	X
<i>Overlays</i>						
Styrene butadiene-modified cement mortar	M	M	M (40°C)	-	-	X <sup>b</sup>
Epoxy-modified cement mortar	M	M	M (40°C)	-	-	X

a: organic, inorganic or biogenic acids, b: no brand name provided, c: only high temperature was mentioned in the reference  
 E: Excellent, G: Good, M: Moderate, P: Poor; Temp.: Temperature; Ref.: References; SB: solvent-based; WB: water-based; -: information not available.

### *Methods and measurements to evaluate concrete performance in aggressive environments*

A literature review of the available test methods and measurements for evaluating the performance of concrete and concrete repair materials against aggressive environments was conducted. A lack of standardized methods for studying acid attack was found in the consulted literature. Most of the studies reported acid-type immersion tests for evaluating the materials' resistance to acid attack. Other research works included the combined action of chemical (acid immersion) and physical (mechanical brushing) attack, leading to an enhanced/faster degradation of the tested materials. However, several measurements have been reported for assessing materials' performance against adverse conditions, with greater emphasis on the durability (visual inspection, mass loss, pH change, permeability, adhesion, etc.) and mechanical properties (e.g. compressive strength) [15].

In order to define the variables of interest for the materials (concrete, coatings) aging conditions, a search and analysis of the literature regarding tests in acidic environments were performed. Table 3 summarizes a selection of the consulted references and the representative experimental parameters for each study.

**Table 3. Review of Details for Acid Immersion Testing from Literature**

Acid type (concentration or pH)	Temperature (°C)	Immersion time (days)	Material*	Tests	Ref.
HNO <sub>3</sub> (0.025 - 0.5 mol/L)	RT	> 200	Concrete	Immersion, brushing	[17]
H <sub>2</sub> SO <sub>4</sub> and HCl (3-5 %)	RT	56	concrete	Immersion	[18]
HNO <sub>3</sub> (pH=1)	RT	**	concrete	Immersion	[19]
HNO <sub>3</sub> and H <sub>2</sub> SO <sub>4</sub> (pH=1)	RT	360	concrete	Immersion	[20]
H <sub>2</sub> SO <sub>4</sub> (1- 3 %)	RT	144	concrete	Immersion, w/d cycles, brushing	[21]

RT: room temperature, w/d: wet-dry cycles, \*: different types of concrete. \*\*: up to serious damage, Ref.: reference.

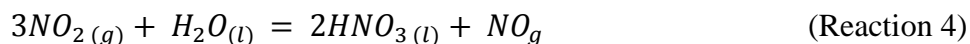
Even though the HCAEX tunnel environment carries nitric acid fumes (vapors of HNO<sub>3</sub> and nitrogen oxides-NO<sub>x</sub> in a gas state), the literature review compiled in the table not only included the use of nitric acid solutions, but also sulfuric acid (H<sub>2</sub>SO<sub>4</sub>) and hydrochloric acid (HCl) solutions that are very common in different scenarios. From the literature review and the table analysis, it can be concluded that the effect of variables such as acid type, acid concentration and concrete type on the concrete performance (durability and mechanical properties) were widely used. On the contrary, as a general trend, the temperature was not considered a significant variable for acid attack testing, due to the fact that all tests were carried out at room temperature conditions. Immersion-type experiments were chosen for all the consulted literature [17], [19], [20-21], and in some cases, a combination of immersion, brushing and cyclic tests (e.g., wet/dry cycles) to increase concrete degradation were selected.

The results of this review have been used and will be used for the design of bench-scale testing for the development and evaluation of aged concrete surfaces (phase 1) and the evaluation of selected concrete repair materials applied on aged and non-aged concrete substrates (phase 2).

### *Theoretical foundations behind the use of immersion-type tests*

This section describes how the acid fumes inside the tunnel attack the concrete surface, information which is necessary in order to support the bench-scale testing (primarily immersion-type tests). One of the questions that needs to be answered is: How do the HCAEX tunnel conditions support concrete acid attack?

To obtain nitric acid, water (H<sub>2</sub>O) in a liquid state and nitrogen dioxide (NO<sub>2</sub>) gas (acid fumes) are necessary [22]. The following chemical reaction (4) represents the formation of nitric acid.



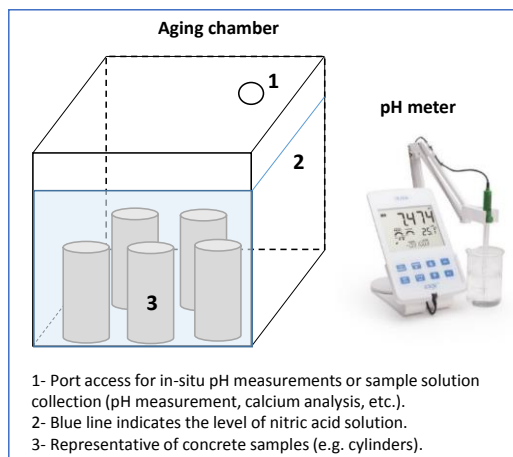
At the tunnel conditions, 80-90 % RH and ~40°C (105°F) temperature), no water vapor condensation is possible, in agreement with the air psychrometric chart. However, initially capillary condensation and hygroscopicity surface phenomena may facilitate water condensation and nitric acid formation [23]. Later, nitric acid attacks concrete (see reaction 1), forming nitrate salts that promote hygroscopicity, water condensation and acid formation. Hygroscopicity depends on the salt composition, relative humidity and temperature. Due to the hygroscopicity phenomenon, some salts like calcium nitrate (Ca(NO<sub>3</sub>)<sub>2</sub>) (found on the degraded concrete tunnel walls) have shown the formation of solution droplets above 10% RH [23]. Then, the already degraded concrete surface will promote water vapor condensation on the surface due to nitrate salts hygroscopicity which is also supported by capillarity and deliquescence.

### **Subtask 18.3.2: Materials and Methods**

The materials and methods described here support the preliminary testing of concrete specimens exposed to simulated aggressive conditions. The obtained results will support phase 1 of a multiphase project that will be dedicated to the development and evaluation of aged concrete under accelerated aging tests. The purpose of performing accelerated tests is to be able to develop aged concrete surfaces similar to the HCAEX tunnel walls (after 60 years of operation) in a short period of time.

Based on the literature review findings, immersion-type test experiments at two levels of nitric acid (HNO<sub>3</sub>) concentration, 0.025 mol/L (low concentration) and 0.5 mol/L (high concentration), were used to simulate the accelerated aging conditions of concrete surfaces. The high concentration was selected to simulate the worst scenario inside the HCAEX tunnel, and the lower concentration to simulate a mild acid condition inside the tunnel, in agreement with consulted references [17-21]. A polypropylene heavy duty tank with lid (dimension 8 in length x 8 in width x 8 in depth), was the aging chamber used for the immersion tests. Figure 47 shows a schematic of the immersion tests setup used. For health and safety reasons related to nitric acid fume working environments, the aging chamber was located inside a fume hood. A volume of 3 L for each of the concentrated solutions (0.025M and 0.5M) was prepared and the pH (1.6 and 0.3, respectively) was measured with an ORION Star A111 pH benchtop meter.





**Figure 47. Schematic of the acid aging chamber.**

Four concrete cylinders with 3 in diameter and 1 in thickness were used for the immersion test. Three of them were used as replicates (identified as 2, 3 and 4) and one as a control sample (identified as 1). The concrete samples were donated from the Civil Engineering Department (Florida International University). Currently, new samples with a concrete mix design similar to the HCAEX tunnel are being prepared. The donated concrete samples correspond to a conventional concrete (NSC), with mix proportions summarized in Table 4 [24]. Concrete specimens were immersed in lime water (calcium hydroxide saturated solution) for curing purposes. Before starting the test, at first, the concrete specimens were taken out from the lime water, washed with tap water (to remove excess of lime water) and the excess water on the surface was gently dried out with absorbent paper towel. Later, the concrete samples were weighed with an OHAUS Adventurer precision balance. In addition, pictures were taken and visual inspection of the samples was conducted and the recorded information was considered as the as-received condition. Then, the concrete samples (except the control) were immersed in the acid solution.

**Table 4. Mix Proportions of Conventional Concrete [24]**

Constituents	Quantities
Portland cement (kg/m <sup>3</sup> )	297 <sup>a</sup>
Fine aggregates (kg/m <sup>3</sup> )	757
Coarse aggregates (kg/m <sup>3</sup> )	979
Fly ash (kg/m <sup>3</sup> )	74
Air-entraining agent (mL)	325
Water (kg/m <sup>3</sup> )	127.5
Water-to-cement ratio	0.43

<sup>a</sup>: Portland cement Type II

Once the immersion test started, the pH of the nitric acid solutions (low and high concentration) was measured with time (almost on a daily basis and more frequent at the beginning of the immersion) in order to control and keep the concentration constant. By using the pH formula ( $pH = -\log c(H^+)$ ), where  $c(H^+)$  is the concentration (in mol/L=molar (M)), the concentration of the acid solution was determined every time the pH was measured and the calculated concentration was compared with the original fixed value (0.5M or 0.025M). The deviation from the original value would indicate acid consumption due to the concrete acid attack (acid-base

reaction). The deviation value calculated was used to determine the volume of concentrated acid necessary to be added to keep the concentration of the bath constant.

Due to the acid attack, the concrete samples experienced a weight loss with time. The weight loss was determined (almost on a daily basis) by a gravimetric method, weighing the samples before (initial) and after (final) immersion in the acid bath. In line with this, concrete samples were taken out from the acid bath, the excess of acid solution on the surface was gently dried out with absorbent paper and then, the weight of the specimen was recorded. After weighing the samples, the surfaces exposed to the acid solutions were visually inspected, pictures (top, bottom and sides) were taken (when surface still wet) and the samples were finally returned to the acid chamber.

### Subtask 18.3.2: Results and Discussion

In this section, the results and discussion of the accelerated aging of concrete immersed in two different concentrated  $\text{HNO}_3$  acid solutions are presented. Visual inspection, weight loss and pH changes (test solution) data with time confirmed the abovementioned.

#### Visual Inspection

Figure 48 shows the progress of the concrete degradation with exposure time. In general, no matter the concentration of the acid solution, concrete samples experienced a fast and intense degradation with immersion time characterized by 1) loss of material (cement paste and sometimes coarse aggregates), 2) fragile and powdery surface (to the touch), 3) pores widening and 4) color change. The degradation of the concrete followed a heterogeneous pattern, more intense (hollowing) in the coarse aggregates than in the paste (Figure 48). It seems that the nature of the coarse aggregate used (limestone, with ~50% of calcium carbonate), determined the greater intensity of the attack. However, the HCAEX tunnel concrete surface showed significant erosion with protruded aggregate (see Figure 48), which may be related to the schist-type coarse aggregate used in the tunnel construction [12].



**Figure 48. Images of concrete specimens (sample 2) immersed in 0.025M (top) and 0.5 M (bottom) nitric acid solutions. (The numbers 1 and 2 identify the same coarse aggregate for the two tested specimens at different times. Samples were wet when the pictures were taken, except for the control sample).**

Also, concrete coarse aggregates (limestone) experienced certain change of color (from white to yellow-brown), which was more evident on those samples immersed in the solution with low acid concentration (0.025M) than in the concentrated solution. It seems that the color could be associated with the formation of a thin film on top of the coarse aggregates, which was easily removed by touch and it was very soluble in water. Further experiments will be necessary to characterize the abovementioned aged surface, including this film. Even though three samples were tested for each acid solution, only the replicates identified as 2 are in the figure.

### Weight Loss

Figure 49 depicts the weight loss with time of the concrete samples immersed in nitric acid solutions with low (0.025M) and high concentration (0.5M). The fastest and greatest weight loss was confirmed for those samples exposed to the 0.5M acid solution that lost an average of ~ 45% (~118 g) of their weight in only 3 days (72 h). However, samples submitted to the 0.025M acid solution experienced a slower weight loss, up to ~ 13% (~ 34 g) of their average weight in 30 days (720 h). The mass loss results are in agreement with the visual inspection findings.

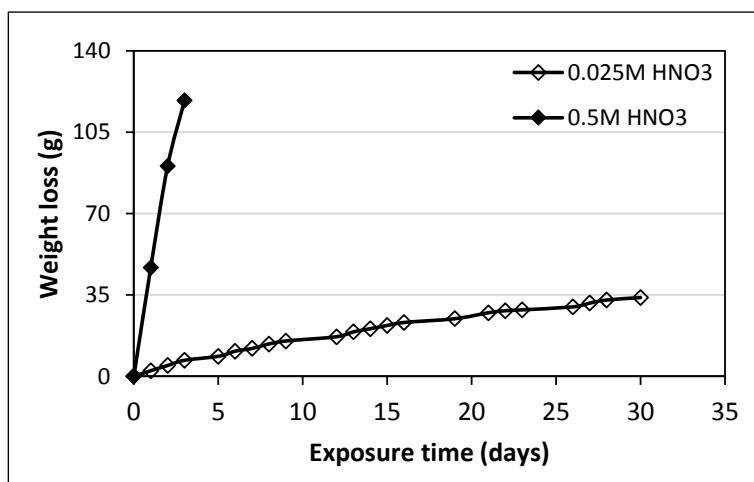
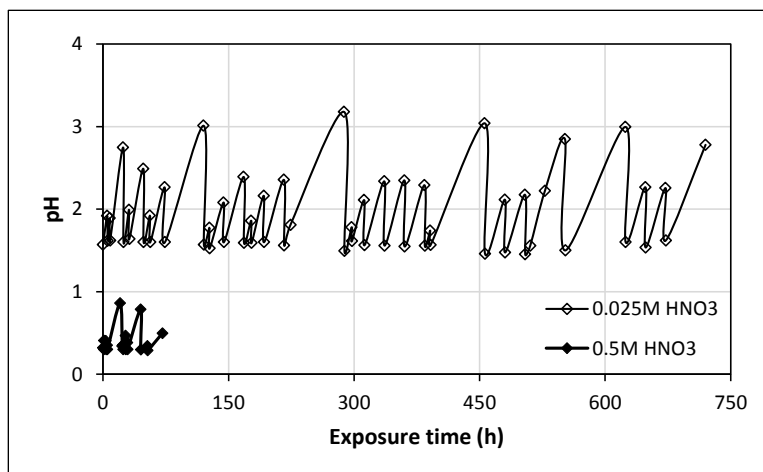


Figure 49. Average weight loss of concrete immersed in 0.025M and 0.5M nitric acid solutions.

### pH Changes

The pH change of the acid solutions was also monitored with time, as shown in Figure 50. The pH change is an indicator of the occurrence of acid attack on the concrete surfaces due to an acid-base reaction (reaction 1) that will lead with time to a pH decrease of the solution. Consequently, the pH and alkalinity of the concrete samples will be affected leading to the material deterioration. The figure shows variation of the solution pH with time, which was faster at initial immersion times than after some days of testing. The pH variations are represented by peaks out of the expected pH values for the 0.025M solution (pH=1.6) and 0.5M solution (pH=0.3), indicating acid consumption. The concentrations of the acid solutions were adjusted by adding concentrated acid.



**Figure 50. pH Changes of the 0.025M and 0.5M Nitric acid solutions with time.**

The strong nature of the nitric acid combined with the high concentration of the acid (pH < 2 for both solutions) influenced the degradation observed. This is in agreement with previous studies [17-21] related to concrete acid attack that demonstrated the key role of the type of acid, the concentration, the type of concrete, etc. on the intensity of the degradation. In addition, preliminary research findings confirmed a good correlation among the monitored parameters (visual inspection, weight loss, pH of the solution).

### Subtask 18.3.2: Conclusions and Future Work

From the literature review findings, the acid attack, carbonation and erosion were the primary degradation mechanisms identified on the concrete walls of the HCAEX tunnel, motivated by the aggressive environment inside this facility. Potential repair materials (coatings and overlays) to mitigate concrete deterioration of the tunnel walls were also identified. From the consulted references, most of the coatings (organic, inorganic or hybrid) applied as a system (several layers) or combined (e.g. ceramic inorganic/organic) showed better resistance to acids, high temperature and abrasion with respect to the overlays. A number of experimental methods and measurements for evaluating chemical attack (mainly nitric acid) and erosion were studied. Preliminary bench-scale testing of concrete specimens (mix design different to the tunnel) was carried out. The immersion-type test demonstrated to be an adequate and feasible method to perform accelerated aging of materials in a short-term period of time providing valuable insights regarding the aging process. The greater deterioration of the limestone coarse aggregate observed will not support the development of aged concrete surfaces with protruded aggregates like the HCAEX tunnel walls. Hence, new concrete samples with schist-type coarse aggregates, found on the HCAEX tunnel walls, are necessary to be able to develop aged surfaces with protruded aggregates for the coatings evaluation phase. The 0.5M nitric acid solution (high concentration) proved to be the most aggressive environment leading to the fastest and most intense degradation of the concrete samples in just 72 hours. Finally, a good correlation among the tested parameters (visual inspection, weight loss, and pH) was evidenced for the two aging conditions (high and low acid concentration).

**Subtask 18.3.2: References**

1. Gilliam, Bob J., Ray, J., and Giddings, B. “Inspection and assessment of the H-Canyon ventilation system at The Savannah River Site”. Phoenix, Arizona. s.n., 2015. Waste Management Conference.
2. Staff Report, Defense nuclear facilities safety board. “H-Canyon exhaust tunnel fragility analysis input and assumptions”. 2018.
3. Nuclear energy standards coordination collaborative. “Codes and standards for the repair of nuclear power plant concrete structures: Recommendations for future development”. 2013.
4. ACI 546.3R-14. Guide to materials selection for concrete repair. American Concrete Institute, 2014.
5. Kim, H. S., Lee, S.H. and Moon, H.Y. “Strength properties and durability aspects of high strength concrete using Korean metakaoline”. *Constr. Build. Mater.* 21 (2007), pp. 1229-1237.
6. Goyal, S. et al., “Resistance of mineral admixture concrete to acid attack”. *J. Adv. Concr. Technol.*, 7 (2009), pp. 273-283.
7. Pan, X. et al., “A review on concrete surface treatment Part I: Types and mechanisms”. *Constr. Build. Mater.* 132 (2017), pp. 578-590.
8. Perrin, F. et al., “Degradation study of polymer coating: improvement in coating weatherability testing and coating failure prediction”. *Prog. Org. Coat.*, 64 (2009), pp. 466–473.
9. Kumar, A.P. et al., “Nanoscale particles for polymer degradation and stabilization-trends and future perspectives”. *Prog. Polym. Sci.*, 34 (2009), pp. 479–515.
10. Report, Defense Nuclear Facilities Safety Board. Staff. “H-Canyon seismic performance and condition”. 2015.
11. M. G. Serrato et al. “Characterization of Concrete Exposed to the H-Canyon Exhaust”. Savannah River National Laboratory Report. January 2018.
12. Alexander, M., Bentur, A. and Mindess, S. “Durability of concrete. Design and construction”. CRC Press Taylor and Francis Group, 2017.
13. ACI 546.3R-14. “Guide to materials selection for concrete repair”. 2014
14. Wagh, Arun S. et al. “Inorganic phosphate compositions and methods”. US20160068442A9 United States, 2016. Application Patent.
15. Echeverria, M. et al., “Literature Review for the H-Canyon Exhaust Tunnel Study”, Summary Document submitted to DOE –EM under Cooperative Agreement # DE-EM0000598 (FIU-ARC-2019-800006470-04c-263).
16. ACI 515.2R-13. “Guide to selecting protective treatments for concrete”. 2013
17. Pavlík, V. “Corrosion of hardened cement paste by acetic and nitric acids. Part I: Calculation of corrosion depth”. *Cement and Concrete Res.*, 24 (1994), pp. 551-562.

18. Jagannadha, K. et al., "Acid resistance of quaternary blended recycled aggregate concrete". *Case Studies in Const. Mater.* 8 (2018), pp. 423–433.
19. Matakah, F. Salem, T. and Soroushian, P. "Acid resistance and corrosion protection potential of concrete prepared with alkali aluminosilicate cement". 2018, *J. Build. Eng.*, 20 (2018), pp. 705–711.
20. Diab, Ahmed M. et al., "Effect of nanomaterials additives on performance of concrete resistance against magnesium sulfate and acids". *Const. Build. Mater.* 210 (2019), pp. 210–231.
21. Gu, L. et al., "Evaluation of accelerated degradation test methods for cementitious composites subject to sulfuric acid attack; application to conventional and alkali-activated concretes". *Cement Concrete Comp.* 87 (2018), pp. 187-204.
22. Cheremisinoff, Nicholas P., "Handbook of pollution prevention and cleaner production. Volume 3. Best practices in the agrochemical industry". Elsevier. 2011
23. Liu, Y. J. et al., "Investigation of the hygroscopic properties of  $\text{Ca}(\text{NO}_3)_2$  and internally mixed  $\text{Ca}(\text{NO}_3)_2/\text{CaCO}_3$  particles by micro-Raman spectrometry". *Atmos. Chem. Phys.*, 8 (2008), pp. 7205-7215.
24. Farzad, M. et al. "Corrosion macrocell development in reinforced concrete with repair UHPC". Paper No. 11580. NACE Corrosion 2018.

## TASK 19: PIPELINE INTEGRITY AND ANALYSIS

---

### Task 19: Executive Summary

Structural integrity of pipe lines and transfer systems is one of the significant concerns for Hanford and other nuclear waste sites in the US. To address this issue, Washington River Protection Solutions (WRPS) implemented a fitness-for-service (FFS) program to assess the structural integrity of pipelines, tanks and tank farm waste transfer system. The purpose of the program was to inspect primary piping, encasements, and jumpers for corrosion/erosion which has been accomplished in the previous years. FIU has been supporting this work which includes previous efforts in the evaluation of ultrasonic transducers that can provide real-time thickness measurements for transfer system components. Previous work included market study and down selection of commercially available ultrasonic transducer systems according to the requirements listed by the WRPS/DOE personnel. One of the down selected UT sensor system from Permasense was acquired and bench scale and engineering scale validation tests have been conducted on a custom built pipe loop. This year's work included exposure of the UT sensors to elevated temperatures (up to 120°F) and humidity (up to of 99%) conditions in order to study their performance under varying environmental conditions. Test results indicated that the sensors were able to survive under high temperature and humidity values as exposed on the sites, thus validating the sensors for potential use in the nuclear sites for cold testing. The second type of sensor system used to test the structural integrity of the pipelines is based on fiber optics for leak and damage detection in carbon steel pipe sections similar to those at Hanford site. Talks between DOE officials, a commercial vendor and FIU resulted in obtaining and installing the Fiber Strike sensor system from Cleveland Electric Laboratory (CEL) at FIU. Initial testing with the sensors is currently being conducted. Additionally, FIU has been collaborating with scientists at SRNL to validate their custom built erosion coupons on the FIU flow loop. The coupons were used to measure slight changes in mass loss due to erosion and also to quantify the thinning in the pipe diameter on a precise level using the UT pencil sensor probes. Further, the coupons were able to provide the visual erosion when inspected under the microscope/SEM.

Structural integrity of non-metallic materials is also being investigated under the current research work. Nonmetallic materials used in the Hanford Site Tank Farm waste transfer system include the inner primary hoses in the hose-in-hose transfer lines (HIHTLs), Garlock<sup>®</sup> gaskets, ethylene propylene diene monomer (EPDM) O-rings, and similar other nonmetallic materials. These materials are exposed to radiation, caustic solutions and elevated temperature and pressure stressors. While the individual effect of these stressors has been well established, their combined effect is of significance to the Hanford site. FIU has been supporting this task by developing a test loop and testing the non-metallic materials under simultaneous stressor exposures. Previous testing included aged HIHTL and material coupons for 6 months and 1 year using elevated temperatures and exposure to caustic material as well as exposure to water only at 170°F for 1 year. The mechanical and material properties of the samples were characterized and compared with those of the unexposed samples (baseline). Evaluations included burst pressure tests of the EPDM hose-in-hose transfer lines and material tensile strength test of EPDM dog-bone coupons. It was summarized that both the tensile strength of the EPDM material dog bones and the burst pressure of the HIHTLs significantly decreased with the increasing temperature and increasing exposure time.



This task will provide information that will assist engineers with understanding the wear rates in metal pipes and transfer lines along with the effect of various stressors on nonmetallic components. The research will aid in determining the remaining useful life of both metallic and non-metallic components by establishing more detailed/accurate guidelines and avoiding unexpected failures in transfer lines.

## **Subtask 19.1: Pipeline Corrosion and Erosion Evaluation**

---

### **Subtask 19.1: Introduction**

The Hanford Site Tank Farm has implemented a Fitness-for-Service (FFS) program for the Waste Transfer System. The FFS program, based on API-579-1/ASME FFS-1, examines structural parameters of the waste transfer systems in order to develop erosion/corrosion rates for relevant system components. The FFS information is acquired from opportunistic evaluations of pipelines that have been removed from service. FIU-ARC engineers work closely with key Hanford high level waste (HLW) personnel and the contractor, Washington River Protection Solutions, LLC (WRPS), to support the FFS program, deliver solutions for sensor evaluations, conduct bench-scale testing followed by data acquisition and analysis for corrosion and erosion assessment. Previous efforts at Hanford included the installation of sensors on a number of the POR 104 components, to provide real time pipe wall thickness measurements. Due to various limitations, alternative approaches for remote permanently mounted pipe wall ultrasonic thickness measurement systems are being investigated.

FIU efforts to support this scope have included investigating key options available in the market for remote permanently-mounted ultrasonic transducer (UT) systems for HLW pipe wall thickness measurements. Specific applications include straight sections, elbows and other fittings used in jumper pits, evaporators, and valve boxes. FIU assessed the use of various ultrasonic systems that are either commercially available or used previously at Hanford and selected the most promising systems for further evaluation. One of the two down selected systems (Permasense UT sensor system) was acquired and initial bench-scale validation testing was conducted. Following the initial bench scale tests, engineering scale testing was implemented on an in-house designed and installed test loop. The design loop has been established using 2- and 3-inch diameter straight and bends pipe sections to mount the sensors. The loop was eroded using sand-water slurry and the Permasense sensors were used for thickness measurements. The sensors were also tested for their performance in extreme environmental conditions under high humidity and temperatures. In addition to the Permasense UT sensors, two other systems were evaluated for erosion and corrosion detection in the pipe loop at FIU. These included the SRNL coupons with the Pencil UT sensor and the Fiber optic sensors from CEL.

Currently, FIU is in the process of testing the Permasense sensors under the effects of radiation, working with the SRNL team to evaluate their erosion coupons and to use CEL's Fiber optic sensor system for leak detection in carbon steel pipe sections. The benefits of this research include providing validation for new methods and technologies that will assist engineers in understanding the fault potential of HLW nuclear waste transfer components due to corrosion and erosion. By providing insights into determining if and when lines need to be removed, the unneeded excavation of transfer lines can be avoided saving valuable time and resources. Also, more detailed and accurate guidelines can be developed governing the life expectancy of the

transfer system and its components. By being able to have accurate predictions of points of failure from erosion, and by being able to monitor an entire pipeline's status in real-time, resources can be targeted to tackle preventative measures instead of reactive.

### **Subtask 19.1: Objectives**

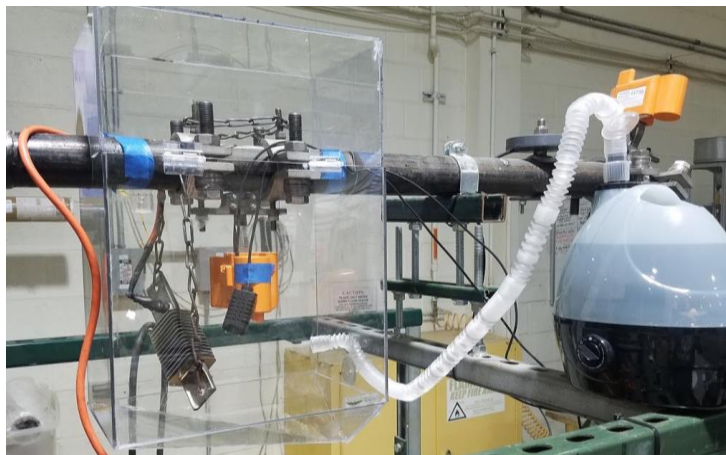
The objective of the current task is to assist DOE and WRPS in providing realistic estimates of the remaining useful life of the components and to incorporate those estimates into future design plans. This task includes the investigation of various sensor systems to detect thinning in pipes and tanks along with real-time evolution of the wear using SRNL's mass loss/erosion coupons. Hence, there are three objectives for this task for structural health monitoring using various types of sensors. Including:

- Environmental testing of Permanence UT sensors.
- Erosion and wear detection in pipes using SRNL coupons.
- Pipe leak and anomaly detection using CEL's fiber optic sensors.

### **Subtask 19.1: Methodology**

#### **Environmental testing of Permasence UT sensors**

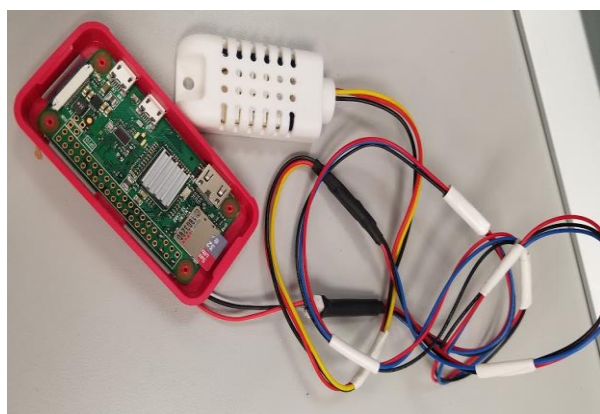
Previous year's research included evaluation of the Permasense UT sensors for bench and engineering scale testing on FIU's pipe loop. Upon successful validation, this year's work incorporated the environmental assessment of the sensors for use in the actual sites. Input from WRPS scientists resulted in obtaining the actual humidity and temperature conditions that the sensors would be exposed to at the sites. Based on their input, a clear environmental chamber has been designed that has been placed around one of the UT sensors on the flow loop. Heat and humidity were introduced into the enclosure to detect the sensor's response under elevated temperature and pressure conditions. The experimental set up as shown in Figure 51 contained the environmental chamber mounted on the 2-inch carbon steel pipe and houses the ultrasonic sensor. To heat the air inside, a 400W ceramic insulated strip fin-heater [1] was suspended from the pipe using a metal chain. The ultrasonic humidifier supplied saturated air at room temperature to the heated chamber through a small inlet. Both units were controlled by an InkBird [2] control unit that measures relative humidity and temperature inside the chamber and cycles the units on or off accordingly in order to achieve the desired temperature and humidity conditions. The humidity and temperature sensors were placed on the ultrasonic sensor mounted on the pipe to acquire most accurate measurements closer to the sensor.



**Figure 51. Experimental set up with heater and sensors in the chamber.**

Initial experiments were conducted over a period of 40-60 minutes in which temperature and humidity measurements were manually recorded every minute in order to assess the effectiveness of the heating element, humidifier, and control unit, to raise the environment inside the enclosure up to a temperature of 120°F and relative humidity greater than 95%.

Since, the initial set of experiments were conducted manually, the process was tedious. Hence, for the second stage, the process was automated with the building of an in-house data acquisition system using a microcontroller. The data logger consisted of a micro controller (Raspberry Pi Zero) placed inside a case. A DHT22 temperature and humidity sensor [3] was wired to it to act as a probe. A program (python script) was written to log temperature and humidity readings to a file every minute once the device turned on. The log file could then be accessed by either removing the micro SD card or by connecting to the micro controller over Wifi. A picture of the setup is as shown in Figure 52.



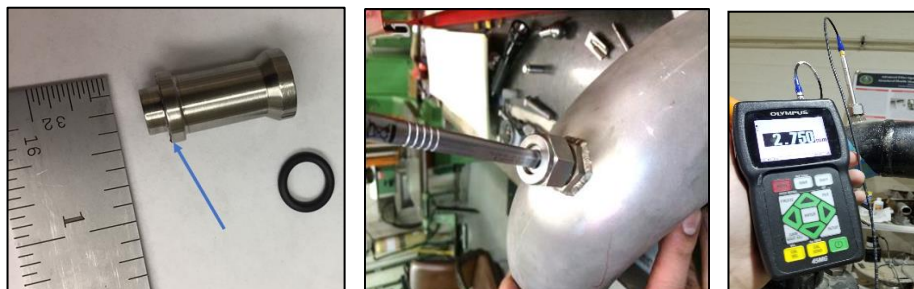
**Figure 52. Data acquisition system (left) and experimental set up (right).**

The experimental set up of the DAQ system along with the temperature and humidity controller and ultrasonic humidifier is as shown in Figure 52 (right). The environment in the chamber was set to 40°C (104°F) and 100% RH and the test duration was 6.5 hours. During the test, temperature and humidity readings were recorded at one minute intervals and pipe thickness measurements from the UT sensors were recorded every 30 minutes. The heating element and

humidifier were turned off at the 6 hour mark to check if the cool down period resulted in any change in reading. Experimental results and discussion are presented in the next section.

### **Erosion and wear detection in pipes using SRNL coupons**

Collaboration with SRNL scientists during the previous year led to the initial testing of SRNL coupons for erosion in pipe sections. The process included use of small coupons of carbon steel (Figure 53) made of the same material as used in pipelines across DOE nuclear waste sites. The intention was to measure the changes in thickness using UT sensors and to measure the mass loss on a minute level to detect and quantify pipeline wear.



**Figure 53. a) Erosion Coupon b) UT sensor and coupon [4] c) UT pencil sensor on FIU's loop.**

By measuring the minute erosion of the coupon, the life expectancy of sections of pipelines in the field may be calculated. The coupon is inserted into a coupling welded to the pipe surface and the head of the coupon is made flush with the inside of the pipe. By being subjected to the same abrasive forces as the pipe walls, the coupon represents a fully observable model of the pipe section. The advantage of the coupon is that it is easily removable. Mass measurements of the coupon before and after testing were taken to provide insights into the degradation of that particular pipeline, or a pipeline made of similar material.

The coupons were tested on the pipe loop with varying sand and water slurry mixtures and grit sizes. Previously, the mixture was created using coarse grade sands which resulted in rapid erosion leading to pipe failure within a few hours. Additionally, settling of sand at the bottom of the tank was a major concern. Hence, during this year, the next phase of testing has been initiated with medium grit (30/60 grit) sand to have slower and more uniform wear along the loop with less settling of sand. The pipe loop was thoroughly cleaned by circulating water and the SRNL coupons were inserted as shown in Figure 54.



**Figure 54. SRNL Coupons on the pipe loop, endoscopic images of the pipe internal surface with the coupons.**

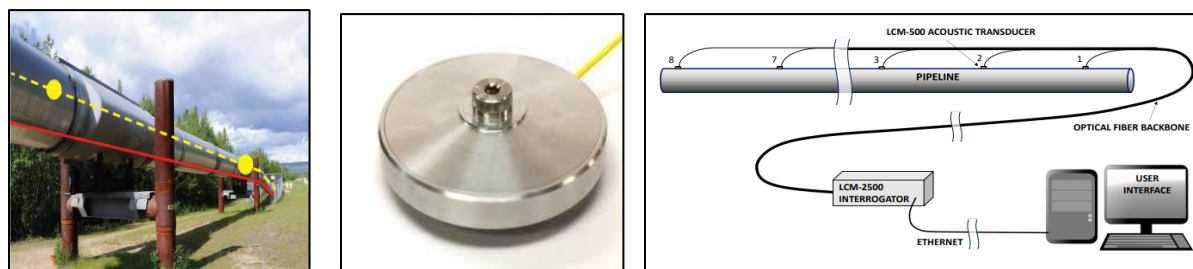
To quantify the erosion taking place in the pipe, the coupons were weighed and measured using a balance and caliper before being inserted. The surface of the coupon head was also viewed under



a microscope and photographed for later comparison after erosion had occurred. During the test, measurements were taken in situ using an Olympus V260-SM UT pencil sensor [5] that was modified to fit specifically in the provided channel within the coupon. Thickness measurements were collected every 30 minutes from both a handheld UT pencil sensor and the permanently mounted UT sensors on the loop. After testing, the coupons were removed from the pipe loop and measurements were taken again in order to quantify mass and height loss, and validate the measurements taken by the pencil sensor. Experimental results are presented in the next section.

### **Pipe leak and anomaly detection using CEL's fiber optic sensors**

In addition to the UT sensors and the SRNL coupons, a new sensor system was also evaluated for structural health monitoring of tanks and transfer lines. The Fiberstrike sensor system developed by an Ohio based engineering firm, Cleveland Electric (CEL) [6], for the purposes of pipeline monitoring, was tested and validated on a bench scale pipe loop. Current monitoring systems on the market rely on measurements such as flow rate, pressure, temperature, etc. These sensors transmit wired or wirelessly and usually must be powered by an electrical source. This can lead to increased operational costs and accidental downtime. In comparison, the Fiberstrike sensors are acoustic transducers based on the principle of optical interferometry, using light to detect the slightest of vibrations. One large advantage is that they require no power source. Only a fiber optic cable linking the sensor to the gateway is required. The sensors emit no form of radiation and therefore cannot interfere with any other nearby equipment. They are also not susceptible to any forms of external interference, making them ideal for harsh, radioactive environments. By measuring the acoustic energy of an object, the power spectral density (PSD) can be observed. A pipeline exhibits an acoustic or vibrational signature, when conditions in and around the pipeline are stable, the signature remains stable as well. This signature is known as the pipeline's power spectral density (PSD), the distribution of power into frequency components. By placing acoustic transducers at intervals along a pipeline, continuous, real time monitoring of the pipeline's PSD can be realized. Under ideal operating conditions the baseline signature is captured and comparisons are made against it to detect anomalies along the pipeline. Any parameter that translates into even the slightest physical movement can be quantified by monitoring the PSD.



**Figure 55. Fiberstrike a) sensor system b) sensor [6] c) monitoring system layout [6].**

Events such as impacts to a section of pipe, drilling, or leakage, can all be translated into unique signatures represented by the change in the pipeline's PSD. The location of the event can then be determined by comparing the magnitude of signatures on neighboring sensors. The higher the magnitude ratio of sensor A to sensor B, the closer the event has taken place to sensor A. By relying on fiber optics, near instantaneous, measurements can be made with a maximum reported latency of 3 seconds and a nominal latency of 1.5. All sensors on the pipeline have no electrical

components and are connected via non-conductive optical fiber. This allows for the sensors to be located more than 20 km from the monitoring equipment.

The sensors resemble a small metal disk approximately 6 inches in diameter with a center hole. When installed they have a thin plastic shell the same shape. The sensors are mounted on a threaded stud that may be welded to the surface of the pipeline or a tank wall. The sensors may also be attached using a metal clamp with a threaded stud. Direct physical contact is required for optimal signal integrity, and the sensors need to be fastened tightly to avoid any movement or shifting from continuous vibrations. The interval at which the sensors are installed on a pipeline varies depending on configuration; for long straight sections it has been shown that spacing can be more than 500 meters apart, but for geometries such as elbows or complex configurations with valves and pumping stations, more frequent placements of sensors is necessary. Use of the LCM-500 transducers requires a fiber optic “backbone” to be installed on the pipeline containing single-mode SMF-28 fibers. The cabling is then connected to an LCM-2500 which serves the purpose of an optical interrogator. Finally, the interrogator(s) can be connected either directly to a local station via Ethernet, or to a router for remote access. A layout of the monitoring system along with the transducer locations is as shown in Figure 55.

The FIU loop previously described was used to install the fiber optic sensors as shown in Figure 56. In this set up, both straight and 90° elbow sections were used and joined by a reducer. The pipe sections were welded and the sensors were installed per the manufacturer’s instructions. A threaded boss is attached to the exterior of the pipe. Typically, it is physically attached to the pipe by clamping it with an industrial rated strap or clamp. The transducer shown in Figure 56b is attached to the threaded boss using a supplied nut and washer.



**Figure 56. a) Fiber optic sensors on the loop; b) single transducer (LCM-500); c) LCM-2500 Interrogator and user control station.**

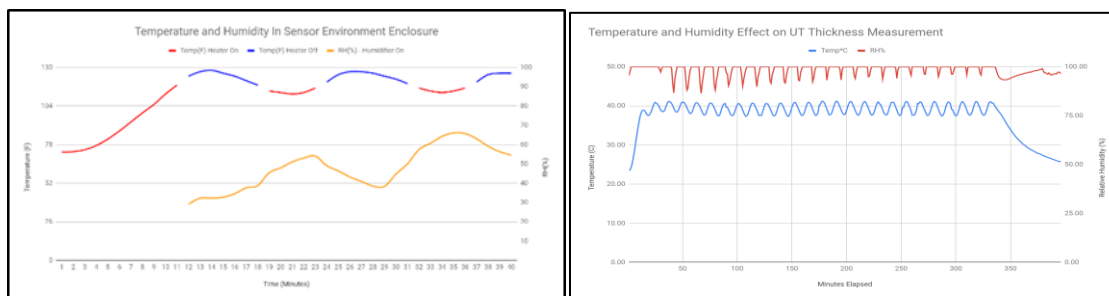
Figure 56b shows the installation of one of the three LCM-500 acoustic transducers mounted on a 2 in. section of pipe. Once installed, each sensor must have their pigtail fiber cables fusion-spliced into the fiber optic backbone cable that travels the length of the pipeline to the interrogator. Figure 56c shows the monitoring station placed several feet away from the scale pipeline with a laptop sitting on top of the LCM-2500 interrogator. Testing included circulating the sand water mixture similar to the previous cases.

## **Subtask 19.1: Results and Discussion**

### **Results from the environmental testing of Permasense UT sensors:**

Environmental chamber testing for the Permasense sensors was conducted in three phases. Phase one was to check the proper functioning of the chamber and the heater. The temperature was varied between 75°F and 120°F while the humidity ranged between 30% RH and 65% RH.

Sample test results of phase one experiments are as shown in Figure 57. It is evident from the graph that the heater takes about 11 minutes to heat up to the temperature set point of 120°F from the initial point of 75°F (room temperature). Once the desired temperature is achieved, the controller unit turns the heater off until the temperature is lower than to 117°F before turning back on. Hence, it is evident that the heater could be controlled with a temperature fluctuation of 3°F. Relative humidity change is also shown in the same graph. Humidity was introduced into the chamber at the set point temperature and it changed between 30% RH and 65% RH over a period of 40 minutes. As expected, the humidity peaks were achieved when the heater was off (temperature reduced) and vice versa.



**Figure 57. Results obtained during the environmental chamber testing, a) manual and b) automated.**

During the experiment, the Permasense UT sensor measurements were recorded and no changes in readings were observed. Hence, it is concluded that the UT sensors are not affected by the set point temperature of 120°F and 65% relative humidity. Fluctuations in temperature and humidity during the test can be explained by the hysteresis of the heating element. Once the temperature set by the controller is reached, the heating element turns off; however, the thermal mass of the element continues to induce a temperature rise in the chamber. This effect causes the temperature in the enclosure to slightly increase above the set point. In addition, once the temperature drops below the set point, the heating element requires several minutes to attain the set point temperature and heat the enclosure again. This causes the temperature to drop several degrees below the set point before starting to increase. While the heating element is turned on, the humidity in the enclosure reduces as hot air becomes less saturated with moisture. On the other hand, when the heating element is turned off, humidity slowly increases due to cooling of the air and condensation of the moisture occurs due to over saturation.

During phase one testing, the data was acquired at frequent intervals manually which was tedious and hence a data acquisition system was built to automate the process. Results obtained by the automated process are as shown in Figure 57b. In the figure, the drop in humidity almost coincides with a drop in temperature which is against the physics of the problem. This can be explained as a result of the delay in the response time of the humidity sensor when compared to the temperature sensor. Also, the peaks in the humidity readings gradually reduce with time, stabilizing the system. This can be explained by the cycling of the heating element (On and off) and the gradual saturation of air at high temperatures.

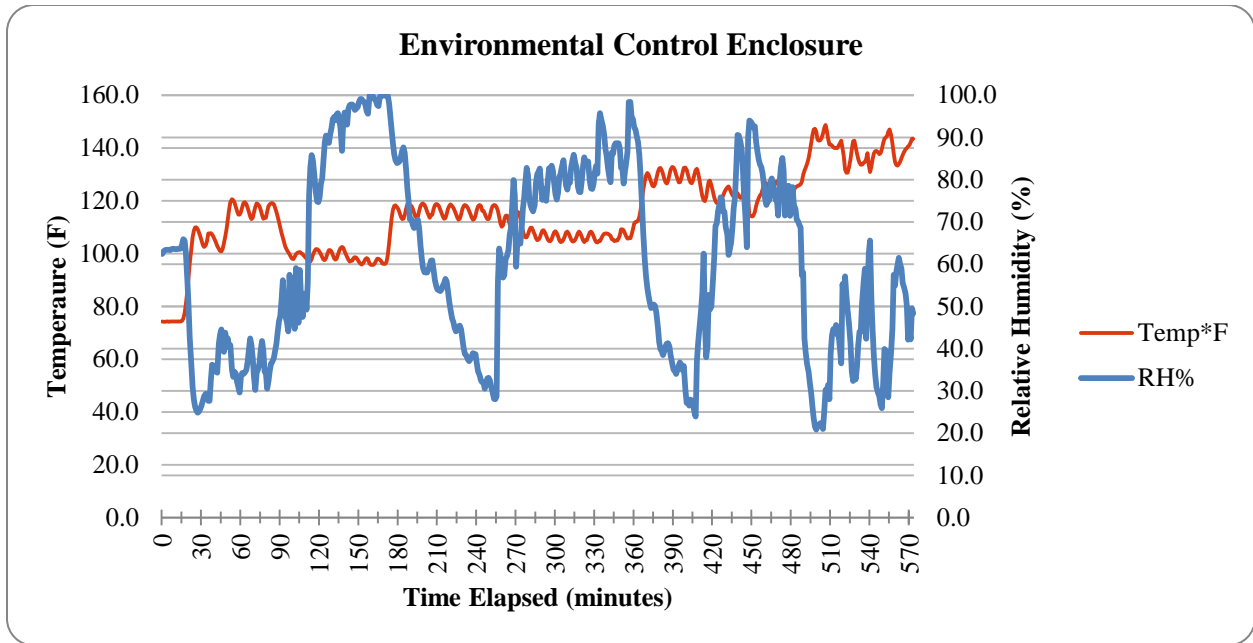
Thickness measurements from Permasense UT sensors were recorded every 30 minutes and are tabulated in Table 5. As seen from the table, the readings are consistent to 2 decimal places in mm during the entire 6.5 hr. period of testing. Overall, the test has successfully proven that the Permasense UT sensor can consistently take precise measurements at 40°C and almost 100% RH conditions as provided by the site engineers.



**Table 5. UT Sensor Measurements during the Experiment**

Time (Minutes)	Temperature (C)	RH (%)	Thickness (mm) (Permasense UT sensors)
0	23.50	95.40	3.62
30	38.60	99.20	3.61
60	40.20	99.90	3.61
90	39.60	96.40	3.61
120	37.60	99.90	3.61
150	40.30	99.90	3.62
180	39.80	99.90	3.61
210	37.60	99.90	3.61
240	40.90	99.90	3.61
270	39.20	96.30	3.61
300	37.60	99.90	3.61
330	41.00	99.90	3.61
360	30.30	96.20	3.61
390	26.10	96.40	3.62

The third phase of testing included real world dynamic condition testing. In order to test the Permasense UT sensors under realistic conditions and varying stresses, sensor measurements were taken over a 10 hour period in which temperature and humidity were fluctuated frequently. Humidity was varied between 20% and 99% while the temperature was increased from 75°F to 145°F. A previously developed automated data acquisition (DAQ) system using a microcontroller (Raspberry Pi) was used to log the temperature and humidity data at 1 minute intervals. Variations of the environmental conditions in the chamber enclosing the sensor are as shown in Figure 58. Previous tests were focused on maintaining a specific temperature and humidity to validate the sensor's ability to operate under those static conditions, while the objective of the present testing was to see if rapid changes in the environment would affect the sensor's ability to compensate for the conditions.



**Figure 58. Dynamic environmental conditions in the UT sensor’s testing chamber.**

The Permasence sensor measured pipe thickness during the experiment and the results at several data points (temperature and humidity) are presented in Table 6. It is evident from the table that the thickness measurement varied by a maximum of  $\pm 0.01\text{mm}$ , which is the manufactured specified tolerance on the UT sensor, thus validating its operational ability under varying conditions of temperature and humidity.

**Table 6. UT Sensor Measurements during the Experiment**

Time Elapsed (min)	Thickness (mm)
0	3.62
30	3.62
60	3.62
90	3.62
120	3.62
150	3.62
180	3.62
210	3.61
240	3.62
270	3.61
300	3.61
330	3.61
360	3.61
390	3.61
420	3.61
450	3.62
480	3.61

510	3.61
540	3.61
570	3.62

**Results of SRNL coupon experiments:**

SRNL coupons were inserted at 5 locations on the 3-inch pipe sections. Three coupons (1, 2 and 3) were placed at the top and the other 2 coupons (numbers 4 and 5) were placed at the bottom. Sand-water slurry with varying grain sizes and volume concentrations were circulated to erode the pipe sections.

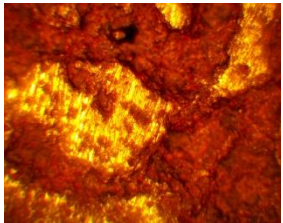
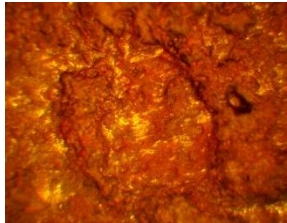

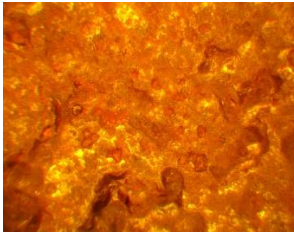
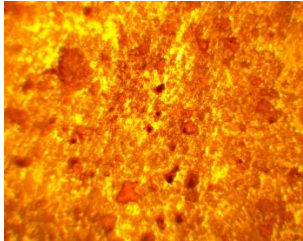


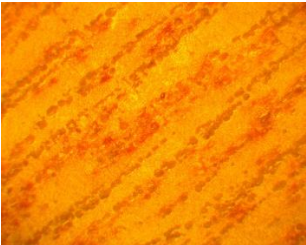
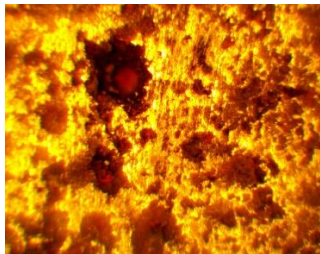
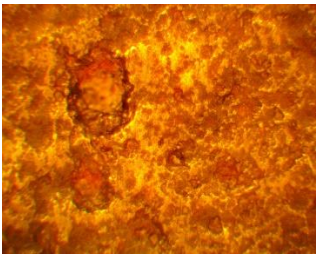
This year’s testing included one new coupon (never tested) and 4 old coupons (tested previously) to have an accurate erosion measurement and comparison with the baseline. Tests were conducted ranging from 1-7 hrs. Gravimetric measurements of the coupons were conducted before and after the tests. A sample set of results in weight changes obtained during the 7 hr tests are provided in Table 7. It is evident from the table that the coupons 3 and 4 have considerable mass loss of 2.3 mg, while coupon 2 (placed at the top) has the lowest mass loss.

**Table 7. Mass Loss in the SRNL Coupons during the Experiment**

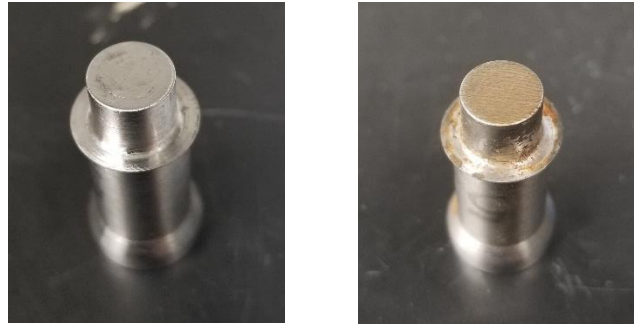
Coupon	Weight (gm)		
	Before	After	Mass Loss
1	7.9634	7.962	0.00140
2	7.77746	7.777	0.00046
3	7.85333	7.851	0.00233
4	8.5063	8.504	0.00230
5	7.95348	7.952	0.00148

Microscopic images of the coupons were captured using the Olympus BH3 microscope with 5X magnification. These images are as shown in Figure 59. The same location on each coupon was pictured before and after testing in order to allow for more direct comparison and show visually how surfaces on the coupons changed from erosion.

Previously it was believed that much of the pitting seen on the surfaces of the coupons was caused by corrosion, however, it appears now (after the testing) that much of the pitting was actually caused by the sand particles eroding the surface of the coupon. Coupon 4 was a new coupon without any previous use in the pipeline system. After the experiment, scores appear in a uniform direction across the surface. Upon closer inspection, the lines are tiny pits on the surface, all occurring in the direction of flow in the pipe. The other coupons can see similar effects after testing. Smaller pits that were on the surface have become larger, and the number of pits increased. The new coupon before and after testing is shown in Figure 60.

Coupon #	Before	After
1		
2		
3		
4		
5		

**Figure 59. Microscopic images of the coupon surfaces (5X magnification).**

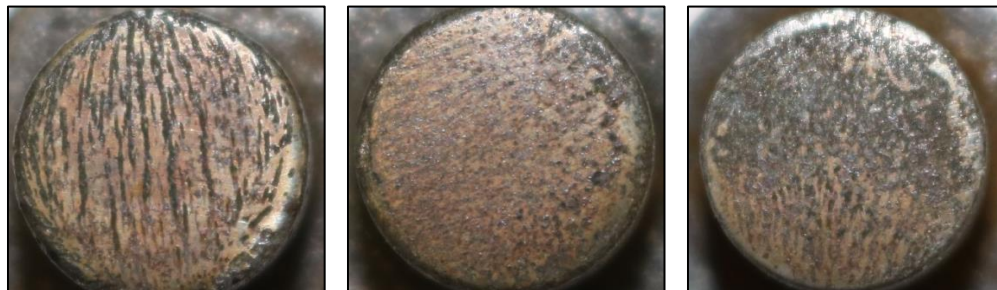


**Figure 60. SRNL coupon (new) a) before the test and b) after the test.**

The next set of experiments were conducted with coarse sand particles which resulted in higher erosion rates. Surface profile changes for the five coupons involved in the test can be seen in Figure 61 and Figure 62. The sand slurry was circulated through the pipe loop for approximately 7 hours and measurements were taken before and after. It should be noted that coupons 1-3 were placed on the top of the pipe section and coupons 4-5 were placed on the bottom directly below. The surface of the new coupon after being turned on a lathe can be seen in Figure 61.a, representing the starting surface condition of all five coupons used in the test. It is extremely noticeable that the coupon heads exposed to the pipe ceiling (1-3) all exhibit similar wear pattern, long and deep surface scarring; coupons placed on the bottom of the pipe (4-5) exhibit a much more uniform erosion pattern and none of the deep scar characteristics of coupons placed on the pipe ceiling.



**Figure 61. a) New coupon surface; b) Coupon 1 (after testing); c) Coupon 2 (after testing).**

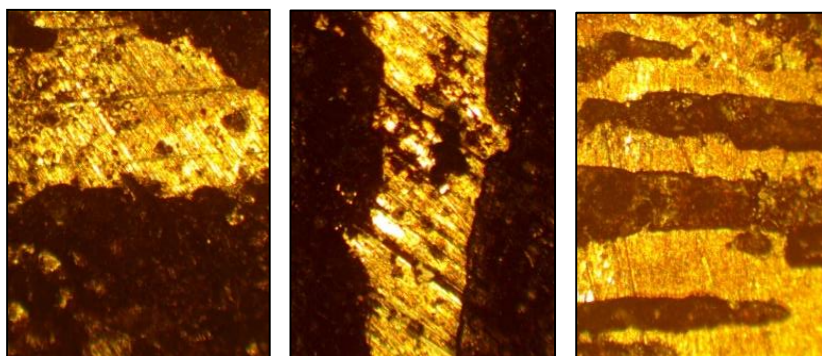


**Figure 62. a) Coupon 3 (after testing); b) Coupon 4 (after testing); c) Coupon 5 (after testing).**

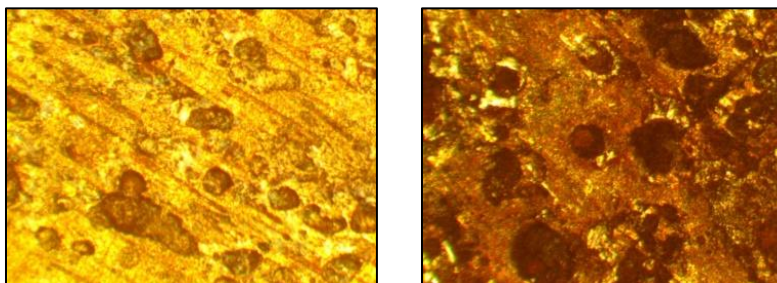
The current hypothesis for the uniquely different forms of erosion is that sediment particle velocity plays the largest role. While traversing the pipeline horizontally, sediments tend to settle



on the floor of the pipe and move at velocities less than the nominal rate of flow in the pipe. In addition, a higher percent of sediment settling covers a larger surface area many particles thick. This results in a continuous sanding of pipe wall at lower speeds. Evidence of this can be seen in the smaller pit diameters and depth, and the more uniform coverage of erosion. Meanwhile, particles impacting the ceiling of the pipe may be carried in currents of turbulent flow, accelerating particles at speeds greater than the nominal flow. In addition, because the density of the particles (sand) is much greater than that of the medium (water), and the particles do not exhibit any coagulating properties, the ceiling of the pipe is subjected to individual particle strikes at high speed. Particles introduced into the same streams of turbulent flow may follow a similar trajectory, subjecting certain areas of the pipe surface to high levels of erosion while neighboring regions experience very little erosion. Evidence for this can also be seen in the microscopic images (Figure 63 and Figure 64). Surface scars are long and deep, however, between scars there appears to be much less relative erosion.



**Figure 63. Microscopic images (5X magnification) of coupon surfaces for coupons 1, 2, 3 respectively.**



**Figure 64. Microscopic images (5X magnification) of coupon surfaces for coupons 4 and 5 respectively.**

After testing, erosion was quantified by taking mass and height measurements. As expected, there were significantly different changes for erosion taking place on the pipe floor as opposed to the pipe ceiling. In Table 8, the height change and mass loss of the coupons can be seen. Notably, coupons on the ceiling exhibited lower mass loss but higher height loss, whereas the coupons mounted on the pipe floor exhibited higher mass loss and lower height change.

**Table 8. SRNL Coupon Mass and Height Loss**

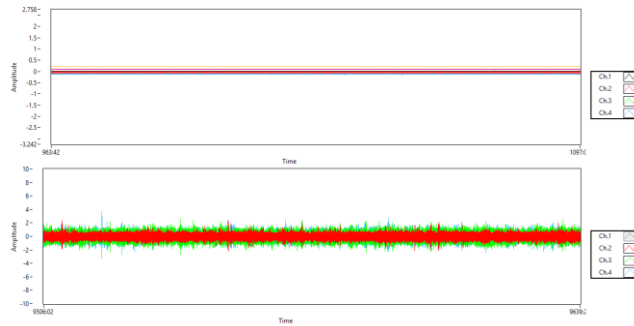
<b>Coupon #</b>	<b>Starting Mass (gm)</b>	<b>Starting Height (mm)</b>	<b>Ending Mass (gm)</b>	<b>Ending Height (mm)</b>	<b>Mass Loss (gm)</b>	<b>Height Loss (mm)</b>
1	7.872	25.50	7.868	25.46	0.004	0.04
2	8.469	25.79	8.462	25.76	0.007	0.03
3	7.691	25.51	7.683	25.48	0.008	0.03
4	7.76	25.50	7.753	25.48	0.007	0.02
5	7.851	25.44	7.835	25.42	0.016	0.02

In addition to the measurements detailed in Table 8, the Olympus UT probe was also used to take measurements in situ during the test. After comparing the results of the UT pencil sensor to caliper readings taken after testing, it can be shown that the accuracy of using the UT pencil probe during operation can yield thickness measurement changes accurate to 0.025mm (0.001”) and a reproducibility of measurement on the same coupon of 0.0127mm (0.0005”).

#### **Results from Fiber-optic Sensors:**

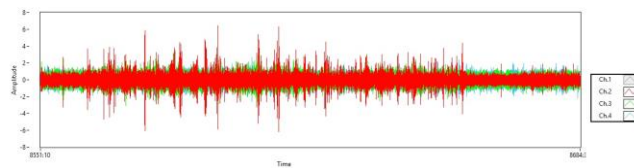
Bench scale testing of the sensors consisted of capturing data from the pipeline during operation while unique events occurred in order to identify event signatures and ensure that the sensors were able to routinely detect occurrences of the same event. Each sensor represents one channel and captures roughly 36,000 data points per second in order to effectively measure all energies across a frequency spectrum of 0 Hz to 100 kHz that the pipeline emits. A set of experiments were conducted by mounting three sensors at approximately equal intervals throughout the test pipeline. No issues with signal attenuation were experienced with the sensors due to their mounting; however, small radius bends and kinks in the fiber optic cable did cause temporary signal degradation that was fixed once the bends and kinks were removed. The event signatures were created by striking the pipeline with a hammer or opening a hole in a section of the pipe. Detecting an event on the pipeline requires capturing the baseline signature and then comparing any deviations. The baseline is defined as the continuous flow inside the loop when the pump is operating. As it will be shown by the data, each event creates a unique signature that would allow a remote monitoring system to identify not only the type of event, but also the relative location and severity.





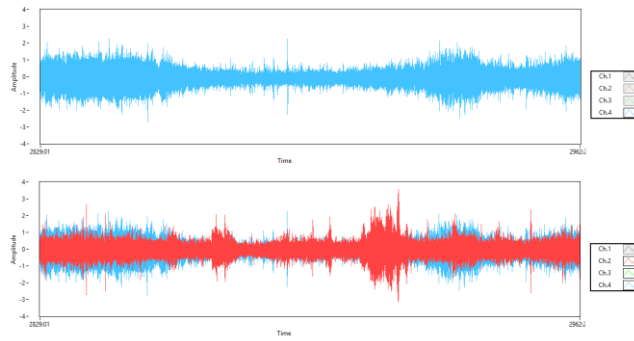
**Figure 65. Sensor baseline profile of pipe loop (no activity - top and pump operating - below).**

Compared to when the pump is running, a dramatic change in acoustic energies can be seen when it is not. Figure 65 compares the signature of the pipeline with no activity (pump is off and no throughput) and the baseline (pump is on and water is flowing). For sections of pipelines near pumping stations, the signature of the pipeline can be used to easily identify pump failures, and to also monitor the health of the pump in real time. Minor changes in acoustic energy emitted from the pump through the pipeline may go unnoticed to personnel nearby; however, by analyzing changes in the PSD signature captured by the acoustic transducers, a monitoring system can make judgements on overall pump performance.



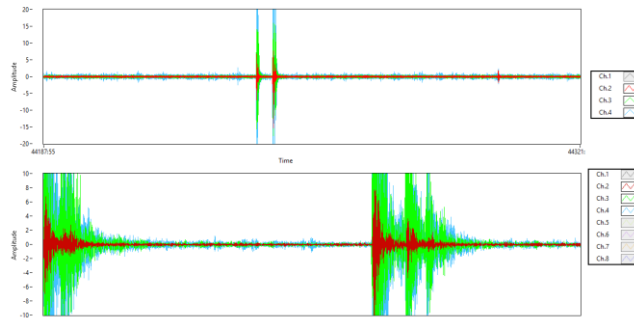
**Figure 66. Sensor profile (0.25" hole opened and closed).**

To simulate the puncturing of the pipeline and a leak, a 0.25-inch hole was opened and then closed. The expected change in physical conditions within the pipe would be a change in pressure and increased turbulent flow. In Figure 66, one can see the signature of a leak occurring and then being plugged during a 13 second interval. The hole is located closest to channel 2 - represented in red - on a vertical section of pipe. It is important to note that little effect is noticed on the signatures of channel 3 (green) and channel 4 (blue) which are mounted on the pipeline in horizontal sections further down the line. It should also be noted that when the hole is plugged, the signature returns to its baseline. While the leak is active, reverberations inside the pipe from the turbulent flow are picked up from the nearest sensor, channel 2 (red). As expected, not all holes or leaks in a pipeline will emit the same frequency response and have the same PSD signature in all places. The signatures in Figure 67 below represent a 0.5 inch hole being opened and then closed during a 13 second interval. The hole was located on the furthest end of the pipeline, closest to the channel 4 sensor (blue). In addition, the hole was located on the top of the pipeline. When opened, a vacuum occurred and air was pulled into the pipeline, unlike the previous event where a 0.25" hole was opened and water escaped.



**Figure 67. Sensor profile (0.5” hole opened and closed).**

Instead of an increase of amplitude in the channel as seen in the previous test, we see a sudden decrease in the amplitude of channel 4 (blue). Due to air entering the closed system, there is less water in this section of the pipeline and hence a damping of the acoustic signals traveling along the pipeline since air is not as conductive as water. As soon as the hole is closed, the PSD of channel 4 returns to its normal signature.



**Figure 68. Sensor profile (pipeline strike 13 sec - top and 2 sec magnified - below).**

In another attempt to capture a unique signature, the pipeline was repeatedly struck. One of the most common forms of damage to a pipeline is during construction in the area. Buried pipes are often struck by stakes, shovels, or earth moving equipment. By striking the pipeline in different areas with a hammer, researchers were able to capture the unique signature of a strike against a metal pipe, and identify the relative location of the event. Figure 68 shows the pipeline being struck consecutively with a hammer between the sensors represented by channel 3 (green) and channel 4 (blue). The strike can be characterized by the sharp change in amplitude of all channels followed by the rapid dissipation of vibrations and the amplitudes returning to the baseline. It should be noted that the closer to the strike the sensor is mounted, the larger the amplitude spike and the longer the regression to the baseline. This strike took place at approximately the midpoint between channel 3 and 4, and the near identical shifts in amplitude corroborate. This gives evidence that a monitoring system would be able to identify where a machine or person has accidentally struck the pipeline. In other tests researchers were able to successfully guess the relative location of the strike to a sensor by looking at the amplitudes and attenuation times of the disturbances measured by each channel and comparing them. In this instance, the pipeline was not dented or punctured, however, if it had been, the signature of the pipeline would not return to its baseline. Instead, a signature like Figure 68 may appear, representing that the pipe was leaking.

### **Subtask 19.1: Conclusions and Future Work**

The current task involves verification and validation of several sensor options that can be used at the nuclear waste sites across the US for challenging structural integrity issues. In this regard, three sensor systems are being tested at FIU. One of the sensor systems is the Permasense wave guided UT sensor system for use with pipelines. These sensors have been tested for their precision (0.01 mm), repeatability and reliability of operation. Additionally, the real environmental conditions similar to those at the sites were also tested. Based on several tests conducted over a year, it is concluded that the Permasense sensors are a good option to be considered for deployment to the sites for detecting thinning of carbon steel pipe sections. Future work will involve the radiation exposure of these sensors to investigate their ability under various levels of radiation. This is being planned in the next year's scope of work.

Current research also verifies and validates the use of the SRNL coupons on an engineering scale test bed for their ability to detect pipe wear and erosion on a minute level in real-time. From the data obtained from the SRNL coupon testing, the erosion rates of the ceiling versus the floor of the pipe could easily be calculated after several hours of experimentation. On an average, the bottom of the pipe showed 1.6mg/hr and 0.0028mm/hr mass loss and thickness loss respectively, while the ceiling of the pipe lost 0.9mg/hr and 0.0047mm/hr. In addition, extremely valuable insights into the method of erosion were gained from the ability to remove and inspect the coupons after a test. Under typical circumstances, the thickness change measurements recorded by a UT sensor would lead to the conclusion that more mass is being lost from the ceiling of the pipe section due to the fact that it has a higher average height change; however, by being able to inspect the surface of the coupons subject to wear, it is clear that average height change and mass loss are not as closely correlated. This could be due to the uneven surfaces resulting from particle agglomeration, settlement to severe flushing with high velocities. Compared to conventional forms of wear testing in the field, the SRNL coupon system is vastly superior for reasons outlined in this research so far. By being replaceable, the coupons allow for accurate testing of erosion in a field environment but with the added benefit of being able to start with a fresh surface and a controlled location to take measurements. These factors alone reduce the errors resulting from improper probe angle and placement when taking measurements, not to mention surface defects and corrosion on the inner surface of the pipe that can lead to inaccurate UT measurements. By being able to remove the coupons and collect highly precise mass measurements, very specific erosion quantification can be achieved while previously, the assumptions on the relationship between mass and thickness change were forced to be made. The findings of the bench scale test performed during this research indicate that the SRNL coupon system will be an impactful new technology for waste management facilities, and many other applications requiring erosion measurement as well. Further testing of longer duration is required to prove validity on larger scale systems where tests may last months instead of hours. Also, modifications to the current bench scale pipe loop are planned to quantify more variables such as pressure and flow rate inside the pipe. With these added values, more complex models of erosion can be determined from the quantities extracted from the coupon system. Finally, the coupons must be assessed for failure potential and expected lifetime usage. For operational pipelines that are not solely for experimental conditions, mounting the coupon system on a section of pipe must prove to be a permanently safe operation. Degradation of coupon components during normal operation and exposure to the elements must be analyzed in future.

This work has also attempted to investigate the functionality and application of acoustic transducers interpreted by optical interferometry, and the possible application in nuclear waste facilities where pipelines must be monitored. The CEL Fiberstrike system was assessed for its ability to detect unique events such as impacts and leaks on a carbon steel pipe loop located near an active pump. This sensor system is capable of registering numerous types of pipeline events in real-time with little to no visible delay. By using 2 in. and 3 in. pipe sections, the bench scale testing documented in this work provides basis for the sensor system's potential implementation in various DOE sites when transferring hazardous materials through a pipeline that requires real-time monitoring. This will ensure that any fault is detected immediately and will reduce the impact. While all analysis of captured data was done by researchers, it can easily be seen that through training a machine learning model with various types of pipeline fault signatures, an automated real-time monitoring system could be realized. Further investigations into applying this same technology to monitoring the storage of static vessels containing hazardous liquids are planned. In addition, data collected from the erosion coupons show promise for creating a methodology for assessing a waste transfer system's erosion potential in situ, or for testing the erosion susceptibility of new materials in the design process. Introducing a radioactive simulant into the test parameters will be very useful for measuring the additional effects on pipeline degradation and to see if there is any interference with the acoustic sensors. The previously mentioned work will be investigated in the future while potentially conducting experiments and onsite tests at a DOE facility.

### Subtask 19.1: References

1. [https://in.omega.com/pptst/FSH\\_HEATER.html](https://in.omega.com/pptst/FSH_HEATER.html)
2. <https://www.amazon.com/Inkbird-Temperature-Controller-Thermostat-Variations/dp/B07GR31TBW>
3. [https://www.mouser.com/ProductDetail/Adafruit/393?qs=GURawfaeGuA6CBjDa3Dvow%3D%3D&gclid=CjwKCAiA6vXwBRBKEiwAYE7iS46G2fuX7u3KplDfb4WUtm31UFN0q\\_gn\\_GfvC5OvdH3FMpe2yUp-BoCU6YQAvD\\_BwE](https://www.mouser.com/ProductDetail/Adafruit/393?qs=GURawfaeGuA6CBjDa3Dvow%3D%3D&gclid=CjwKCAiA6vXwBRBKEiwAYE7iS46G2fuX7u3KplDfb4WUtm31UFN0q_gn_GfvC5OvdH3FMpe2yUp-BoCU6YQAvD_BwE)
4. [https://srnl.doe.gov/tech\\_transfer/tech\\_briefs/SRNL\\_TechBriefs\\_UltrasonicThicknessMassLossMeasurement.pdf](https://srnl.doe.gov/tech_transfer/tech_briefs/SRNL_TechBriefs_UltrasonicThicknessMassLossMeasurement.pdf)
5. <https://www.olympus-ims.com/en/shop/item/269-productId.570437480.html>
6. <http://www.clevelandelectriclabs.com/wp-content/uploads/2016/08/Cleveland-Electric-Labs-Marketing-Pipeline-Monitoring-with-Fiber-Optics.pdf>
7. Aravelli, A., Thompson, M., McDaniel, D., Krutsch, M., McNeilly, M., Imrich K., Wiersma B., "Advanced Fiber Optic and Ultrasonic Sensor Systems for Structural Health Monitoring of Pipes in Nuclear Waste Sites", IMAPS 52<sup>nd</sup> International Symposium on Microelectronics (IMAPS), Boston, MA, Sep 30-Oct 3 2019, IMAPS (2019).
8. Aravelli A., McDaniel, D., Davila, C., "Real-time Erosion-Corrosion Detection in Waste Transfer Pipelines using Guided Wave Ultrasonic Sensors", Proceedings of the Waste Management Symposia 2018, Phoenix, AZ, March 18-22, 2018.
9. Aravelli, A., McDaniel, D. and Davila C., "Assessment of Guided Wave Ultrasonic Transducer Systems for Wall Thickness Measurements", Summary Document submitted

to DOE –EM under Cooperative Agreement # DE-EM0000598 (FIU-ARC-2016-800006470-04c-242).

10. Aravelli A., D. McDaniel, A. Abrahao, A. Awwad, C. Davila, “Thermal Measurement and Modeling of Nuclear Waste in the Double Shell Tanks at Hanford Nuclear Waste Site Using Miniature Sensors,” International Microelectronics Assembly and Packaging Society (IMAPS) 2016, Pasadena, CA, October 11-13, 2016.

## **Subtask 19.2: Evaluation of Nonmetallic Components in the Waste Transfer System**

---

### **Subtask 19.2: Introduction**

Nonmetallic materials are utilized in the waste transfer system at the Hanford tank farms; these include the inner hose of the hose-in-hose transfer lines (HIHTLs), Garlock<sup>®</sup> gaskets and ethylene propylene diene monomer (EPDM) O-rings. These materials are exposed to simultaneous stressors including  $\beta$  and  $\gamma$  radiation, elevated temperatures, caustic supernatant as well as high pressures during normal use. In 2011, the Defense Nuclear Facilities Safety Board recommended to the U.S. Department of Energy (DOE) to conduct post service examination of HIHTLs to improve the existing technical basis for component service life. Suppliers of the nonmetallic components often provide information regarding the effects of some of the stressors, but limited information is available for simultaneous stressor exposure.

An extensive test plan was developed by Sandia National Laboratories to understand the simultaneous effects of the aforementioned stressors [1]; however, this test plan was never executed. Additional studies conducted by Lieberman provide information on HIHTLs at elevated temperature and pressure, but little information is gained regarding the synergistic effects with the caustic supernatant [2]. Florida International University (FIU) has been tasked with supporting this effort by conducting multi stressor testing on typical nonmetallic materials used at the Hanford tank farms. Previous years' research efforts focused on evaluating the aging behavior of EPDM by exposing samples of HIHTLs as well as EPDM dog bone shaped specimens to a 25% NaOH solution at (100°F) and operating (130°F) and design temperatures (170°F) for 6 months and 12 months. This year's efforts focused on exposing HIHTL and the EPDM dog bone specimens to only hot water at 170°F for a duration of one year. A test loop was developed at FIU that allowed for the aging of HIHTL as well as dog bone specimens utilizing only water at 170°F. This report provides the mechanical property testing of EPDM material dog bones as well as the blowout test results for HIHTLs, after a 12-month aging period using water at 170°F. In addition, the baseline specimens and exposed specimens were examined using a JEOL 6330 scanning electron microscope equipped with energy dispersive X-ray spectroscopy (SEM-EDX) to evaluate the changes in surface microstructure and the penetration of ions into the EPDM material from the NaOH solution.

### **Subtask 19.2: Objectives**

In order to reinforce the findings from the previous work, HIHTL coupons as well as EPDM material coupons will be used to run additional experiments utilizing sodium hydroxide and water only at various temperatures. FIU engineers will work with Hanford personnel to develop new experimental combinations. Comparing the results of the testing with previous data will allow a better understanding of how the elevated temperatures and the sodium hydroxide affect the material properties of the components.

### **Subtask 19.2: Methodology**

All material samples had their baseline mechanical performance and properties tested as per ASTM standards prior to any exposure. Once the baseline properties were determined, each material sample was aged, which involved exposing each sample to a water at 170°F for

durations of 365 days. Tests were conducted on both EPDM dog bone as well as HIHTL specimens. After aging/conditioning, the mechanical properties of the samples were again measured as per ASTM standards.

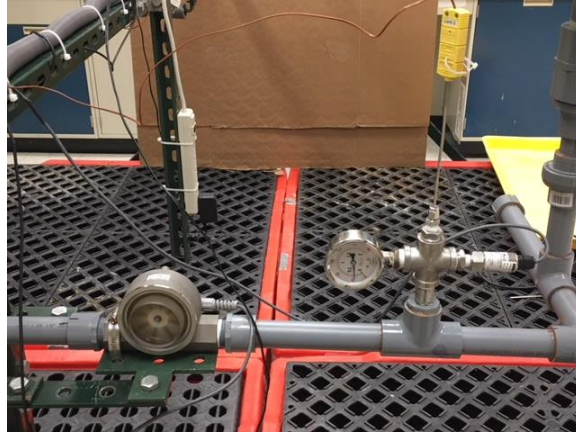
### Specimen Aging

Two HIHTL and 5 EPDM dog bone specimens were aged using only water at 170°F. This test was developed after reviewing the data from the tests conducted last year and consultation with site personnel. Previous tests showed the greatest degradation in hose burst pressure as well as the tensile strength of the material coupons occurred at the highest temperatures (170°F). It was not clear if the degradation to the HIHTL and dog bone specimens was a result of being exposed to the high temperature or if it was a result of exposure to the sodium hydroxide. Thus, for this set of experiments, pure water at 170°F was chosen as the stressor in an attempt to determine whether it is the high temperature or the caustic solution that is causing the degradation in the material. Figure 69 shows the aging loop. It consists of two hose test sections connected to a flow loop made of CPVC tubing. The loop has a high temperature pump as well as a turbine flow meter along with a thermocouple and a pressure transducer to provide the flow rate, temperature and pressure of the flow in the loop (Figure 70).



**Figure 69. Water only aging loop.**





**Figure 70. Flow meter, pressure transducer and thermocouple.**

The dog bone aging setup consisted of an aging vessel filled with six EPDM dog bones submerged in the test loop's storage tank (Figure 71). This resulted in exposing the dog bones to the same conditions as the HIHTL specimens; the circulating fluid is the same water at 170°F.

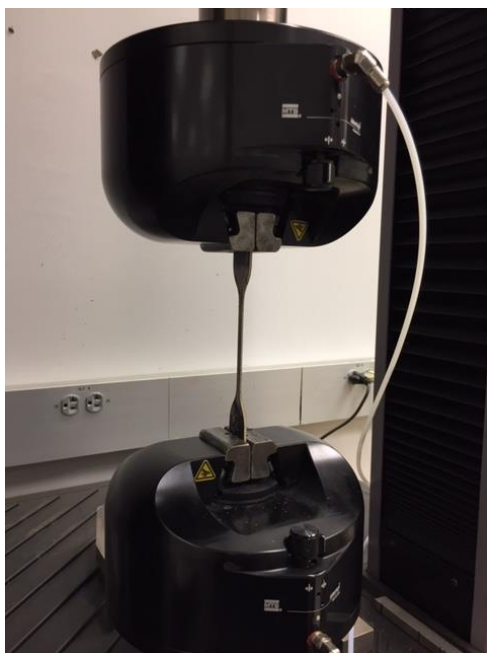


**Figure 71. Coupon aging vessel (left) and EPDM dog bone (right).**

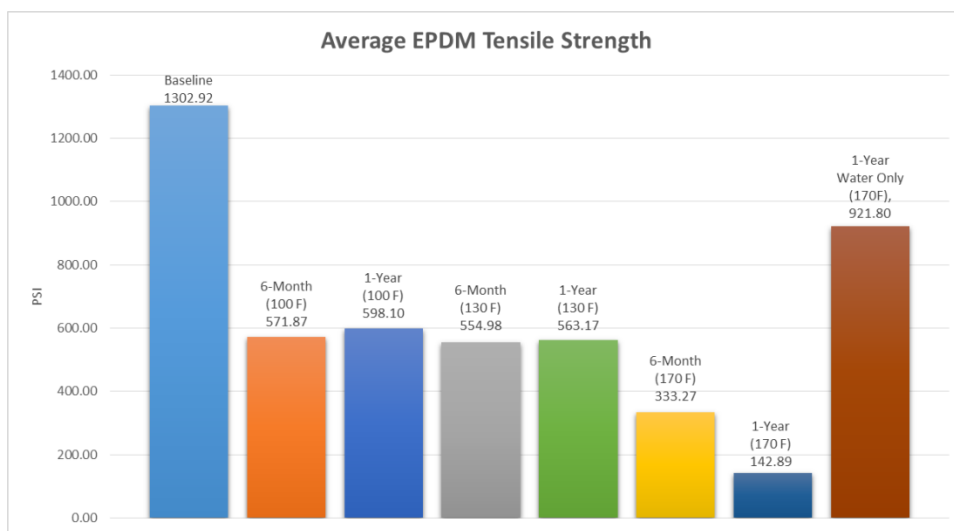
## **Subtask 19.2: Results and Discussion**

### ***Material Tensile Testing***

Six EPDM dog bones were aged in loop's tank maintained at 170°F. All procedures used for testing were derived from the ASTM D412-16 standard [3]. Figure 72 shows an EPDM dog bone being tested and Figure 73 shows a comparison of the tensile strength test results for the EPDM dog bones under various aging conditions.



**Figure 72. Tensile strength testing of an EPDM dog bone.**



**Figure 73. EPDM dog bone tensile strength.**

As can be seen from Figure 73, the tensile strength of EPDM dog bones that were aged with the caustic solution decreased as the aging temperature increased. However, the specimens aged with water only at 170°F observed only a 29% reduction in strength while the specimens aged at with the caustic solution at 170°F observed an 89% reduction in strength. This infers that the sodium hydroxide solution has a greater effect on the degradation of the material strength than just the high temperature alone.

***Hose-In-Hose***

After the aging for one year, the two HIHTL specimens (WO-01 and WO-02) were removed from the 170°F water only loop and pressurized until rupture. Their pressure profiles as well as initial and final lengths were measured. The rupture pressures of the specimens were compared

with the unaged samples (baseline) which ruptured at 2827 psi. Figure 74 shows the rupture test apparatus and a ruptured hose section.



**Figure 74. Hose burst test apparatus.**



**Figure 75. Ruptured HIHTL specimen WO-01.**



**Figure 76. Ruptured HIHTL specimens WO-02.**

Data from the burst pressure tests showed that hose WO-01 burst at 2,287 psi (Figure 77) and hose WO-02 burst at 2,262 psi (Figure 78). This translated to an average burst pressure of 2,275 psi and a difference between both readings of 25 psi, which is within the pressure transducer's accuracy of  $\pm 35$  psi.

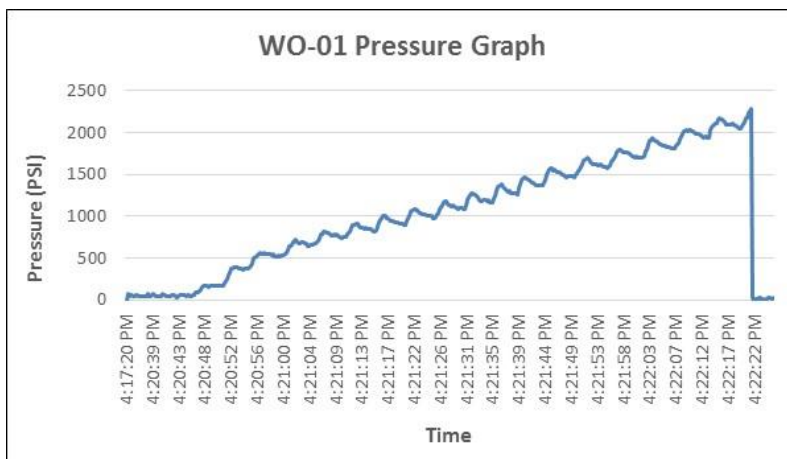


Figure 77. WO-01 burst pressure graph.

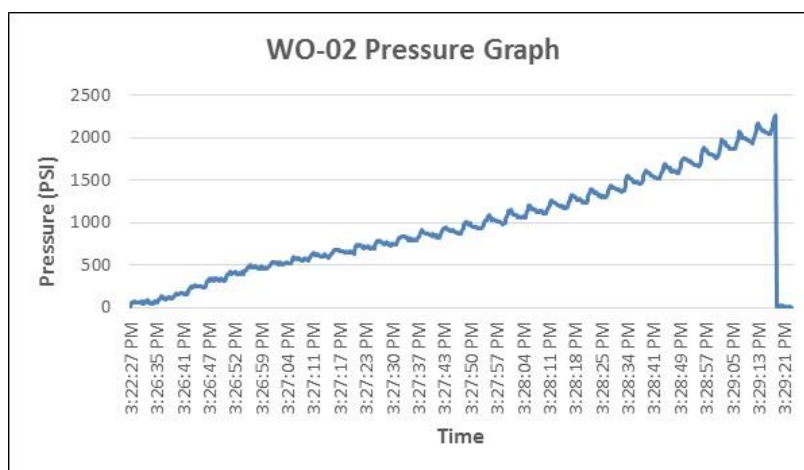


Figure 78. WO-02 burst pressure graph.

When the average burst pressure of the one-year 170°F water-only aged hoses was compared to the average burst pressures of the hoses aged for one-year in a 170°F 25% sodium hydroxide solution as well as the baseline (unaged) hoses (Figure 79), the effect of the circulating fluid’s temperature on the degradation of the hose burst pressure became apparent. The 170°F water-only aged hoses had an average burst pressure 552 psi lower than the average baseline pressure, but 261 psi above the hoses aged in a 170°F 25% sodium hydroxide solution. This indicates that the fluid temperature plays a significant role in the degradation of the hose burst pressure.

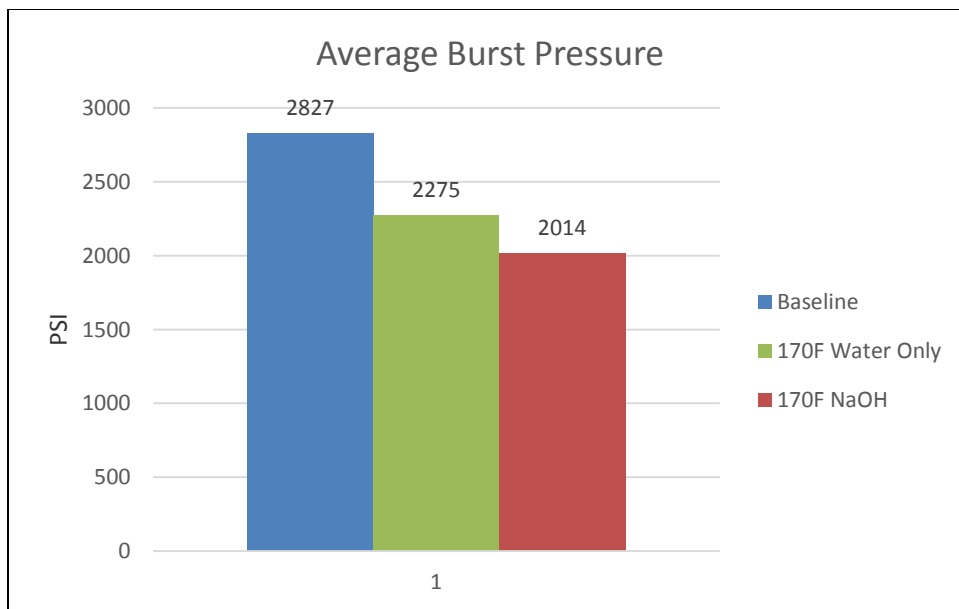


Figure 79. Average hose burst pressure comparison.

**Material surface**

The exposed and baseline EPDM dog-bone specimens were examined visually and by assessment of the captured Scanning Electron Microscope (SEM) images. As shown in Figure 80, the deterioration of the exposed surfaces of the dog-bone specimens aged with NaOH increased with the increasing fluid temperature for both the 6-month and 12-month aged specimens. The levels of surface deterioration were noticeably higher for the 12-month aged samples than those that were exposed for 6 months. However, the dog-bone specimens aged with water only for 12 months did not show as much deterioration as the specimens aged with NaOH.

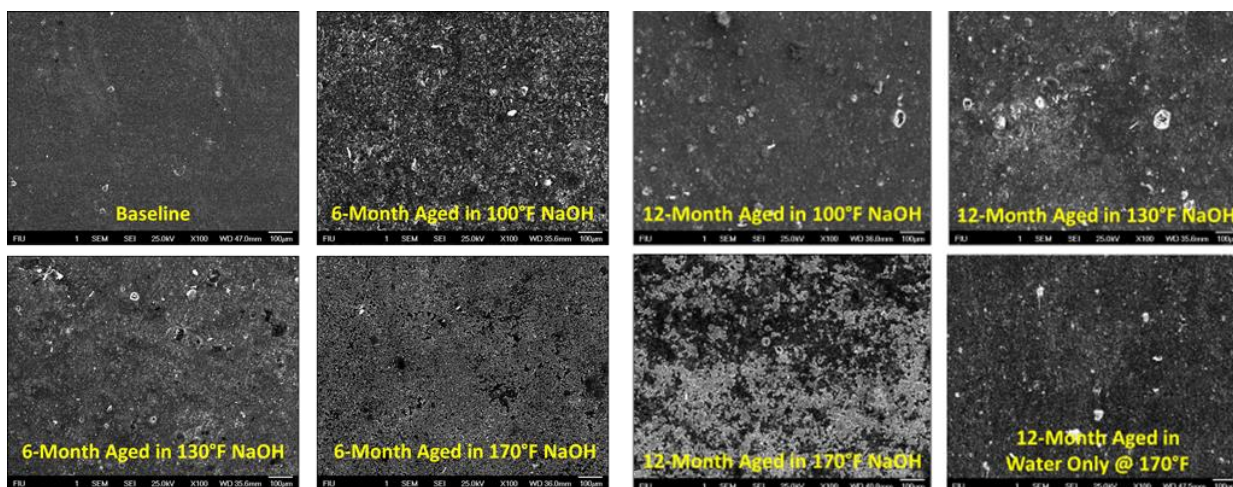
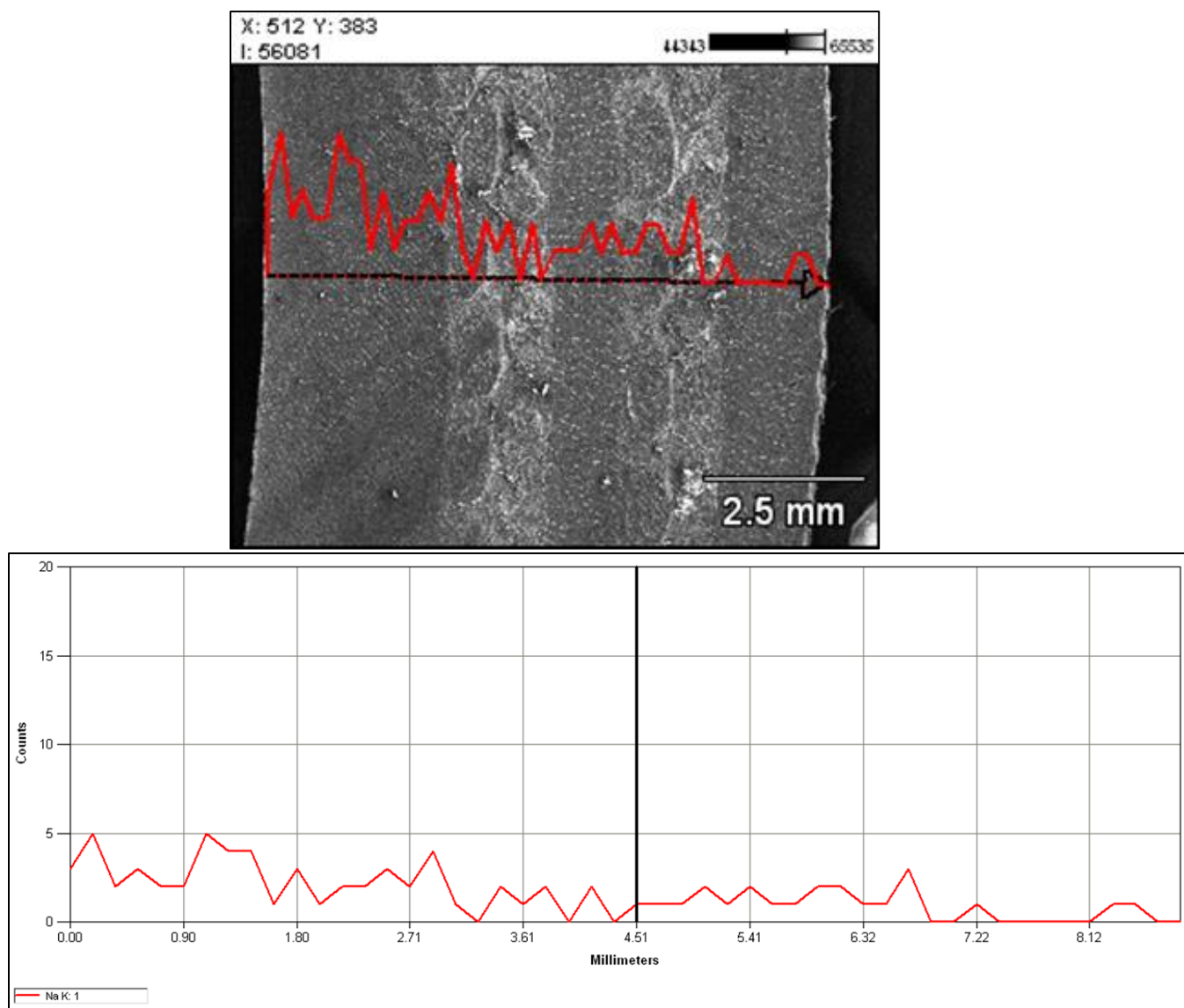


Figure 80. Visual characteristics of the surface of the EPDM (dog-bone) specimens before and after aging.



**Scanning electron microscope analysis**

Comparison of the SEM-EDS scans of a baseline HIHTL specimen and a HIHTL specimen exposed to 25% NaOH solution for both 6 and 12 months at 130°F and 170°F showed that there was ion penetration from the NaOH solution into the exposed EPDM material. Since the baseline sample was not exposed to the liquid, there was no sodium detected within the EPDM material (Figure 81), while the hose samples that were aged for 6 months and 12 months in the 25% NaOH solution at 130°F and 170°F had sodium ions that had penetrated into the EPDM material (Figure 82 - Figure 85). Upon closer investigation of the data from the specimens aged with 25% NaOH solution at 130°F and 170°F, the specimens aged for 12 months had a lower sodium count than the specimens aged for 6 months.



**Figure 81. SEM-EDS scan of baseline hose specimen.**

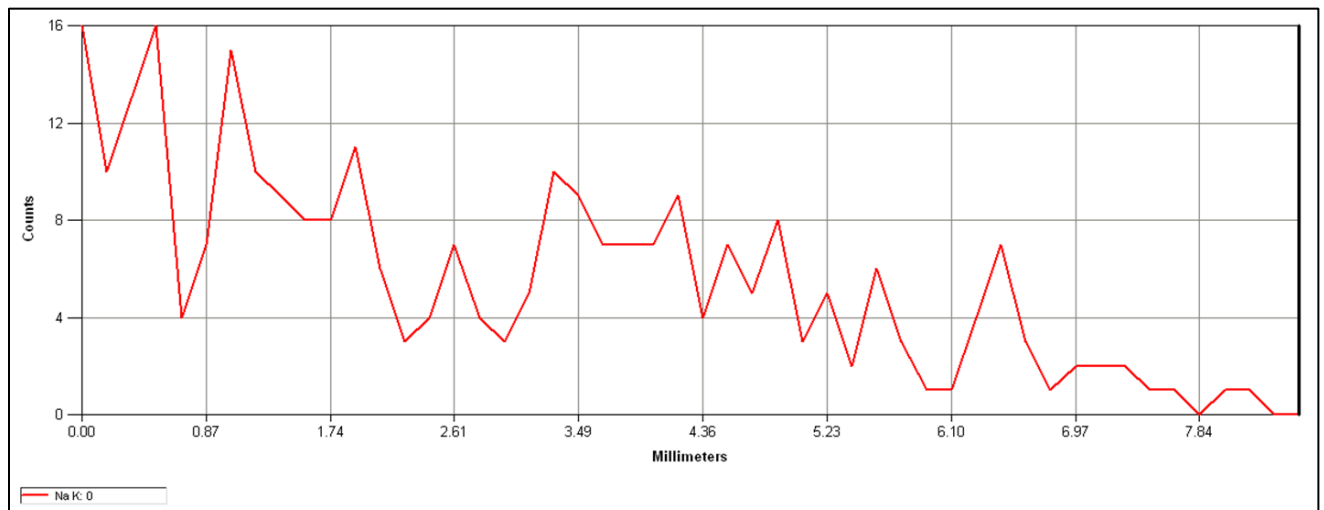
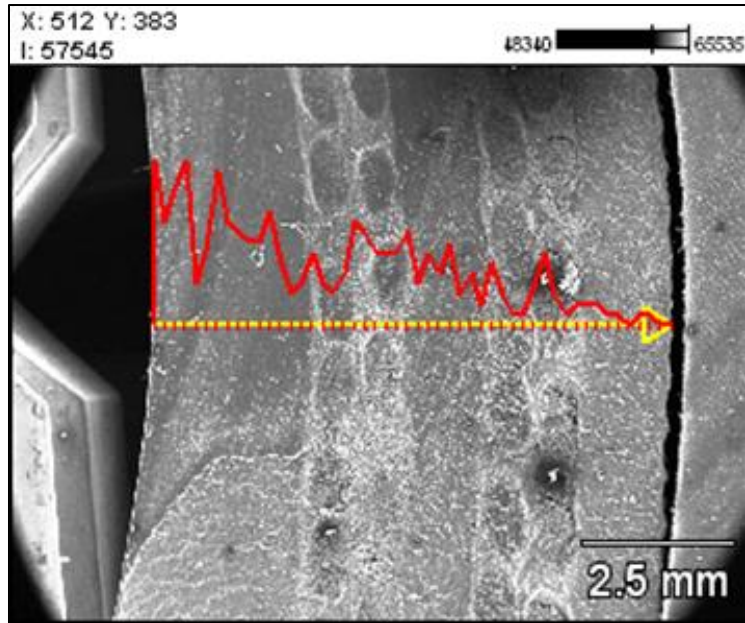


Figure 82. SEM-EDS scan of hose specimen aged for 6-months at 130°F.



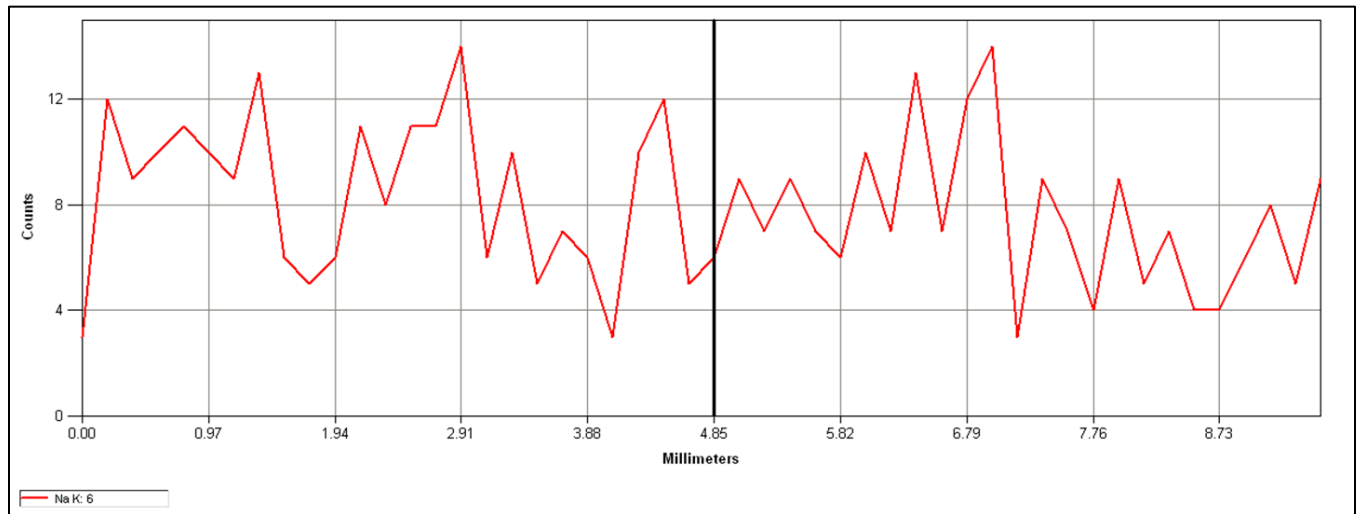
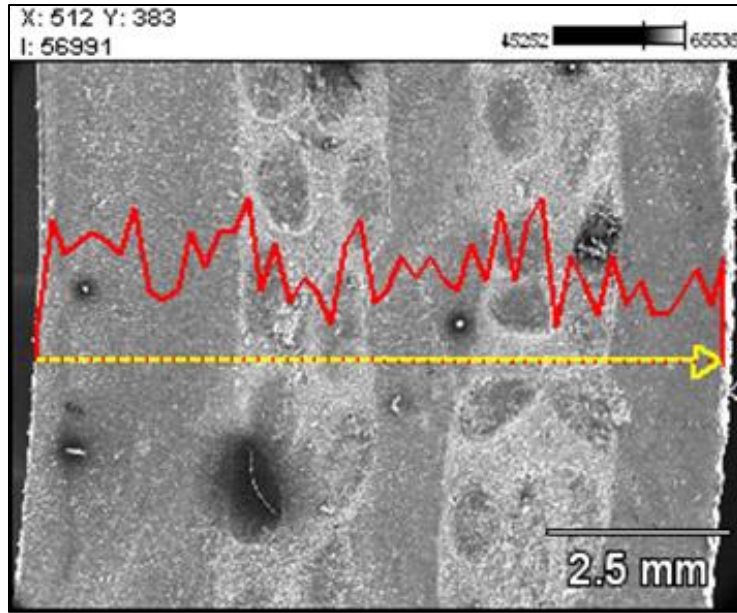


Figure 83. SEM-EDS scan of hose specimen aged for 12-months at 130°F.

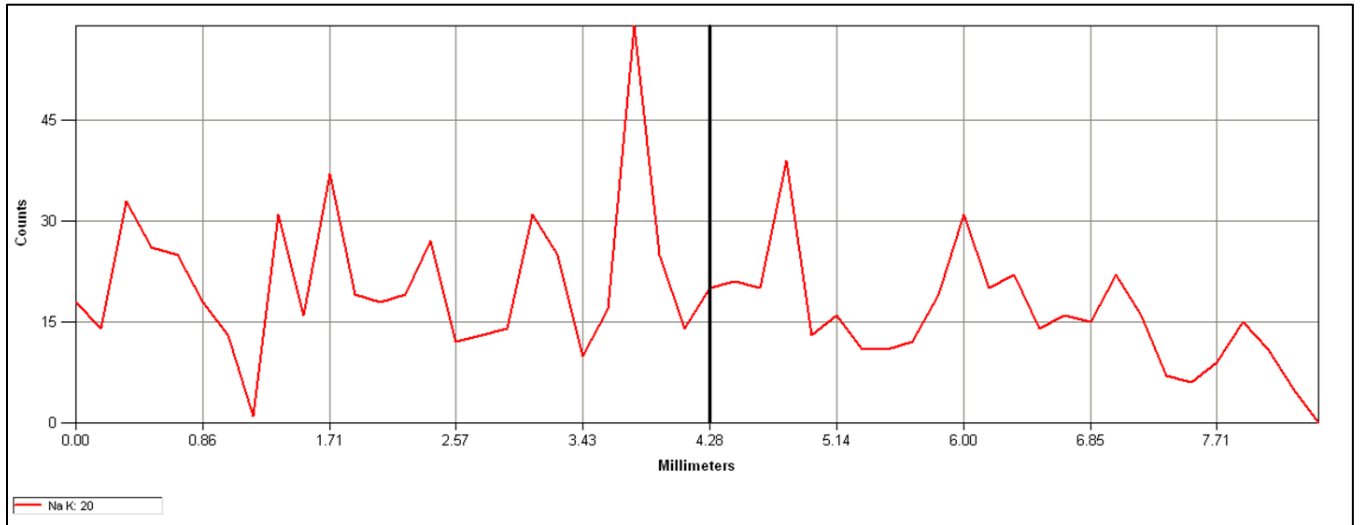
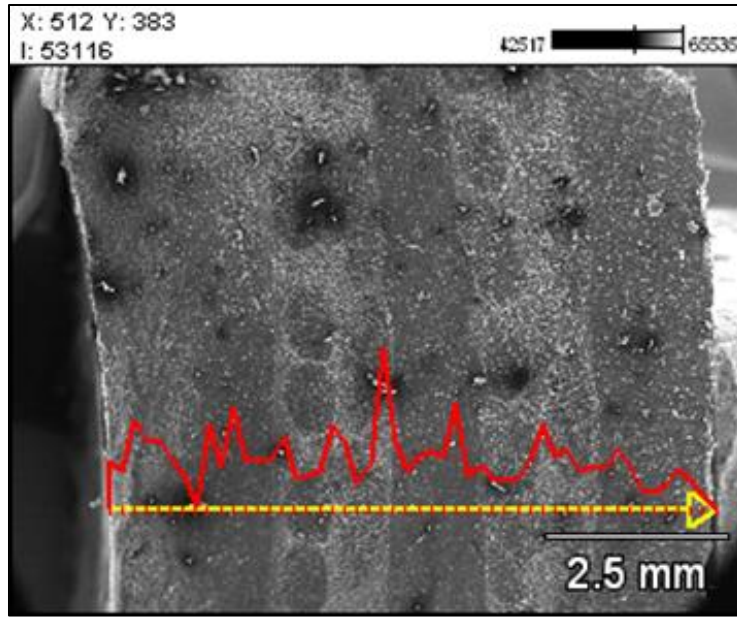


Figure 84. SEM-EDS scan of hose specimen aged for 6-months at 170°F.

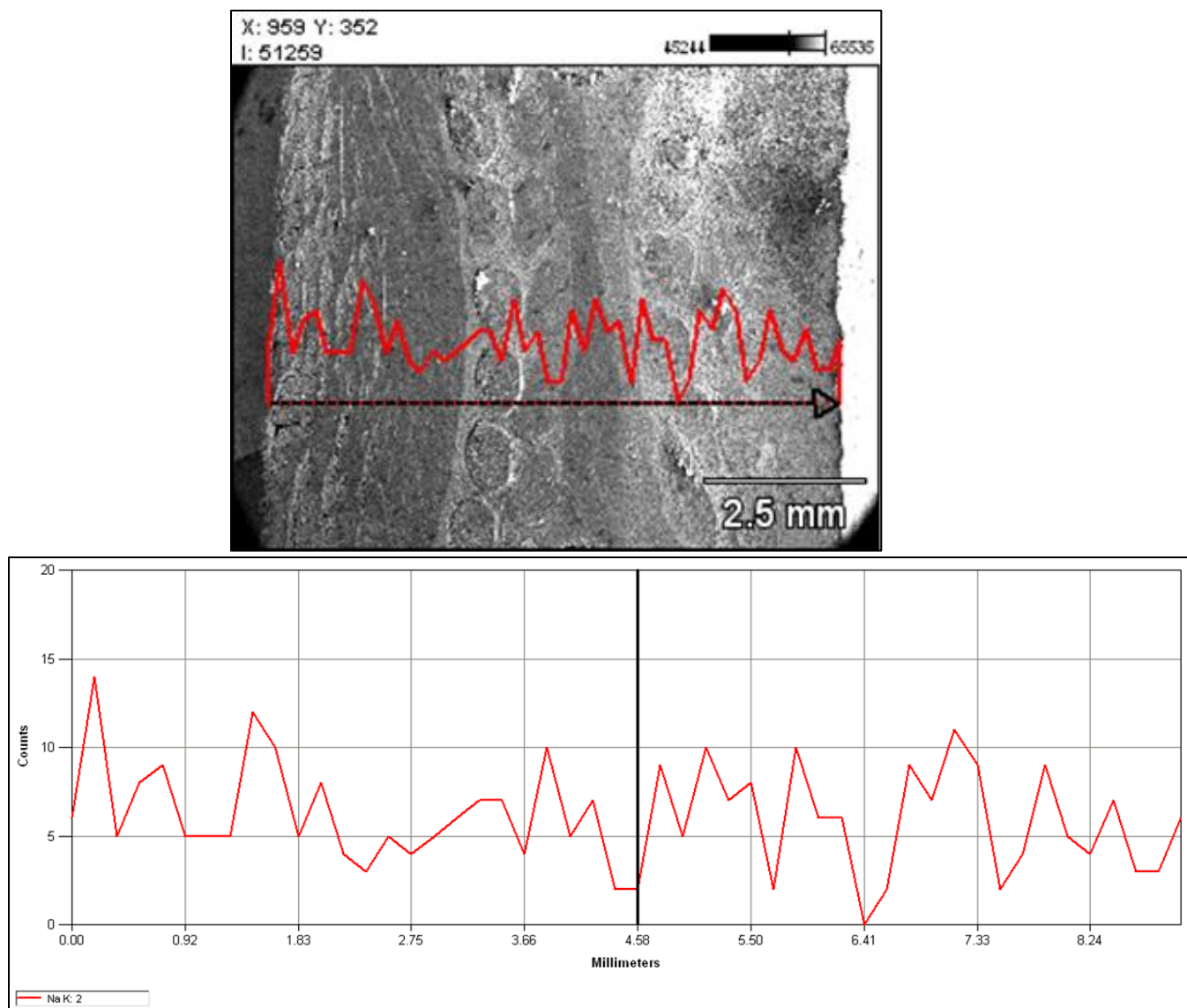


Figure 85. SEM-EDS scan of hose specimen aged for 12-months at 170°F.

### Subtask 19.2: Conclusions and Future Work

After analyzing the experimental data from the samples aged with only water at 170°F for one year, a 19.54% degradation was observed in the bursting pressure of the hoses when compared to the baseline results. However, a greater degradation (28.75%) was observed with the hoses aged with the 25% NaOH solution at 170°F. This indicates that even though exposure to high temperatures causes degradation in the burst pressure strength of the hoses, when NaOH is added into the solution, it has a greater effect on the degradation. Similar results were observed when the data was analyzed from the EPDM dog bone tensile tests. When compared to the unaged (baseline) dog bone results, the dog bones aged with water only at 170°F showed a 29.25% degradation in the tensile strength. However, a greater degradation (89%) was observed with the dog bones aged with the 25% NaOH solution at 170°F. This too infers that the sodium hydroxide solution has a greater effect on the degradation of the material strength than just the high temperature alone.

The next phase of testing will include obtaining 15 additional HIHTL specimens that will be aged with various concentrations of NaOH at 170°F for a duration of one-year. After each set of HIHTL specimens and material dog bones are aged for one-year, their burst and tensile strength will be tested.

### **Subtask 19.2: References**

1. H Brush, C. O. (2013). Test Plan for the Irradiation of Nonmetallic Materials. Albuquerque, New Mexico: Sandia National Laboratories.
2. Lieberman, P. (2004). Banded (Band-It) and Swaged Hose-In-Hose (HIHTL) Assembly Service Life Verification Program. Santa Clarita, California: National Technical Systems.
3. ASTM D412-16 Standard Test Methods for Vulcanized Rubber and Thermoplastic Elastomers—Tension, ASTM International, West Conshohocken, PA, 2016, <https://doi.org/10.1520/D0412-16>

## **ACKNOWLEDGEMENTS**

---

Funding for this research was provided by U.S. DOE Cooperative Agreement DE-EM0000598.

## CONFERENCE PARTICIPATION, PUBLICATIONS & AWARDS

---

### Peer-reviewed publications

Awwad, A., McDaniel, D., Lagos, L., Tansel, B., “Temperature effects on nonmetallic components used in radioactive waste transfer lines exposed to caustic conditions”, *Polymer Degradation and Stability* (In review).

Tashakori, S., McDaniel, D., Tan, Y., Abrahao, A., DiBono, M., Martin, D., Uriarte, P., Lagos, L., “Miniature rover for the inspection of the Hanford high-level waste double shell tanks” (In preparation).

### Oral presentations (presenter is underlined)

Aravelli, A., Thompson, M., McDaniel, D., Krutsch, M., McNeilly, M., Imrich K., Wiersma B., “Advanced Fiber Optic and Ultrasonic Sensor Systems for Structural Health Monitoring of Pipes in Nuclear Waste Sites”, IMAPS 52<sup>nd</sup> International Symposium on Microelectronics, 2019, Sep 30-Oct 3, Boston, MA, 2019.

Zanlongo, S., Bobadilla, L., McDaniel, D., Tan, Y., “Development of Informative Path Planning for Inspection of the Hanford Tank Farm”, International Conference on Robotics and Automation, Montreal, Canada, May 20-24, 2019.

Abrahao, A., Aucott, T., Alrashide, A., Adams, J., Zanlongo, S., McDaniel, D., Lagos L., “Autonomous Radiation Mapping and Quantification using an Unmanned Ground Vehicle” ANS Winter Meeting & Expo, Washington, DC, November 17-21, 2019.

Abrahao, A., Excellent, C., Losada, M., Lagos, L., McDaniel, D., “Development of Robotic Crawlers for Inspection of Radioactive Waste Tanks and Transfer Lines - 19573”, Proceedings of the Waste Management Symposia 2019, Phoenix, AZ, March 3-7 2019.

Tan, Y., Dibono, M., Lagos, L., McDaniel, D., “Development of a Semi-autonomous Miniature Rover for Inspection of Double Shell Tank Floors - 19625”, Proceedings of the Waste Management Symposia 2019, Phoenix, AZ, March 3-7 2019.

McDaniel, D., “Robotic and Sensor Systems for Infrastructure Inspection”, ASME Power Conference and Nuclear Forum, Drone and Robotics Seminar, Salt Lake City, UT, July 18, 2019. (Presentation – no paper)

McDaniel, D. “Inspection Tools for Hanford Tanks and Waste Transport Systems Tank Closure Forum, DOE-EM, September 10, 2019. (Presentation – no paper)

McDaniel, D., Hanford and Savannah River Coordination Meeting, Hanford, WA, March 18, 2019. (Presentation – no paper)

### Poster presentations (presenter is underlined)

Aravelli, A., Thompson, M., McDaniel, D., Krutsch, M., McNeilly, M., Imrich K., Wiersma B., “Advanced Fiber Optic and Ultrasonic Sensor Systems for Structural Health Monitoring of Pipes in Nuclear Waste Sites”, IMAPS 52<sup>nd</sup> International Symposium on Microelectronics, 2019, Sep 30-Oct 3, Boston, MA, 2019 (student poster).

## **WM Student Posters**

Christopher Excellent: Development of a Peristaltic Crawler for the Inspection of the HLW Tanks at Hanford - 19638

Michael DiBono: Miniature Motorized Inspection Tool for DOE Hanford Site Tank Bottoms - 19658

Christopher Suarez, Manuel Losada, Jean Plummer, William Wells, Conor McMahon, Julian Benitez-Muniz: Savannah River Site H-Canyon Tunnel Inspection LiDAR Mapping Solution - 19477

Jason Soto, Anthony Abrahao, Himanshu Upadhyay, Leonel Lagos: LiDAR Mapping & Surveillance of Nuclear Infrastructure - 19717

Mackenson Telusma, Yew Teck Tan, Dwayne McDaniel, Leonel Lagos: Surface Contact Adhesion Force Control via Sensor Fusion and PID Controller - 19715

## **Student awards**

### *WM Undergraduate Student Poster Competition*

1<sup>st</sup> Place: Michael DiBono: Miniature Motorized Inspection Tool for DOE Hanford Site Tank Bottoms - 19658

### *WM Graduate Student Poster Competition*

1st Place: Mackenson Telusma, Yew Teck Tan, Dwayne McDaniel, Leonel Lagos: Surface Contact Adhesion Force Control via Sensor Fusion and PID Controller - 19715

### *DOE Fellows Poster Exhibition and Competition*

Session I (Undergraduate posters):

2<sup>nd</sup> Place: Anilegna Nunez Abreu “Accelerated Aging of Concrete for the Evaluation of Coatings to Protect the HCAEX Tunnel at the Savannah River Site”

1<sup>st</sup> Place: Christopher Excellent “Development of a Crawler for the Inspection of the secondary liners of The Double shell tanks at Hanford”

Session II (Graduate posters):

1<sup>st</sup> Place: Michael Thompson “Advanced Fiber Optic and Ultrasonic Sensor Systems for Structural Health Monitoring of Pipes in Nuclear Waste Sites”



## APPENDIX

---

The following document is available at the DOE Research website for the Cooperative Agreement between the U.S. Department of Energy Office of Environmental Management and the Applied Research Center at Florida International University: <http://doeresearch.fiu.edu>

- Florida International University, *Project Technical Plan*, Project 1: Chemical Process Alternatives for Radioactive Waste, December 2019.